

NOAA Technical Memorandum ERL NSSL-86

Property of
NWC Library
University of Oklahoma

Final Report on the
JOINT DOPPLER OPERATIONAL PROJECT (JDOP)
1976 - 1978

Prepared by STAFF of:
National Severe Storms Laboratory, NOAA/ERL
Weather Radar Branch, Air Force Geophysics Laboratory
Equipment Development Laboratory, National Weather Service
Air Weather Service, United States Air Force

National Severe Storms Laboratory
Norman, Oklahoma
March 1979



**UNITED STATES
DEPARTMENT OF COMMERCE**

Juanita M. Kreps, Secretary

NATIONAL OCEANIC AND
ATMOSPHERIC ADMINISTRATION

Richard A. Frank, Administrator

Environmental Research
Laboratories

Wilmo! N. Hess, Director

NOTICE

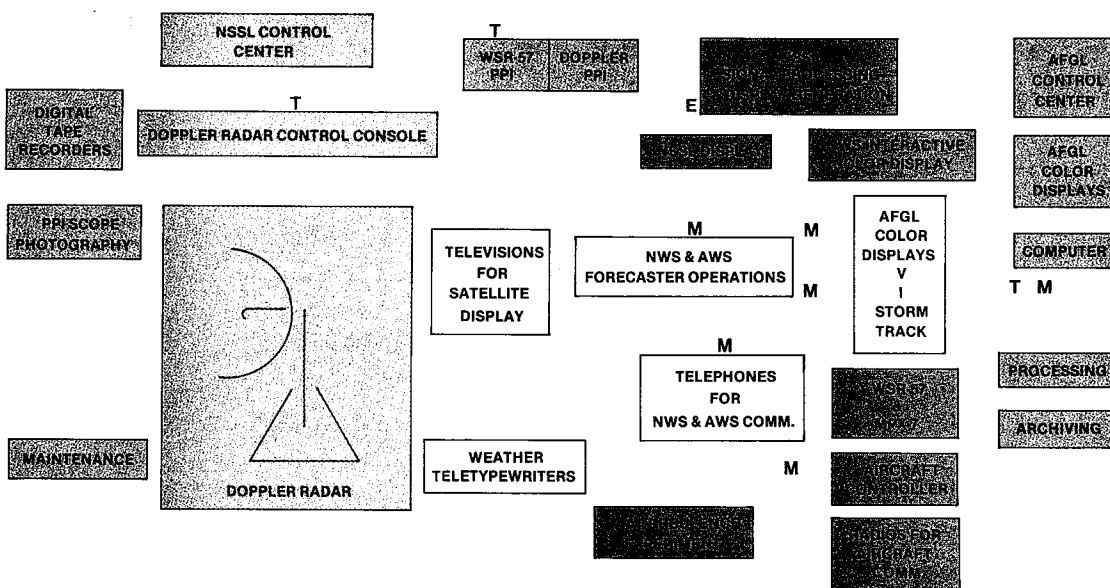
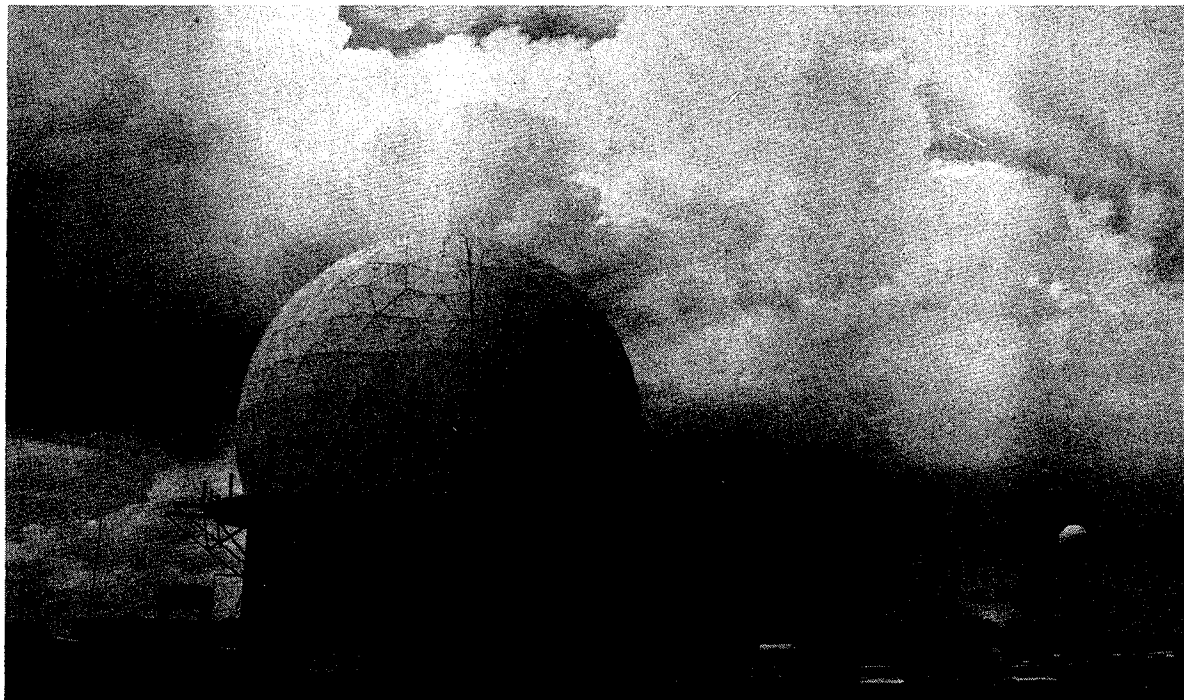
Mention of a commercial company or product does not constitute an endorsement by NOAA Environmental Research Laboratories. Use for publicity or advertising purposes of information from this publication concerning proprietary products or the tests of such products is not authorized.

Final Report
on the
JOINT DOPPLER OPERATIONAL PROJECT (JDOP)
1976-1978

PART I - METEOROLOGICAL APPLICATIONS
Prepared by
Don Burgess, Ralph J. Donaldson,
Tom Sieland, and John Hinkelman

PART II - DOPPLER RADAR ENGINEERING
Prepared by
Dale Sirmans, Kenneth Shreeve,
Kenneth Glover, and Isadore Goldman

APPENDICES
Prepared by
Joel David Bonewitz, Kenneth Shreeve
and Kenneth Glover



Frontispiece--Above: Doppler Radar Facility at the National Severe Storms Laboratory, used as the test facility for the Joint Doppler Operational Project (JDOP), 1977-78.

Below: Placement of staff and equipment during JDOP operations in 1978. Staff included Meteorologists (M), Engineers (E), and Technicians (T) from National Weather Service, Air Weather Service, Air Force Geophysics Laboratory, and National Severe Storms Laboratory working together to process, analyze, interpret, and archive Doppler radar measurements from severe thunderstorms.

THE JOINT DOPPLER OPERATIONAL PROJECT - (JDOP)

Project Coordinator

*Kenneth E. Wilk, National Severe Storms Laboratory, NOAA

Principal Agency Representatives

NOAA Executive Committee

Karl R. Johannessen, National Weather Service
Edwin Kessler, Environmental Research Laboratories, Co-chairman
William H. Klein, National Weather Service, Co-chairman
Merritt N. Techter, National Weather Service

Federal Aviation Administration

*John W. Hinkelman, Systems Research and Development Service

U. S. Air Force

Ray Bonesteele, Air Weather Service
*Tom Sieland, Air Weather Service
*Kenneth Glover, Air Force Geophysics Laboratory

JDOP Staff, Participants, and Advisors

National Severe Storms Laboratory

| | | |
|-----------------|----------------|-------------|
| R. Alberty | J. Dooley | *J. Moore |
| G. Anderson | R. Doviak | P. Ray |
| R. Brown | L. Fortner | *D. Sirmans |
| W. Bumgarner | *L. Hennington | J. Smith |
| *D. Burgess | E. Horwitz | J. Weaver |
| *C. Clark | *J. Lee | A. Zahrai |
| R. Davies-Jones | D. Loggains | *D. Zrnic |

National Weather Service, Silver Spring, Md.

| | | |
|--------------|-----------|-------------|
| T. Blackburn | D. George | J. Nussbaum |
| R. Elvander | D. Greene | *K. Shreeve |
| | D. Holmes | |

National Weather Service, Oklahoma City Weather Service Forecast Office

| | |
|-------------|------------|
| C. Aldridge | *D. Devore |
| R. Crooks | W. Walker |

Air Force Geophysics Laboratory

| | | |
|--------------|---------------|----------|
| G. Armstrong | A. Bishop | M. Kraus |
| K. Barris | *C. Bjerkaas | W. Smith |
| | *R. Donaldson | |

U. S. Air Force, Air Weather Service

| | |
|-------------|----------|
| J. Bonewitz | M. Mader |
| D. Forsyth | M. Snapp |

Federal Aviation Administration

*I. Goldman

*Authors of materials included in this report.

FOREWORD

The Joint Doppler Operational Project has met its initial goal to evaluate real-time Doppler capabilities for identifying tornadic storms. The tests have established that Doppler velocity patterns have great value for recognition of severe storm phenomena; they encourage automation of analytical techniques to provide reliable objective analyses of reflectivity and wind shear signatures.

This report reflects a wide variety of contributions from many meteorologists and engineers; it reflects also the spirit of scientific cooperation which allowed the project to move ahead with minimal funding and diversion of staffs. Participants have the expertise and desire to move ahead together with design and implementation of the next generation weather radar.

The third year of tests scheduled for Spring 1979 will define requirements for data processing, communication, and remote displays to NWS and AWS offices, and further examine techniques for mapping turbulence for use by FAA in Air Traffic Control. The operational agencies must now define their data requirements, and complete the design for remote display systems. Also, suitable computer software must be developed to provide lucid graphic summaries for use at operational offices remote from the radar.

Kenneth Wilk, David Holmes, and
Ray Bonesteele
Agency Coordinators

TABLE OF CONTENTS

| | <u>Page</u> |
|---|-------------|
| FRONTISPIECE | iv |
| FOREWORD | vi |
| LIST OF ILLUSTRATIONS | ix |
| LIST OF TABLES | xi |
| LIST OF ABBREVIATIONS | xii |
| LIST OF SYMBOLS | xv |
| ABSTRACT | 1 |
| INTRODUCTION AND CHRONOLOGY | 1 |
| PART I - METEOROLOGICAL APPLICATIONS | 7 |
| 1. DOPPLER METHODOLOGY | 7 |
| 1.1 Real-time Signature Recognition and Severe Storm Diagnosis | 7 |
| 1.2 Implications of Doppler Radar for Turbulence Detection and Warning | 10 |
| 1.3 Summaries of Illustrative Cases from the JDOP Files | 12 |
| 2. 1977-1978 DATA | 24 |
| 2.1 General | 24 |
| 2.2 Air Weather Service Advisories | 35 |
| 3. JDOP FACILITIES | 38 |
| 3.1 NSSL Doppler Radar | 38 |
| 3.2 JDOP Control Room Configuration | 40 |
| 3.3 NSSL Data Processing and Display | 40 |
| 3.4 The AFGL System - Minicomputer Analysis and Display | 44 |
| 4. CONCLUDING REMARKS | 48 |
| PART II - DOPPLER RADAR ENGINEERING | 51 |
| 1. DOPPLER TECHNOLOGY | 51 |
| 1.1 Historical Background | 51 |
| 1.2 Inherent Characteristics | 52 |
| 1.3 Spectral Moment Estimates | 53 |

| | <u>Page</u> |
|-----------------------------------|-------------|
| 2. RADAR SYSTEM CHARACTERISTICS | 55 |
| 2.1 Design Criteria | 55 |
| 2.2 Detection of Mesocyclones | 58 |
| 2.3 Spectrum Width Considerations | 60 |
| 2.4 Engineering Possibilities | 60 |
| 3. RADAR DESIGN CONSIDERATIONS | 65 |
| 4. NEXRAD | 68 |
| APPENDICES | |
| APPENDIX A - Radar Data Displays | 69 |
| APPENDIX B - Plans for 1979 | 75 |
| ACKNOWLEDGMENTS | 80 |
| REFERENCES | 81 |

ILLUSTRATIONS

PART I

| | |
|---|----|
| Frontispiece: (above) Doppler Radar Facility at the National Severe Storms Laboratory | iv |
| (below) Placement of staff and equipment during Joint Doppler Operational Project | iv |

| <u>Figure</u> | <u>Page</u> |
|---|-------------|
| 1. Displays Used by Project Meteorologists | 5 |
| 2. Time-history of Aircraft Derived Turbulence and Doppler Radar Parameters | 11 |
| 3. Doppler Radar Displays for Gust Front of 28 June 1977 | 13 |
| 4. Track of 5 April 1978 Mesocyclone and Tornadoes | 14 |
| 5. Echo Tracks from Doppler for Storms of 5 April 1978 | 14 |
| 6. Radar Echoes Near the Time of the Lone Wolf Tornado on 5 April 1978 | 16 |
| 7. Comparison of Piedmont Storm Mesocyclone and Braman Storm "Micro"-cyclone | 16 |
| 8. Hail Swath with Radar Echo Overlaid for the 29 April 1978 Storm | 18 |
| 9. Multimoment Display of Divergence Aloft on 29 April 1978 | 18 |
| 10. Time-height Section of Mesocyclone Wind Shear for Piedmont Storm of 30 April 1978 | 20 |
| 11. Damage Path of 30 April 1978 Piedmont Storm | 21 |
| 12. Color Display Illustrations of the Piedmont Storm 30 April 1978 | 22 |
| 13. Multimoment Display Illustrations of the Piedmont Storm 30 April 1978 | 23 |
| 14. Color Displays of Reflectivity, Velocity and Velocity Spectrum Width for Storm of 27 May 1978 | 25 |
| 15a. Multimoment Display | 42 |
| 15b. Color PPI Display | 43 |

| <u>Figure</u> | | <u>Page</u> |
|---------------|--|-------------|
| 16. | Block Diagram of the Echo Track And Significance Estimator (ETSE) | 45 |
| 17. | Example of Echo Track Color Display. Data are from 5 and 29 April 1978 | 47 |

PART II

| | | |
|-----|--|----|
| 1. | The Unambiguous Range--Unambiguous Velocity Coupling for Doppler Radar | 55 |
| 2. | Percent Occurrence of Radial Velocities for Three Tornadic Storms | 56 |
| 3a. | Doppler Mesocyclone Signature of a Rankine Combined Vortex | 59 |
| 3b. | Theoretical Mean Doppler Velocity Azimuthal Profiles Through a Rankine Vortex | 59 |
| 4. | Frequency of Occurrence of Measured Mesocyclone Diameters | 59 |
| 5a. | Measured Mesocyclone Diameters | 61 |
| 5b. | Measured Peak-to-Peak Radial Velocity | 61 |
| 6. | Cumulative Probability of Spectrum Width for Two Tornadic Storms | 62 |
| 7. | Velocity Spectrum Width Versus Range for the Mesocyclone Region | 63 |
| 8. | Pictorial Representation of Signal Schemes that can Relax the Range Velocity Ambiguity | 63 |

TABLES

PART I

| <u>Table</u> | | <u>Page</u> |
|--------------|--|-------------|
| 1 | Project Progress | 3 |
| 2a | Operational Summary for 1977 | 26 |
| 2b | Operational Summary for 1978 | 27 |
| 3 | JDOP Data Summary | 28 |
| 4 | JDOP Advisory/Warning Tabulation for 1977-1978 | 30 |
| 5 | JDOP Critical Success Index | 31 |
| 6 | 1977-78 Doppler CSI for Tornadoes | 32 |
| 7 | JDOP Long Range Verification | 32 |
| 8 | OKC Warning Justification | 33 |
| 9a | 1977 Thunderstorm Penetration Flight Summary | 34 |
| 9b | 1978 Thunderstorm Penetration Flight Summary | 35 |
| 10 | JDOP Military Advisories | 36 |
| 11 | JDOP Military Advisory Skill | 36 |
| 12 | Norman Doppler Radar Characteristics | 39 |

PART II

| | | |
|---|---|----|
| 1 | Illustrative Doppler Radar Characteristics | 66 |
| 2 | Illustrative System and Signal Processing Characteristics (Batch Processing) | 67 |

LIST OF ABBREVIATIONS

| | | |
|--------|---|--|
| AFCRL | = | Air Force Cambridge Research Laboratories, now called Air Force Geophysics Laboratory (AFGL) |
| AFGL | = | Air Force Geophysics Laboratory |
| AGL | = | Above ground level |
| AWS | = | Air Weather Service, U.S. Air Force |
| BW | = | Beamwidth |
| CA | = | Computer Automation mini-computer |
| CMF | = | Coherent memory filter |
| CRT | = | Cathode ray tube |
| CSI | = | Critical success index |
| CST | = | Central standard time |
| dBZ | = | Ten times the logarithm of the reflectivity factor, a measure of range-normalized reflectivity |
| ERL | = | Environmental Research Laboratories |
| ETSE | = | Echo track and significance estimator |
| FAA | = | Federal Aviation Administration |
| FAR | = | False alarm rate |
| FPS-77 | = | Air Force operational radar, 5.3 cm |
| h | = | hour(s) |
| I/O | = | Input/output |
| Isodop | = | Contour of single Doppler velocity |
| JDOP | = | Joint Doppler Operational Project |
| mi | = | mile(s) |
| min | = | minute(s) |
| MMD | = | Multimoment display |
| MPX-7 | = | Aircraft interrogation radar |

MSI = Medium scale integrated circuits
 NEXRAD = Next generation weather radar
 nmi = Nautical mile(s)
 NOAA = National Oceanic and Atmospheric Administration
 NRO DOP = Norman Doppler radar
 NSSL = National Severe Storms Laboratory
 NWS = National Weather Service
 OKC = Oklahoma City, Oklahoma
 OS = Operating system
 POD = Probability of detection
 PPI = Plan position indicator, radar display
 PPP = Pulse pair processor, real-time velocity estimation
 PRF = Pulse repetition frequency
 PRT = Pulse repetition time
 R&D = Research and development
 s = Second(s)
 SCRM = Scan converter refresh memory
 SNR = Signal to noise ratio
 TVS = Tornado vortex signature
 USAF = United States Air Force
 VIL = Vertically integrated liquid water, a radar parameter
 VIP = Video integrator and processor
 WG/NGWR = Working Group/Next Generation Weather Radar
 WSFO = Weather Service Forecast Office
 WSR-57 = Weather Surveillance Radar, original contract 1957, 10 cm
 WSR-74C = Weather Surveillance Radar, original contract 1974, 5.5 cm

WSR-74S = Weather Surveillance Radar, original contract 1974, 10 cm
WWV = Call letters for National Bureau of Standards radio station
giving correct time

LIST OF SYMBOLS

| | | |
|------------|---|-------------------------------------|
| r_a | = | Unambiguous range |
| v_a | = | Unambiguous velocity |
| σ_v | = | Velocity spectrum width |
| C | = | Velocity of light |
| λ | = | Wavelength |
| T_s | = | Pulse repetition time |
| Z | = | Radar reflectivity factor |
| Z_{th} | = | Threshold radar reflectivity factor |



JOINT DOPPLER OPERATIONAL PROJECT (JDOP)
FINAL REPORT: 1976-1978

ABSTRACT

Results of operational tests by the Joint Doppler Operational Project during 1977 and 1978 illustrate the marked improvement Doppler radar offers for early accurate identification of thunderstorm hazards, especially tornadoes and squall lines. Design characteristics are given for a Doppler radar system, suggested as a next generation weather radar system, to meet the integrated requirements of the NOAA National Weather Service, U. S. Air Force Air Weather Service, and Federal Aviation Administration.

INTRODUCTION AND CHRONOLOGY

The relative strengths of thunderstorms can be measured by the well-calibrated weather radars in use today. When used in a meteorological analysis of the convective potential of the airmass, such as that produced routinely by the National Severe Storms Forecast Center, radar data pinpoint probable locations of hail and dangerously heavy rain, and form patterns indicative of damaging winds and tornadoes. However, the WSR-57 and FPS-77 weather radars now used in the National Radar Network measure only reflectivity, and accurate and dependable diagnosis of damaging winds and tornadoes is not routinely possible. Major tornadoes are not dependably revealed by spiral patterns in the precipitation echoes and, by the time of radar detection, are already doing damage. They can be seen with the WSR-57 radar only at relatively short range (< 100 km).

Doppler radars with narrow beams are sensitive to precipitation motion, and enthusiasts have long thought that use of Doppler radar could improve tornado and severe thunderstorm warning. After research findings showing tornado-related signatures in Doppler radar data were published (Donaldson, 1970; Brown, 1973; Burgess, 1975) leading scientists in the field of radar meteorology (e.g., Atlas, 1976) avidly endorsed a field experiment to test Doppler radar for detecting tornadoes operationally, with the hope of developing a better system of weather forecasting.

To be better than present systems, a radar system must provide routine observations like those of today's national radar network and also provide detailed diagnostic data on local storms for warnings of incipient tornadoes and tornado-like winds, large hail, and dangerous turbulence.

In the light of newly recognized Doppler capability, staff from Environmental Research Laboratory Headquarters and from NSSL and National Weather Service Headquarters, in September 1976, discussed merits and limitations of modifying existing NWS radars. The 15 participating engineers and meteorologists proposed a cooperative project to evaluate real-time Doppler capabilities for identifying tornadic storms by operational tests to verify research

findings and to identify specifications for a next-generation radar (NEXRAD). The result was an informal agreement between ERL and NWS to conduct a cooperative program, the Joint Doppler Operational Project, for operational test of Doppler radar. (The agreement was formalized in October 1977.)

The Air Weather Service, which was contemplating procuring a Doppler radar system for the Air Force, joined NOAA and expanded the project to include AWS objectives. The Air Force Geophysics Laboratory (AFGL) also helped plan the joint project since for several years it has supported the AWS plan to study Doppler radar technology to improve weather radar for military operations. By December 1976, a plan was set up to use the experimental Doppler facilities at NSSL and mobile data processing facilities from AFGL for a test operation. Participation by several agencies has brought both direct and indirect contributions to the program from many persons.

Table 1 shows how the 2-year project progressed. During the 90-day period from January to April 1977, NWS and AFGL engineers put together the radar system composed of the NSSL Doppler radar as nucleus, digital memory and processing for color display, and interactive control and storage for playback. At the same time, staffing and training of personnel started (including operational and research meteorologists and engineers), and operating procedures were designated. On May 5, 1977, the display system on the NSSL radar was installed, training was complete, and routine surveillance of storms started. The JDOP operational tests shared the NSSL facility with the ongoing program of severe storms research. Remarkable Doppler capabilities were clearly indicated during JDOP's first 30 days, in spite of limitations imposed by coordination with research activities. Most of the severe storms in Texas and Oklahoma monitored in April and May 1977 were large and tall, easily seen by the narrow-beam NSSL radar, with mesocyclones detected sometimes at ranges of 350 km. Consequently, several advisories were issued to distant Weather Service offices at Fort Worth and Amarillo, Tex. On 20 May, a tornado advisory was issued to Altus Air Force Base (range 195 km) 25 minutes before a tornado occurred that caused substantial damage.

On May 4, 1977, at a special meeting of Agency representatives, a review of the first month's operation revealed that severe-storm advisories issued because of Doppler data were consistently many minutes ahead of warnings resulting from conventional WSR-57 radar data. A mesocyclone occurred near Wichita Falls, Tex. during the meeting, and participants viewed its radar signature in real time.

A conflict of missions occurred on May 20, when several very severe storms developed in central Oklahoma. The NSSL R&D program required multiple Doppler coordinated sector scans (using NSSL's two radars and two other radars in unison). This prevented the JDOP team from controlled surveillance of all storms and delayed recognition of a nearby circulation that passed over Norman moments before initial tornado touchdown at Del City, Okla. Fortunately the meteorologists using the AFGL color display at NSSL's Cimarron radar monitored the mesocyclone in this storm (Bjerkaas and Donaldson, 1978. See also report of first year's operation in Burgess, et al. 1978.) A similar tornado-producing storm occurred in 1978 when JDOP was sole user of the radar, and advisories were greatly improved. Both cases are being studied to determine the best procedures to follow when several severe storms occur simultaneously.

TABLE 1. Project Progress

| | |
|---|-----------------|
| Conception and planning | Oct - Nov 1976 |
| Modification to NSSL radar and requisition of color display | Jan - Feb 1977 |
| Development of NSSL Ling computer software and color display software | Feb - Mar 1977 |
| Assignment and training of NWS and AWS meteorologists | Feb - Apr 1977 |
| Operations | Apr - Jun 1977 |
| Analysis of Doppler advisories and preparation of report on first year's progress | Jun - Sep 1977 |
| First year evaluation and second year planning | October 1977 |
| Advancement of color display control and preparation for AFGL display system | Nov 77-Mar 1978 |
| Assignment and training of new NWS and AWS meteorologists | Feb - Apr 1978 |
| Completion of engineering modifications to provide dual PRF and installation of AFGL color displays | Mar - Apr 1978 |
| Operations | Apr - Jun 1978 |
| Analysis of advisories and completion of radar design specifications | Jul - Sep 1978 |
| Program review | October 1978 |

Occasional small but damaging tornadoes occurred without mesocyclones and allowed no opportunity for advisories. This lesser type of storm is being studied further. If all storms are considered statistically equal, the Doppler radar advisories show significantly better lead times than those from conventional radar.

In 1977, the two displays (Fig. 1a) used by JDOP meteorologists provided a PPI contoured display of all storms within range, and an expanded view of the internal structure of reflectivity and velocity (wind shear) within each storm that seemed likely to be severe. The first display is analogous to current NWS contoured PPI displays of reflectivity except that radial velocity and standard deviation also may be selected, and the contours are presented in color on a refreshed (non-fading) computer-driven terminal. The second display provides totally new information (Burgess *et al.*, 1976). The two displays are interactive, requiring the meteorologist to view three-dimensional data selectively and then to deduce significance from the vertical distribution of reflectivity and velocity signatures.

Before the second phase of the test began in 1978, the experiment gained support of the Systems Research Division of the Federal Aviation Administration. This resulted from recognition of contributions to aviation safety which Doppler radar is likely to make.

During the 1978 tests, the JDOP meteorologists used four new color displays developed by AFGL (Fig. 1b). Three of the displays provided Doppler contours with high clarity and resolution for direction of research aircraft and related high-precision activities. The fourth AFGL display provided a real-time summary of locations, tracks, and extrapolated positions of selected storms, which were valuable to JDOP forecasters.

Following the 1978 tests, JDOP data was organized and summarized for presentation to management officials in the participating agencies, and plans were made to begin the complex process of procuring a new national radar system to supplant the multiplicity of systems now in use. Gradually, JDOP will fade and NEXRAD will become more prominent.

Part I of this report describes JDOP operating procedures, hardware, staffing, and meteorological data recorded. The information is being used to establish the design and performance criteria for NEXRAD and to plan 1979 efforts to develop Doppler sampling techniques that could identify signatures of strong straight-line winds and improve detection of turbulence. Part II discusses Doppler radar technology from the engineer's viewpoint and provides a beginning to preparation of NEXRAD specifications. The Appendices present discussion of data display systems, and plans for Doppler tests in 1979.

Special briefings on JDOP for television meteorologists as well as slide presentations have been conducted at forecast offices. Public Information Offices in the Air Weather Service and Environmental Research Laboratories prepared film and video tape "snapshots" of the Project. These valuable supplements to this report are available from those offices.

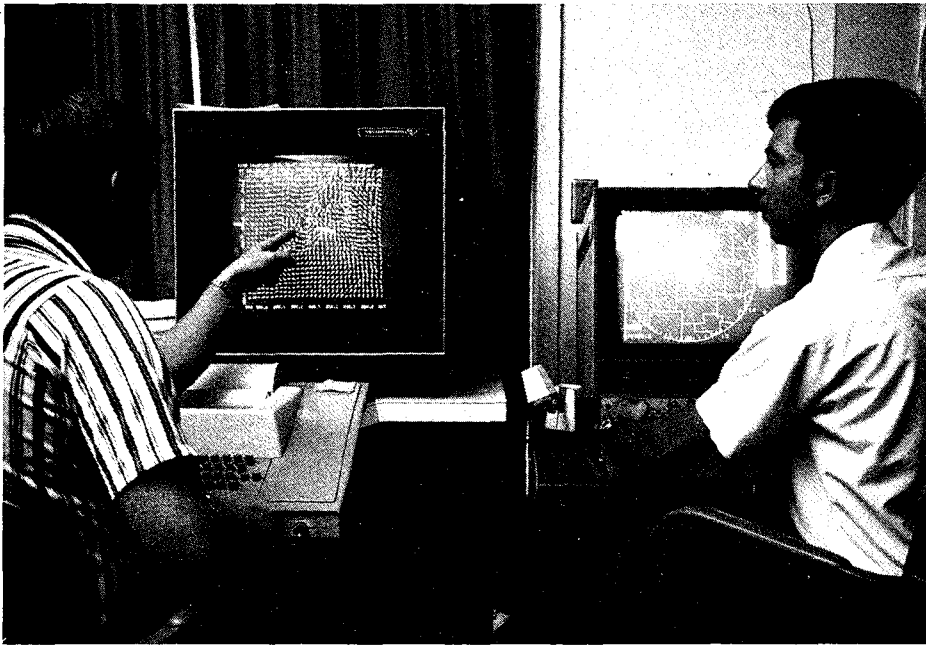


Figure 1. Displays used by project meteorologists. NOAA color display (top right) and NSSL multimoment display (top left) were used with the AFGL displays (bottom) to locate reflectivity and velocity signatures.



PART I

METEOROLOGICAL APPLICATIONS

Prepared by

Don Burgess, Ralph J. Donaldson,
Tom Sieland and John Hinkelman

1. DOPPLER METHODOLOGY

1.1 Real-Time Signature Recognition and Severe Storm Diagnosis

Pulse Doppler radar measures the radial component of motion (i.e., motion parallel to the radar beam) and it is blind to motions perpendicular to the beam. The radial component data readily yield unique signatures for mesocyclones (small intense rotating wind systems) and sometimes the even smaller and more intense tornadoes themselves.

When a mesocyclone much larger than the beam volume is scanned, a characteristic velocity pattern appears, a couplet indicated by azimuthally close and markedly different magnitudes of radial speed. This signature appears because the flow around the circulation is nearly perpendicular to the radar beam that passes through the circulation center. Closed velocity contours (isodops) appear at the radii of maximum wind where the radar beam parallels the swirling flow. The presence of convergence (divergence) rotates or skews the pattern clockwise (counterclockwise) relative to the radial line from the radar to the circulation center.

On the velocity display, mesocyclone signatures are easily recognizable and maintain vertical continuity throughout the storm's lowest 5 to 10 km. Although numerous regions of cyclonic shear appear in severe storms, not all identify mesocyclones. Thus, objective criteria are used to distinguish between shear without significant swirl and a swirling vortex. Initial mesocyclone recognition rules proposed by Donaldson (1970) have been modified as follows into three steps for operational use:

Step 1. Significant azimuthal shear must exist between closed isodops of opposite sign.

When searching for shear, the radar collects data with antenna elevation angles intercepting storm midlevels (3-7 km AGL). Mesocyclone shear is first detected at midlevels and extends downward to the surface with time. Significant shear is defined as $5 \times 10^{-3} \text{ s}^{-1}$ inside 230 km and $1 \times 10^{-3} \text{ s}^{-1}$ beyond 230 km. The shear must be contained between centers of closed isodops with as much as 45° skew between centers permitted. Storm motion component must be removed to obtain closed isodops of opposite sign.

Step 2. Shear pattern and closed isodops must extend vertically for a height interval comparable with horizontal diameter.

To be comparable, the vertical extent can be as small as 50% of the horizontal diameter but never can the vertical extent be less than 3 km. This criterion should be satisfied by collecting of tilt sequence data with vertical resolution of 1 km wherever possible. If storms are randomly distributed inside 230 km, a proposed elevation angle sequence is 1/2°, 1°, 2°, 4°, 8° and 16°.

Step 3. Shear pattern and closed isodops should persist for half the period required for vortex revolution.

The persistence scale (γ_p) is defined by:

$$\gamma_p = \frac{\pi R \Delta\beta}{V_2 - V_1} ,$$

where $\Delta\beta$ = the angular distance in radians between velocity maxima,

R = range in meters,

$V_2 - V_1$ = the velocity difference in meters per second between velocity peaks.

During the time required to satisfy the persistence scale (300 to 1500 s, or 5 to 15 min), early recognition may be achieved if the vertical extent of step 2 is large (6000 m; i.e., 6 km or greater).

Anomalous, isolated large shears with vertical continuity have been detected by single Doppler radars at the location of intense tornadoes and labeled as Tornadic Vortex Signatures (TVS) by Brown and Lemon (1976). These shears, believed to represent the tornadic winds filtered by the beam, are observed only with narrow beamwidth radars and not during all tornadoes. Objective criteria for defining a TVS have not yet been established. The following tentative guidelines were used during JDOP:

The velocity difference should be greater than 30 m s^{-1} across azimuthally adjacent sample volumes separated by 1° or less. This implies shear of about $5 \times 10^{-2} \text{ s}^{-1}$ at observation ranges ($10 > 130 \text{ km}$).

The anomalous shear should have a range extent less than 1 km.

The anomalous shear should extend a few kilometers in the vertical.

The anomalous shear should persist for at least 10 min.

Advisories for these two signatures (mesocyclone and TVS) and wind observations in the lowest km greater than 25 m s^{-1} could be phoned to the Oklahoma City Weather Service Forecast Office (WSFO) or military bases. In the usual procedure, one operator viewed the full coverage range (230-km) reflectivity field. When he observed significant echoes, he passed their coordinates to a second operator who displayed the storm on the graphics display and noted velocity magnitude and shear.* If he observed significant shear he recorded it on a log sheet. Data from the log were used to test for vertical and time continuity. During tilt sequences, the color display operator recalled the lowest elevation velocity data to check magnitude. Strong straight winds were found to be larger in scale than the mesocyclone and could be recognized with coarse resolution.

When the decision was made to issue an advisory, the time was noted and a tape-recorded telephone call was made to the appropriate agency. An excerpt from the transcript of one recorded call illustrates such a communication:

1547 CST 19 May 1977

Station: OK, Don, go ahead.

Devore: OK, Fred, we've got two cells that would be VIP 6 or greater. One of them is 6 miles WNW of Lindsay, the other one is 10 miles E of Duncan. That cell east of Duncan has a little bit of shear--it's the strongest one of all. No mesocyclone yet, but if you don't have a warning there, you might want to issue one.

Station: OK, if you see a mesocyclone, give us a call.

1631 CST 19 May 1977

Devore: We have a circulation that is winding up rapidly. It's a mesocyclone that's NE of Duncan near Purdy. Have you got a warning out?

Station: Yeah, Don, I was getting ready to update it.

Devore: Right, you might consider--we don't have a TVS-- but it's winding up so you might want to put out a tornado warning.

(note. Three tornadoes occurred between 1630 and 1730.)

With NWS staff we discussed methods of notifying the Oklahoma City (OKC) forecaster of signatures and of controlling the type of storm information available at the Doppler radar site. Storm reports from NSSL storm intercept teams in the field and NWS teletype messages filtered to the Doppler team

*Display facilities are discussed in Section 3 and in Appendix A.

from the other NSSL scientists involved in the research program. (See, for example, Wilk et al., 1976.)

The Doppler team was isolated initially to prevent "feed back" information which might complicate later evaluation of the velocity signatures. As the program developed, those directly involved at the Radar Facility noticed that close coordination with the OKC forecaster is needed for a viable new system to develop in an orderly way from the present storm detection and warning system. In the first few storm days, the reactions to telephone advisories to OKC of mesocyclone locations were mixed: in some cases tornado warnings were issued, in other cases, severe thunderstorm warnings were issued, and in a few cases, no action was taken. In retrospect it is not clear why this differentiation occurred except that the duty forecaster reacted according to his subjective evaluation of all data available to him on each occasion. Even though a lengthy seminar was held with the forecasters at OKC, the advisories alone, without discussion of reflectivity, storm height, etc., were obviously difficult to link quickly to other observations available at the OKC WSFO. Thus, the reactions to the advisories were varied.

In May and June of 1977 and all of 1978, the limitations in discussions between Doppler Facility and WSFO staffs were relaxed, and they were encouraged to agree on each storm's reflectivity, height, motion, and probable severity.

1.2 Implications of Doppler Radar for Turbulence Detection and Warning

Doppler radar potential is explored further in aviation experiments related to the FAA portion of JDOP. The JDOP experiment involved the use of an Air Force Systems Command F-4-C jet aircraft equipped to measure wind and turbulence simultaneously in situ with the Doppler radar data collection (Lee, 1977).

The aircraft was tracked by its transponder signal which was mixed electronically into the WSR-57 10-cm weather radar system and displayed simultaneously with contours of radar echo reflectivity. This display provides a position every 20 s, and is photographically recorded. For analysis, straight line interpolation is used between each recorded position. WWV time signals help coordinate aircraft, weather radar, Doppler radar, and voice data. Aircraft data are recorded 50 times each second, and a five-point smoothed average provides 1.0 s values for computation of true vertical velocities (w) and, as a measure of turbulence, derived gust velocities (U_{de}) (Houbolt, et al., 1964). During 1975 and 1976, flight data confirmed the association identified in the mid-1960's; i.e., moderate or greater turbulence is expected somewhere in a storm when the maximum reflectivity factor of the storm is 40 dBZ or more.

Besides reflectivity, other radar associated parameters were considered during the 1975-76 pre-JDOP program, and typical time-history is shown in Fig. 2. Maximum derived gust velocities (turbulence) recorded by the aircraft during each 5 s (approximately 1 km) of flight are shown with the corresponding

(in time and space) Doppler radar observations. The turbulence trend matches the trend in the spectrum width plot; 45 penetrations were analyzed and all show a similar relationship. During these 45 penetrations there were 76 occurrences of moderate or greater turbulence and ninety-five percent had spectrum widths $\geq 4.0 \text{ m s}^{-1}$ (Lee, 1977). In analyzing two of the cases when the spectrum width was less than 4 m s^{-1} but the recorded derived gust velocity exceeded 6.1 m s^{-1} , it appears from the recorded aircraft elevator deflection that the derived gust velocity values were influenced by pilot input (i.e., some component of the vertical acceleration was pilot-induced). The spectrum width may at times be biased as discussed in Part II of this report. This means that there are some non-turbulent areas where the spectral width is large. However, in two tornadic storms studied, the cumulative probability of turbulence when the spectrum width is less than 4 m s^{-1} is only about 30% (Doviak et al., 1978). For non-severe storms the probability is even less; only a small portion of even a severe storm will have an "overforecast" condition.

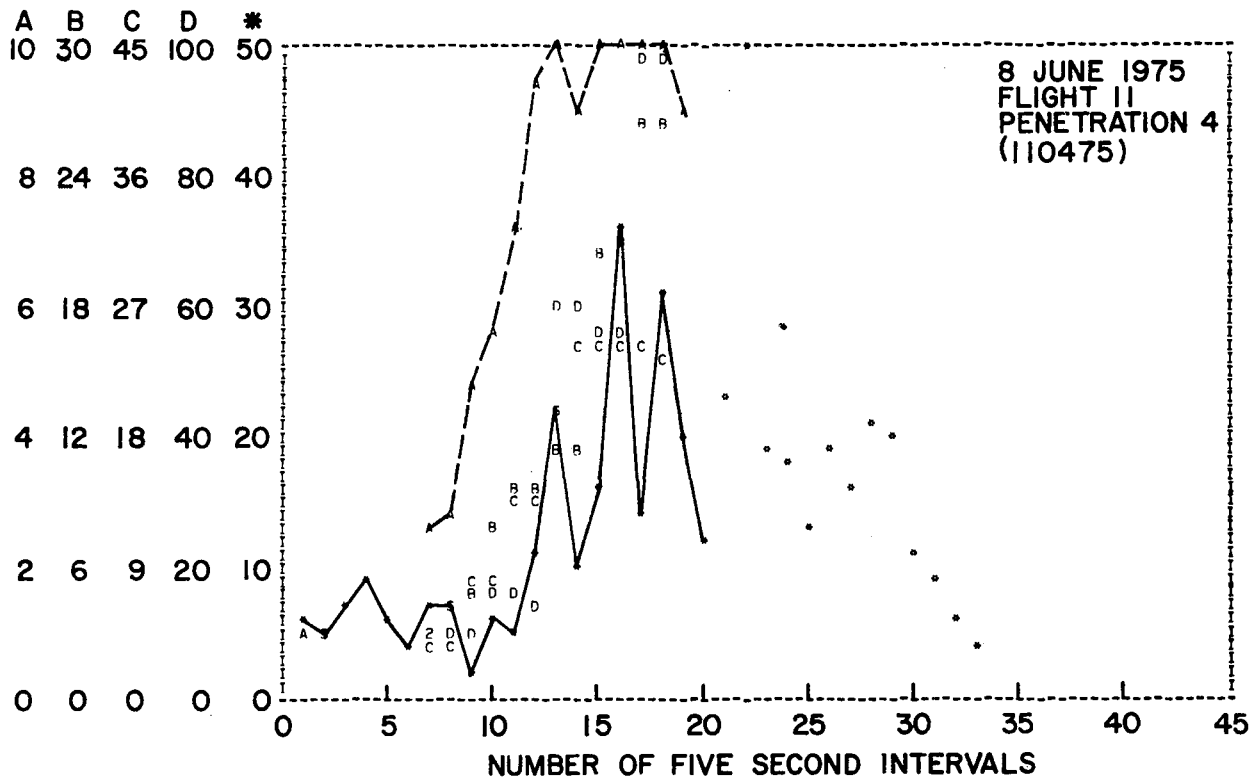


Figure 2. 8 June 1975 penetration 4: Time (space) cross-section for maximum values recorded for each 5 s of flight or corresponding Doppler radar volume during penetration. Derived gust velocity = $\ast(\text{ft s}^{-1})$; spectrum breadth = A (m s^{-1}); velocity gradient = B ($\text{s}^{-1} \times 1000$); gradient of the gradient = C ($\text{s}^{-1} \text{ m}^{-1} \times 1000$). Dashed line connects values of spectrum breadth, and solid line, the derived gust velocities. D = Laplacian; 2 = two data points at the same place.

1.3 Summaries of Illustrative Cases from JDOP Files

Case Summary: 28 June 1977 (squall line with winds)

This case illustrates Doppler radar ability to depict distributions of wind and rain intensity within squall line convection. Fig. 3 photographs show the radar reflectivity, radial velocity, and multimoment Doppler radar displays for June 28, 1977. The squall is just north of Oklahoma City and is moving southeastward. The gust front is very evident in the velocity display and contains particularly high winds in regions not suspected from viewing the reflectivity display. The spectrum width (arrow heads) shows weak turbulence in the gust front. Doppler radar indicated that wind speeds and turbulence were similar to those recorded on the NSSL instrumented KTVY-TV 1500 ft tower as the front went by. This illustrates Doppler radar's potential use in terminal areas for aviation weather advisories and air traffic control.

Case Summary: 5 April 1978 (right-moving tornadic storm)

The automated storm track display provided by the Air Force Geophysics Laboratory (see Section 3.4) was used when a storm in southwest Oklahoma became right-moving as it started producing tornadoes. The Doppler-derived, precise position of severe phenomena, when combined with an accurate motion forecast, provides the best possible warning.

A tornado advisory based on a TVS south of Lawton, Okla. (Fig. 4), was issued at 1945 CST. The resulting NWS tornado warning combined this with an unverified public report of a tornado northeast of Ft. Sill. The warning indicated a tornado (T in Fig. 4) at the northeast edge of the military reservation, moving northeast, the same movement direction as other cells previously detected. At NSSL, a check of the AFGL echo track display revealed an eastward storm motion (Fig. 5). Therefore, an update to OKC was issued at 2000 that redefined the correct position of the mesocyclone (near Pumpkin Center, Okla.) and new direction of movement.

A wide tornado touched down at 1956, passed Pumpkin Center just after 2000 and dissipated near 2010. Eleven homes, 5 trailer houses, and 21 barns were damaged or destroyed. Although the initial NWS warning (with county boundaries) covered the area of damage, residents complained of no specific warning because the tornado location and movement were reported earlier well to their north. Such confusion could be alleviated by issuing warnings to smaller areas defined by Doppler radar.

A second tornado formed just southeast of Marlow, Okla. at 2024. It damaged four lake cabins and a church before destroying the farm house of the Byrd family. The Byrds reported that they went to their storm cellar because of the second NWS tornado warning that placed the tornado at Pumpkin Center, moving east.

Doppler analysis (Fig. 4) shows two TVS's rotating around the mesocyclone but offset as much as 10 km south of center. The mesocyclone center moved to

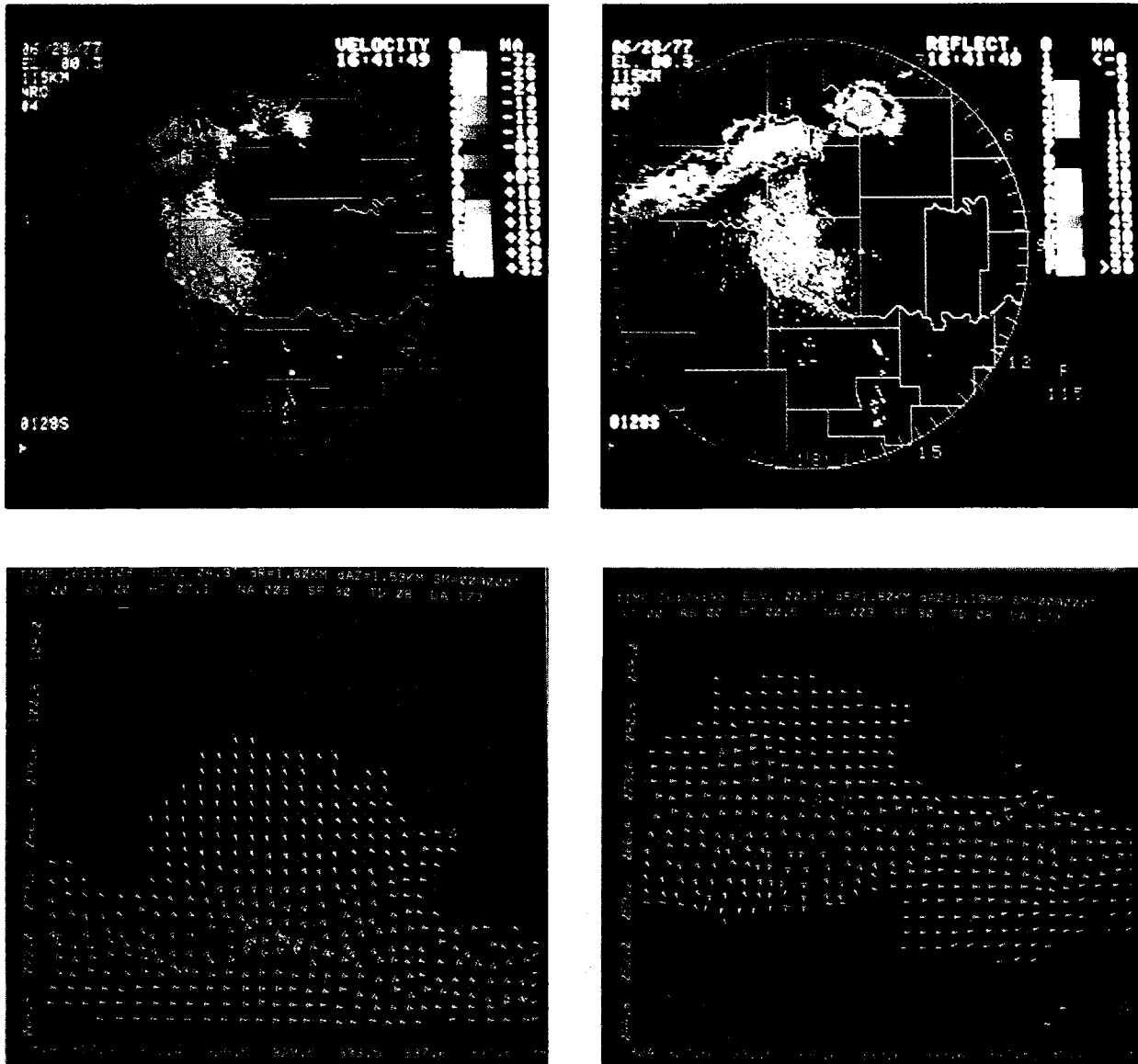


Figure 3. PPI displays of velocity (upper left) and reflectivity (upper right) during squall line of 28 June 1977, as gust front forms northwest of display center. Multimoment "window" view of gust front cell shows start of the downdraft aloft (lower left) that reached the ground (lower right) 15 min later as a strong gust front. The multimoment display is described in Section 3.3.

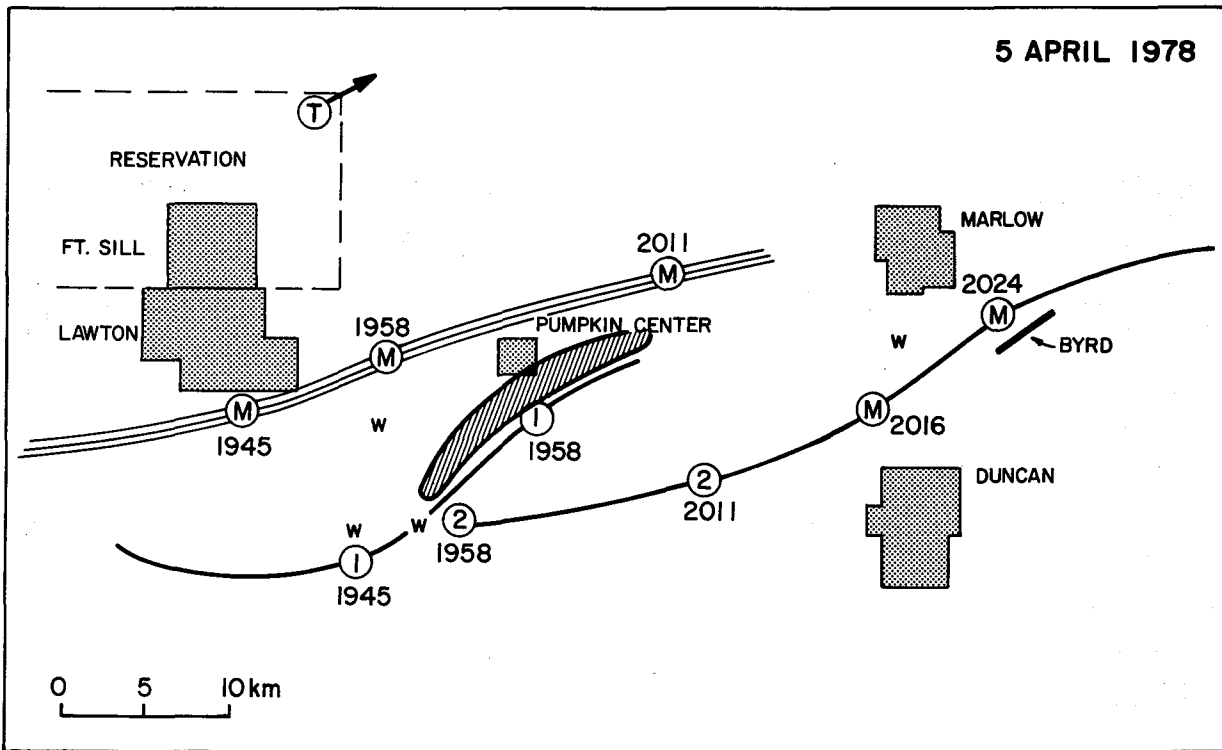


Figure 4. Track of 5 April 1978 mesocyclone (M) and two TVS's (1) and (2). Times are CST. Pumpkin Center tornado damage path is hatched and Marlow tornado is thick line. The circled "T" indicates tornado position given in NWS warning and W's are straight wind damage.

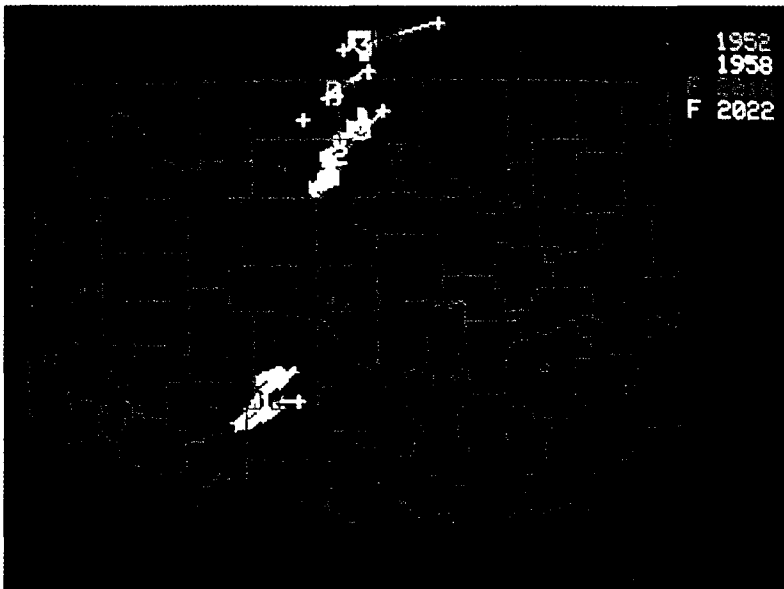


Figure 5. Echo track from AFGL system valid at 1958 CST on 5 April 1978. Bright areas are current (1948 CST) locations with color coded "plus" marks indicating past and forecast locations.

location TVS(2) before the Marlow tornado. The mesocyclone was tracked eastward until 2200. Several reports of funnel clouds, damaging straight wind and large hail verified its continued severity.

Case Summary: 18 April 1977 and 5 April, 17 April and 11 May 1978
(Unforecast tornadoes)

The lesson of this case is knowledge of the broad range of vortices which fit the current definition for tornado. Although most tornadoes, and apparently all maxi-tornadoes, are accompanied by mesocyclones, some small tornadoes are not. It is probably not feasible to design an operational radar to detect these small and ephemeral phenomena.

Several non-damaging tornadoes and funnel clouds occurred on 18 April 1977. No shears were detected by Dopplers in the rainshowers across Oklahoma. The synoptic environment included warm ground and a cold-core low pressure area aloft. Severe thunderstorm potential was not indicated. The vortex formation mechanism may be similar to that of waterspouts and these phenomena over land are called cold air funnels (Cooley, 1978).

Unforecast, small-scale tornadoes that produced damage developed under similar conditions and in nearly the same manner on three different days. On 5 April 1978 (Lone Wolf storm) and 11 May 1978 (Braman storm) single condensation funnels were reported. On 17 April 1978 four closely-spaced tornadoes were reported simultaneously beneath the same cloud (Newkirk storm). All these funnel clouds and tornadoes occurred during the developmental stages of the storm systems at the time of initial rapid growth of echoes on radar. One tornado (Lone Wolf) formed five min before first radar echo (Fig. 6). None of the storm's radar echoes indicated severe weather and no supercell characteristics were observed at tornado time. Storm environments indicated severe potential with substantial thermal instability, strong tropospheric wind ($50-75 \text{ m s}^{-1}$ jet stream), and extreme vertical wind shears ($5-7 \times 10^{-3} \text{ s}^{-1}$).

Post analysis confirms lack of mesocyclone signatures before, during, or immediately after the unforecast tornadoes. However, all the storm systems cited above produced mesocyclones during later mature stages and associated tornadoes were then correctly forecast. Thus early during the Braman storm (Fig. 7, right side), strong shear was absent on the mesoscale, though present on the microscale. This contrasts with the Piedmont storm (Fig. 7, left side) which contained a strong mesocyclone during development of a maxi-tornado (see a later case summary). Maximum observed shears range from $1 \times 10^{-2} \text{ s}^{-1}$ for the Braman case to $5 \times 10^{-2} \text{ s}^{-1}$ for the incipient Piedmont tornado. With the 1-2 km resolution of the real-time displays, it is apparent why warning was possible for the Piedmont storm and no warning was possible for the Lone Wolf, Newkirk and Braman storms.

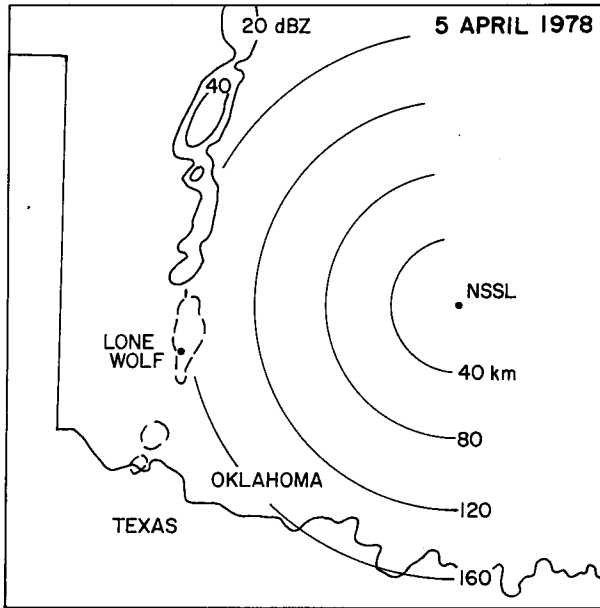


Figure 6. Radar echoes for 5 April 1978 at 1745 CST (solid lines) and new echoes at 1755 (dashed lines). Tornado was on the ground near Lone Wolf from 1745 until 1755 in conjunction with developing cell.

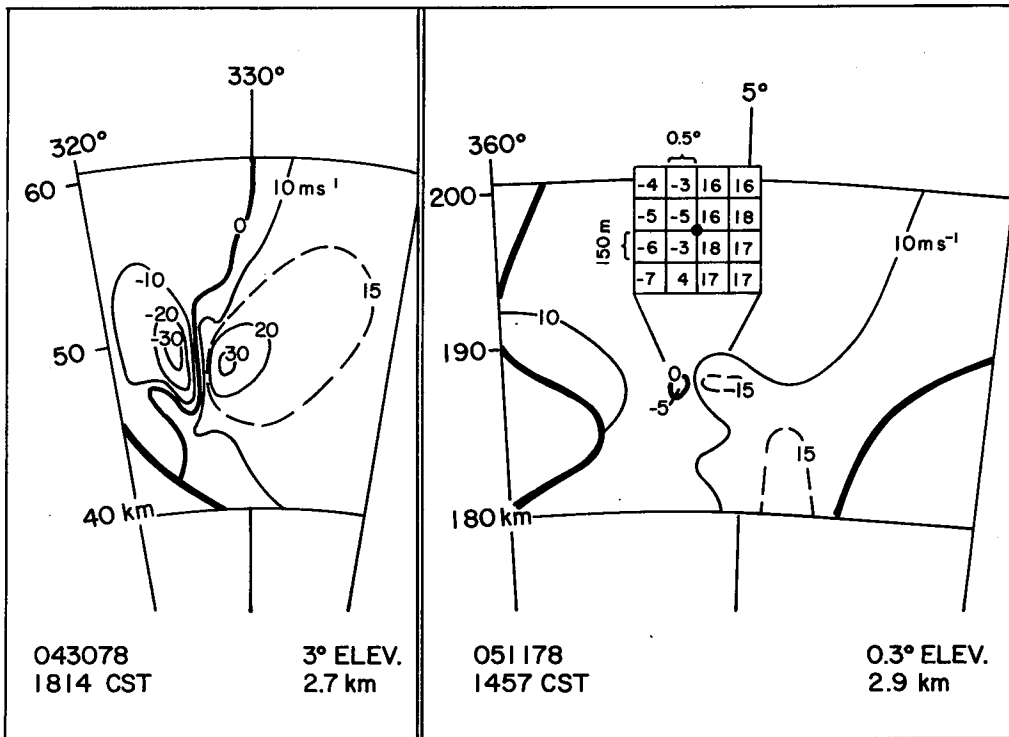


Figure 7. Comparison of different scales for the strong mesocyclone with the Piedmont storm (left) and "micro"-cyclone of the Bramean storm (right). Signature at left allowed for forecast of a maxi-tornado, but the signature at right was too small to be correctly identified in real time.

Scales and perhaps even tornado formation mechanisms obviously differ for the two storm types. Mr. Donald Crow of rural Braman, Okla. an eye witness of the Braman storm, describes the formation and character of a smaller-scale tornado as follows:

I first saw a large (dust devil) whirlwind on the ground southwest of Braman. The whirlwind was moving northeast by east about 1 1/2 miles behind the west edge of the storm cloud. There was no visible connection between the whirlwind and the cloud at this time and no visible funnel.... As long as it (whirlwind) was over wheat it was invisible, until it crossed a dirt road. A small funnel appeared in the cloud approximately 5 miles west and 1 3/4 miles south of Braman.... Then when the whirlwind crossed the dirt road 3 miles west and 1 1/4 south of Braman, it twisted and uprooted trees. From this point on, the funnel and whirlwind were visible but ever changing.... Where I was south of the tornado, there was no rain or hail or wind (before, during or after the tornado). I only heard thunder one time, after the cloud was over Braman. Very strange!

Case Summary: 29 April 1978 (severe hailstorm)

This case shows that Doppler radar can provide new warning information from estimates of updraft speed. The convergence signature at the updraft base (seen at near ranges) and divergence signature at the updraft summit (seen at nearly all ranges) are both used to help identify severe updrafts capable of growing large hail. Doppler radar can determine if the high reflectivities (hail and rain) are associated with dangerous outflows (gust fronts).

The Doppler data collection mode includes antenna tilt sequences, which makes it possible to visualize storm structure (weak echo regions sometimes bounded....WER and BWER) to further elucidate updraft strength. Lemon et al., 1977 have provided a technique to identify WER's by mapping precipitation held aloft at mid-storm levels without any echo at low levels, i.e., the echo overhang on the upwind side of the storm.

The 29 April data set is an excellent illustration of the use of Doppler information to detect and advise of a severe hailstorm near Ada, Okla. which dropped softball-size hail (10 cm or 4 in in diameter). Observation of strong, newly-developed divergence (Fig. 9) and large echo overhang at 1830 CST prompted an advisory for the young storm near Stratford, Okla. (Fig. 8) when reflectivities were only 50 dBZ (VIP 4 to VIP 5).

Damage surveys revealed a continuous swath of hail from Stratford to well southeast of Ada with the largest stones falling in the City of Ada at 1925, doing several million dollars damage. At several locations, the hail-fall was severe enough to strip bark from trees.

Extreme echo overhang (more than 15 km across) and very strong divergence ($7 \times 10^{-3} \text{ s}^{-1}$) were seen with the Doppler at 1925 when maximum reflectivities reached 63 dBZ (VIP 6). The hailswath (and storm motion) turned to

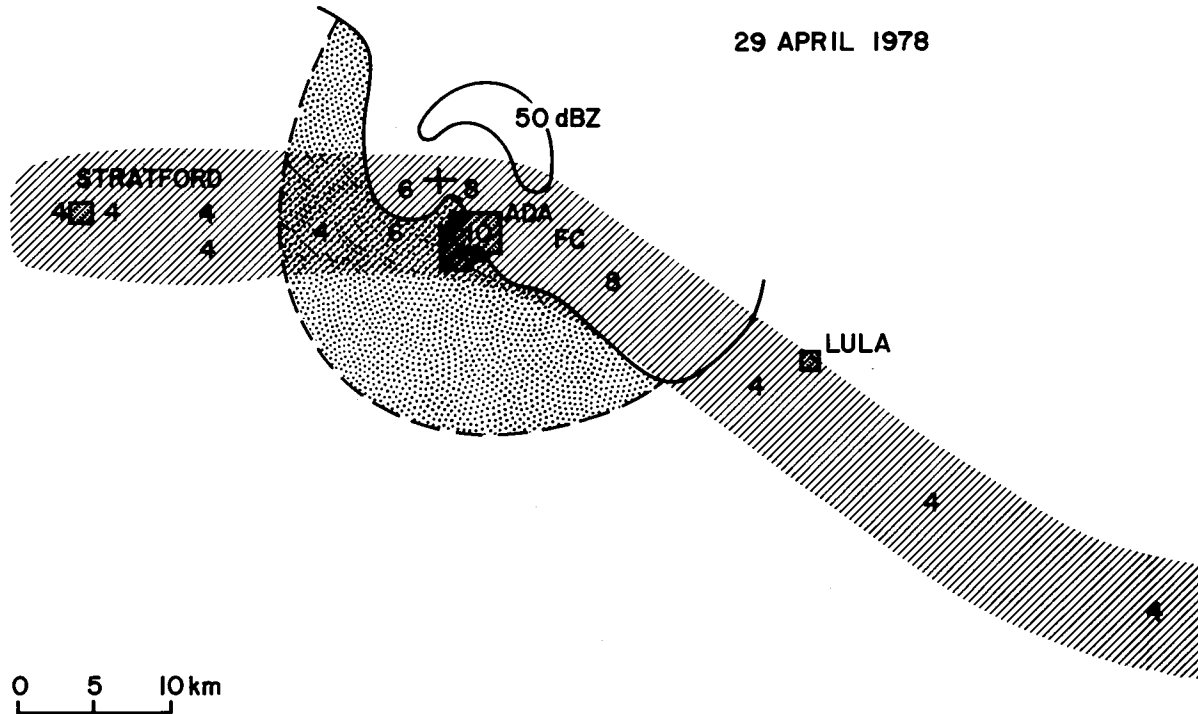


Figure 8. Hail swath for 29 April 1978 (hatched) with low-level radar echo (20 and 50 dBZ), mid-level overhang (stippled) and top position (+) at 1925 CST near time of largest hail at Ada, Oklahoma. Numbers indicate hail size in cm, and FC marks location of funnel cloud.

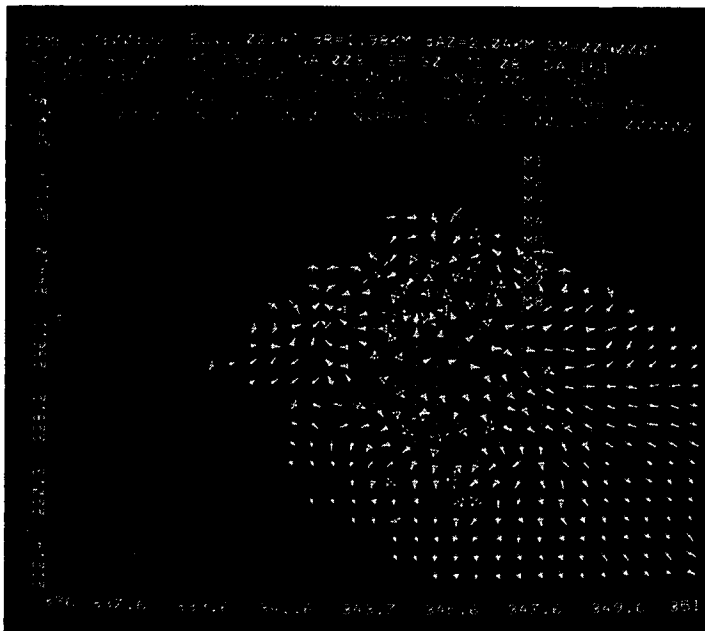


Figure 9. Multimoment view of divergence aloft in the newly developed Ada hail-storm.

right about the time of largest hail. A mesocyclone was confirmed just east of Ada at 1940, and a funnel cloud was observed by NSSL chase teams at 1946. Its turn to the right may be a response to cyclonic rotation within the updraft.

By using the Doppler data, the JDOP forecasters were able to determine that the high reflectivities were not accompanied by strong low-level winds (gust front). Nowhere along the storm's path was there damage other than that produced by hail.

Case Summary: 30 April 1978 (forecast maxi-tornado)

This case illustrates the advantage of Doppler radar in identifying and precisely tracking a maxi-tornado during a widespread outbreak of severe weather. When many storms exist simultaneously, Doppler radar with a narrow beam can be used to diagnose storm potential quickly and accurately.

This day had the only Spring 1978 environment capable of sustaining maxi-tornadoes. A stationary front lay southwest to northeast across Oklahoma with low pressure centered southwest of Oklahoma City. As an upper disturbance approached from the west, severe thunderstorms formed during the afternoon along and north of the front in Oklahoma, Kansas, and the Texas panhandle. Later storms developed along a dryline in northcentral Texas giving the JDOP participants opportunity to collect data during a widespread outbreak with many severe storms within range of the Norman Doppler.

A storm formed 80 km west of Norman about 1630 CST and moved slowly northeast along the front. Significant cyclonic shear, first detected at 1720 (Fig. 10), intensified and lowered toward the surface with time. A tornado advisory based on a mesocyclone with TVS was issued at 1742. The storm's first tornado touched down in El Reno at 1740 (Fig. 11). It consisted of a dust swirl at the ground beneath a short funnel cloud and produced very minor damage. The Doppler data revealed a TVS (T1) aloft south of the mesocyclone center, a second anticyclonic TVS (T2) between T1 and the mesocyclone center (M) where a third TVS was located. Near 1800, three tornadoes were on the ground simultaneously in conjunction with three TVS's. Doppler data strongly indicate that one of the tornadoes was anticyclonic.

About 1810, cyclonic shears near the mesocyclone center intensified (Fig. 10) and a fourth TVS (T3) was identified. This circulation center lowered to the ground and became very strong. A JDOP update of a suspected maxi-tornado just southeast of Piedmont was phoned to the NWS at 1823. The Doppler signature closely fits the path of an intense tornado on the ground from 1820 until 1835. The tornado did F4 intensity damage along a path 2 km wide and nearly 10 km long. Although 15 homes in Piedmont and 10 rural homes were destroyed, no deaths or injuries were reported. Examples of real-time displays during the maxi-tornado can be found in Figs. 12 and 13.

Note the detailed vortex information in Fig. 10 available from Doppler radar. In terms of mesocyclone intensification and maxi-tornado development

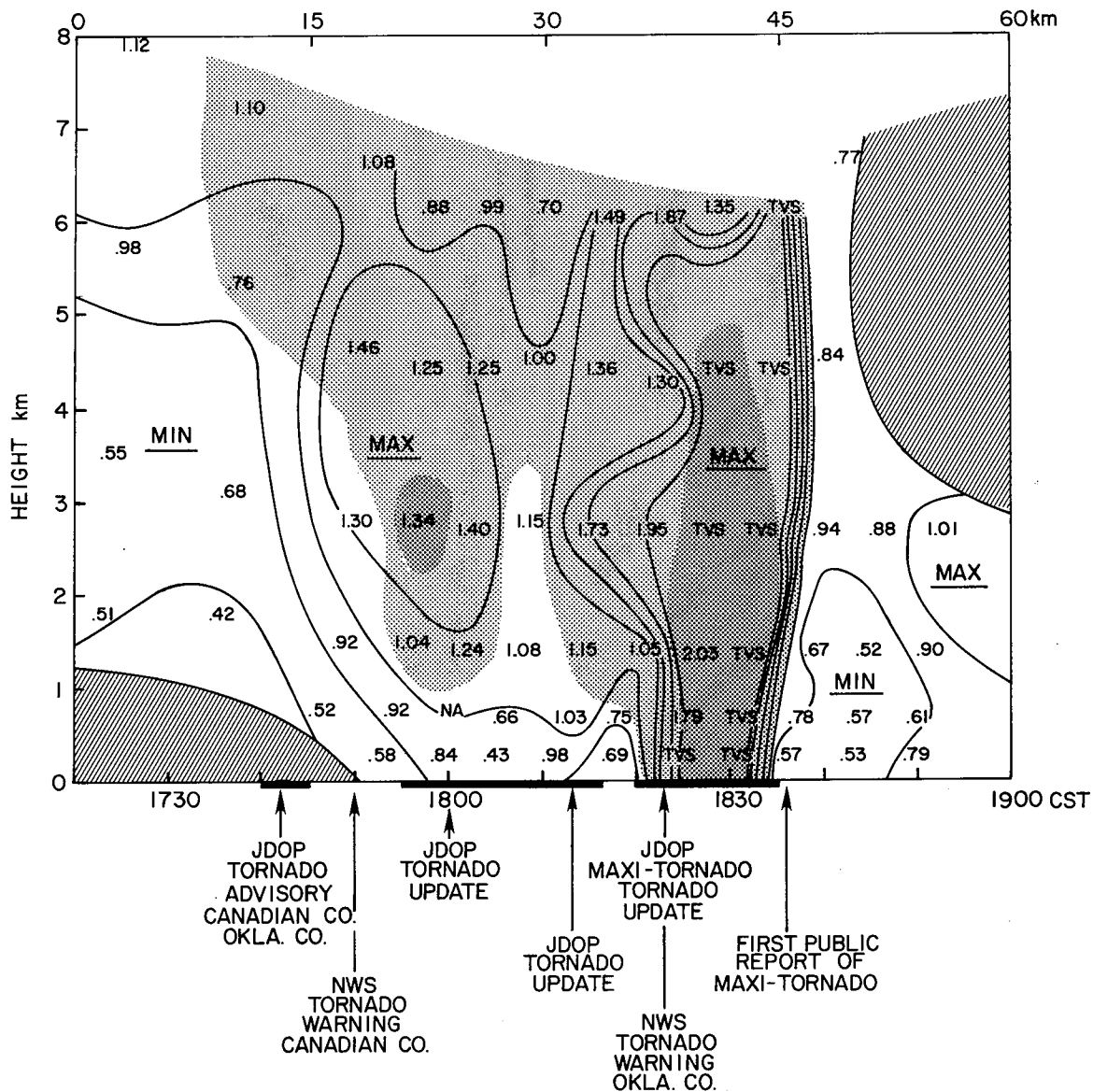


Figure 10. Shear for Piedmont mesocyclone with units of 10^{-2} s^{-1} . Hatched areas indicate no mesocyclone and light and dark stippling indicate presence of TVS and maxi-TV S, respectively. Dark bars along time line show when tornadoes were on the ground. Note descent of strong shear toward ground with time and pronounced weakening of mesocyclone as last tornado dissipates. Letters "TVS" indicate where mesocyclone size shrinks to same order of magnitude as tornado.

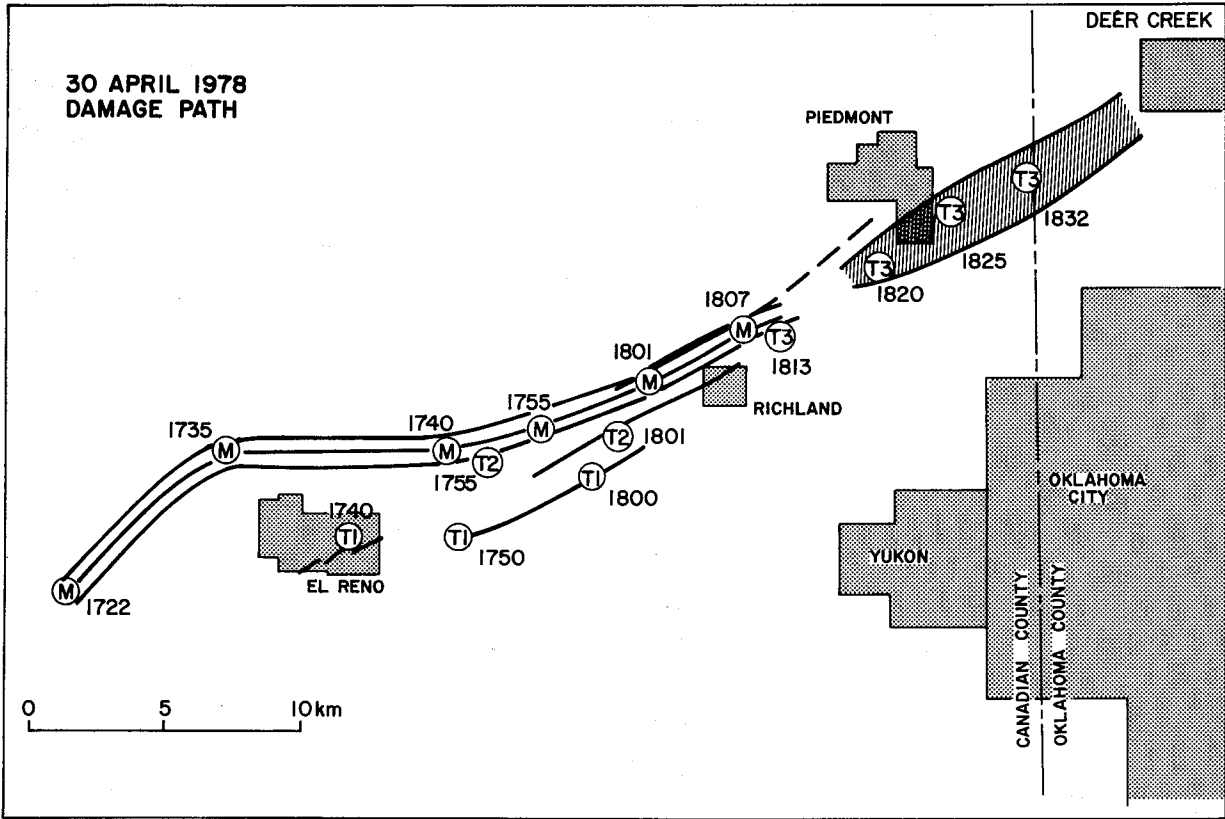


Figure 11. Damage path of 30 April 1978 Piedmont storm. Thin solid lines indicate small tornadoes on the ground and hatched area marks maxi-tornado swath. Mesocyclone center (M) and TVS' (T1, T2, T3) are located from Doppler data used in real time.

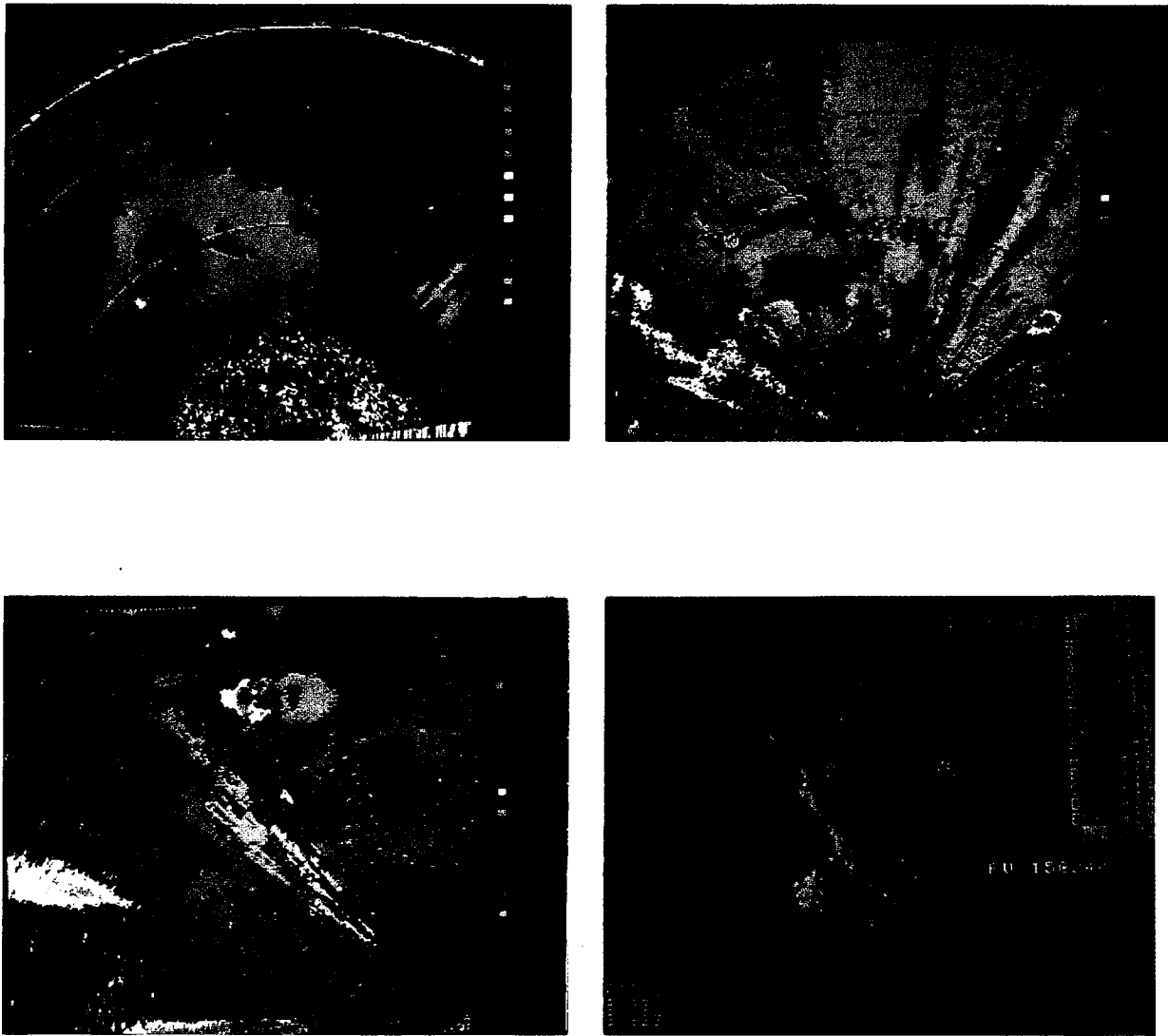


Figure 12. Color displays of the Piedmont storm 30 April 1978. Reflectivity (upper left) and expanded velocity (upper right) during early tornadoes show hook echo and mesocyclone arrows. Expanded velocity (lower left) indicates TVS and full scope velocity (lower right) shows only mesocyclone during maxi-tornado.

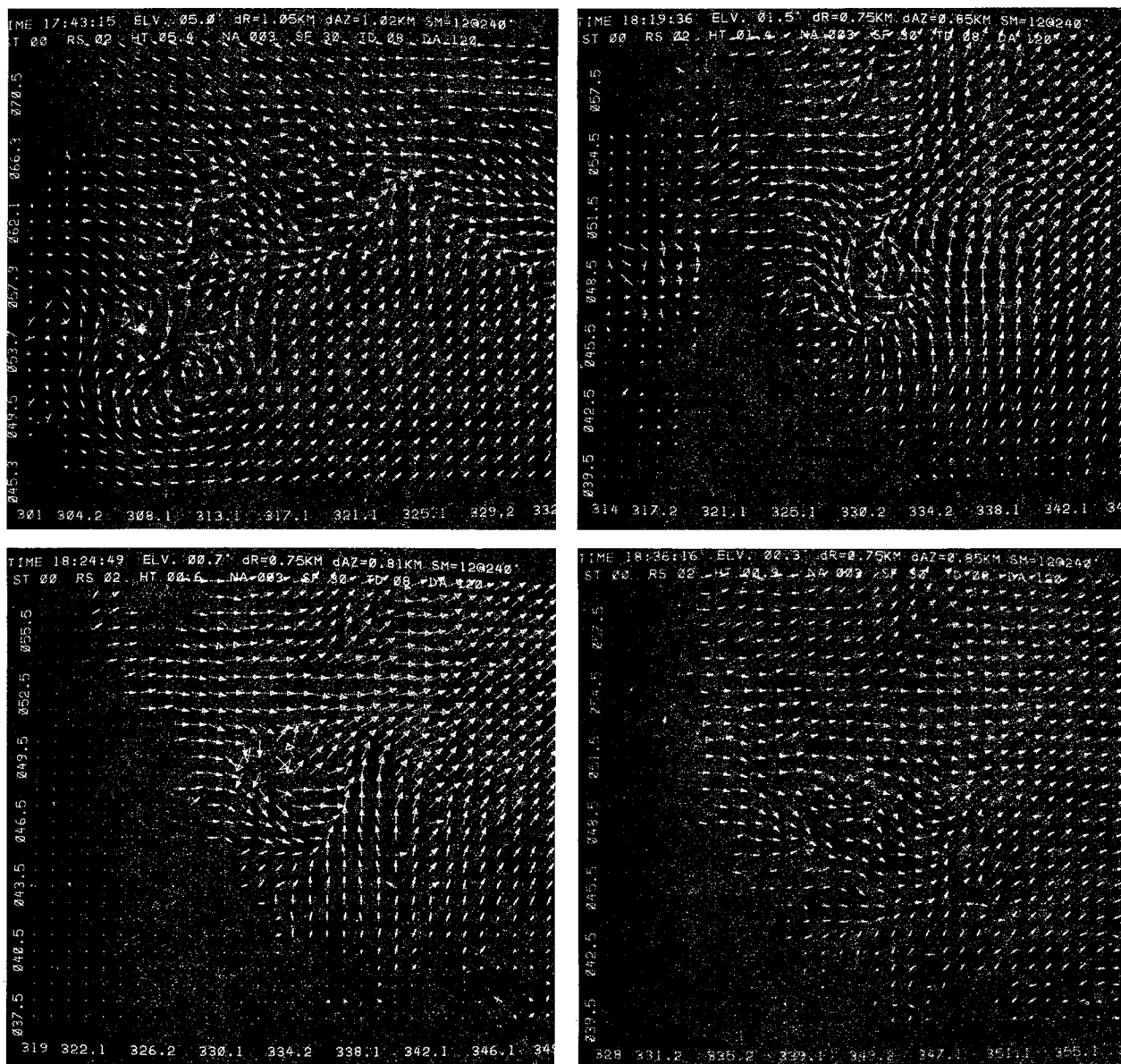


Figure 13. The Piedmont storm as seen on the JDOP multimoment display used in real time for making decisions and locating vortices precisely. Arrows are *not* streamlines; the centers of apparent swirl and locations where arrow directions are highly variable are the places of greatest weather interest. Upper left: High resolution view of developing mesocyclone aloft; upper right: Intensifying low-level mesocyclone; lower left: TVS on ground during maxi-tornado; lower right: Mesocyclone remnants just after tornado dissipation. The multimoment display is described in Section 3.3.

and rapid dissipation, this type of warning input is not available with current radars. Accurate tornado locations (to the nearest km) and warnings with increased emphasis (when maxi-tornado disaster potential is great) are possible with Doppler technology.

Case Summary: 27 May 1978 (Turbulence)

This case illustrates a use of Doppler radar for turbulence detection. Figure 14a, b, and c show the Doppler radar observations of reflectivity mean velocity and spectrum width at approximately 6 km altitude for a storm on May 27, 1978. This storm, in the vicinity of Lawton, Okla. also was penetrated by the F-4-C turbulence research aircraft. Analysis of the aircraft data and pilot comments recorded during the penetrations on an east-west track at 6 km show severe turbulence in the region where the spectrum width is large, thus corroborating the spectrum width indication. These figures also show that for this case the storm's high reflectivity is displaced to the north of the maximum velocity, both of which are west of the broad spectrum width area, illustrating the need to include all three parameters in designing a system for use in air traffic control.

Small scale vortex motion is also a hazard. Burgess (see Section 1.1) found that most severe thunderstorms rotate, and when present the mesocyclone (vortex) extends through a considerable depth. The parent mesocyclone has a characteristic signature readily apparent in the Doppler display. Aircraft should avoid these turbulent areas.

2. 1977-1978 DATA

2.1 General

Advisory operations for National Weather Service and Air Weather Service, with breakdowns by advisory and storm type during 1977 and 1978 are detailed in Tables 2a and 2b and summarized in Table 3. A total of 168 advisories were issued on 49 days: 152 to National Weather Service Offices and 16 to Air Force Bases. Data were collected during 303 hours (but not recorded continuously). In general, three times as many advisories were issued with a threefold increase in storms scanned during spring 1978 as compared to spring 1977. Sharing of the radar between NSSL research experiments and JDOP limited the number of storms scanned and data recorded on tape during spring 1977.

The largest number of severe storms in the primary verification region (Oklahoma City WSFO area of responsibility) occurred in April 1978 and May 1977 with fewer events in May 1978 and almost none in April 1977 or either June. Twenty-eight tornadoes occurred during May 1977 (with an outbreak on 20 May), and fourteen tornadoes occurred in April 1978.

Verification information was collected carefully from standard sources of OKC WSFO severe weather log and newspaper clippings. In addition, data were available from NSSL storm intercept logs, NSSL mesonetwork and hail

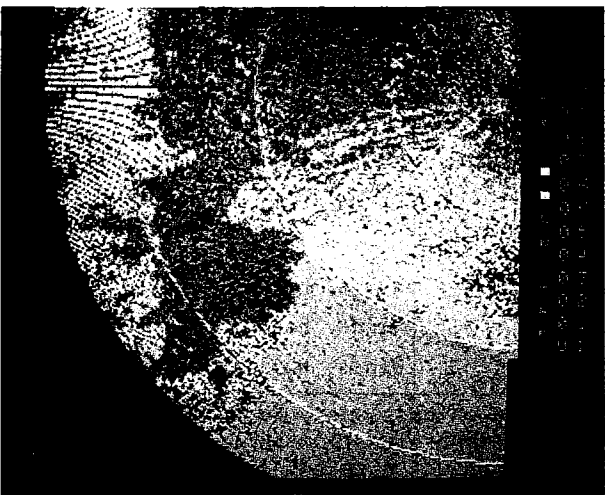


Figure 14. Contoured displays of reflectivity (top left), velocity (top right), and velocity spectral width (left), showing patterns characteristic of severe thunderstorms in Oklahoma. During JDOP these configurations were studied carefully in three dimensions to locate mesocyclones, tornadoes, and regions of very heavy rain and hail for the Oklahoma City WSFO, and to locate areas of turbulence and gust fronts which then were penetrated by the F4-C research aircraft.

Table 2a. Operational Summary for 1977 *

| Date | Time Period (CST) | No. of Tilts | Advisories | | No. of Meso's | Weather |
|----------|-------------------|--------------|------------|-----|---------------|---|
| | | | NWS In | Out | | |
| 1 Apr | 1600-2300 | 8 | | | | |
| 3 Apr | 1544-2342 | 9 | | | | |
| 13 Apr | 1409-1631 | 5 | | | | |
| 14 Apr | 1444-2155 | 10 | | | | |
| 17 Apr | 1538-1835 | 11 | | | | |
| 18 Apr | 1256-1848 | 20 | 1 | 1 | 1 | Cold-air funnels, F1 tornadoes, flash flood, hail |
| 19 Apr | 1431-2318 | 18 | | 3 | 3 | F1 tornadoes |
| 20 Apr | 1439-2156 | 19 | | | | |
| 28 Apr | 1520-2102 | 15 | 2 | | 1 | Hailstorm |
| 29 Apr | 1327-2033 | 18 | | | | |
| 1 May | 1545-2246 | 18 | 2 | 1 | 3 | Hailstorms |
| 3 May | 1629-0004 | 18 | 2 | 1 | 1 | |
| 4 May | 0930-1205 | 7 | | | | |
| 4 May | 1437-1824 | 11 | | 2 | 1 | |
| 5 May** | 1345-2153 | 19 | | | | Winds, hail |
| 9 May | 1253-1732 | 12 | | | | |
| 13 May | 1250-1639 | 7 | | | | |
| 14 May | 1512-0056 | 24 | 4 | 1 | 3 | Winds, hail, funnel cloud |
| 15 May | 1827-2254 | 12 | 3 | | 1 | F4 tornadoes, hail |
| 16 May | 1300-2200 | 22 | 3 | 1 | 2 | F4 tornadoes, hail, winds flash flood |
| 19 May | 1205-2201 | 19 | 5 | | 1 | F2 tornadoes, winds |
| 20 May | 1325-2329 | 17 | 8 | | 2 | F3 tornado outbreak |
| 26 May** | 1100-1812 | 18 | | | | Winds, hail |
| 27 May | 1807-2030 | 6 | 1 | | 1 | Hailstorm |
| 28 May | 1105-2000 | 30 | 1 | | 1 | Winds, hail |
| 30 May | 1500-2330 | 19 | 2 | | | Winds, hail |
| 28 June | 1545-2030 | 8 | 1 | | 1 | Winds, hail |

* Tables 2a and 2b list digital data collected on each operational day. "Tilts" refer to PPI data collected at different antenna elevation angles. The total number of tilts per day is an important measure of data set size. Tilt sequences were more frequent during 1978 when the JDOP held first priority during the Oklahoma observational season. NWS advisories "In" refer to those in the primary verification region (OKC area). Tornado occurrences are accompanied by F-scale intensity (Fujita, 1973).

**There was a failure in the real-time display, hence no advisories were issued.

Table 2b. Operational Summary 1978

| Date | Time Period (CST) | No. of Tilts | Advisories | | | No. of Meso's | Weather |
|--------|------------------------|--------------|------------|-----|----------|---------------|--|
| | | | NWS | | Military | | |
| | | | In | Out | | | |
| 3 Apr | 1415-2053 | 20 | 1 | 3 | | 2 | F1 tornado, hail |
| 5 Apr | 1415-2320 | 29 | 6 | | 3 | 1 | F2 tornadoes (TVS), winds, hail |
| 9 Apr | 1407-2046 | 38 | 5 | | | 2 | Flash flood, winds, hail |
| 17 Apr | 1248-2055 | 24 | 1 | 10 | | 3 | F2 tornadoes, hail |
| 22 Apr | 1355-2100 | 32 | 7 | 2 | 3 | 4 | TVS, funnel, winds, hail |
| 24 Apr | 0945-1156 1409-1740 | 12 | 1 | 1 | | 1 | Hail |
| 28 Apr | 1405-2023 | 18 | | | | | |
| 29 Apr | 1703-2350 | 22 | 5 | | | 1 | Hail, funnel |
| 30 Apr | 1409-01/0115 | 56 | 9 | 5 | 1 | 4 | F4 tornadoes (TVS), funnels, winds, hail |
| 2 May | 0750-1945 | 42 | 1 | 1 | | 1 | Non-severe gust front |
| 6 May | 1510-2335 | 23 | 3 | 1 | | 1 | Hail |
| 10 May | 1215-1630 | 5 | | | | | |
| 11 May | 1325-2147 | 61 | 1 | 12 | 1 | 6 | F2 tornadoes (TVS) funnels, winds, hail |
| 12 May | 1204-1625 | 15 | | 8 | | 4 | F1 tornado, winds, hail |
| 17 May | 1719-2016 | 6 | | 1 | | 1 | Hail |
| 18 May | 1715-19/0056 | 42 | 4 | | 1 | 1 | Hail |
| 19 May | 1251-2018 | 51 | 2 | 1 | | 1 | Squall line, winds, hail |
| 27 May | 1514-2222 | 70 | 10 | | 2 | 1 | Flash flood, funnels (TVS), winds, hail |
| 28 May | 1537-1728 | 4 | | | | | |
| 31 May | 1543-2040 | 10 | | | | | Squall line |
| 1 Jun | 1010-1122 | 37 | | | | | |
| 7 Jun | 1509-1642 | 12 | | | | | |
| 14 Jun | 1504-1700 | 3 | | 1 | | 1 | Windstorm |
| 20 Jun | 1807-2044 | 25 | 2 | | | 1 | Hail |
| 21 Jun | 1200-1300 | 4 | 2 | | | | Squall line, wind, hail (Radar failure) |

Table 3. JDOP Data Summary

| 1977 Summary | | | | | | | | | | | | | |
|--------------|---------|----------------|------|-----------|-------|-----|-------------|------|-------|----------|------|------|-------|
| Days | Data | Advisories | | | | | | | | | | | Mon |
| | | NWS (OKC Area) | | | | | NWS (Other) | | | Military | | | |
| | | Sev. Storm | Tor. | Wind Hail | Meso. | TVS | Sev. Storm | Hail | Meso. | Hail | Wind | Tor. | |
| 11 | 62.5 h | 3 | NA | | 2 | | 4 | NA | 3 | | | | Apr |
| 12 | 108 h | 32 | | 10 | 16 | 6 | 6 | | 6 | 1 | 2 | 2 | May |
| 1 | 5 h | 1 | | 1 | | | | | | | | | Jun |
| 24 | 175.5 h | 36 | | 11 | 18 | 6 | 10 | | 9 | 1 | 2 | 2 | Total |

| 1978 Summary | | | | | | | | | | | | | |
|--------------|---------|----|---|----|----|---|----|---|----|---|---|---|-------|
| 9 | 58 h | 29 | 6 | 14 | 9 | 3 | 21 | 8 | 9 | 1 | 3 | 3 | Apr |
| 11 | 61 h | 20 | 1 | 14 | 3 | 1 | 24 | 1 | 13 | 2 | 2 | - | May |
| 5 | 8.5 h | 4 | - | 2 | 1 | - | 1 | - | 1 | - | - | - | Jun |
| 25 | 127.5 h | 53 | 7 | 30 | 13 | 4 | 46 | 9 | 23 | 3 | 5 | 3 | Total |

| 2 Yr. Summary | | | | | | | | | | | | | |
|---------------|-------|----|----------------|-----------------|----|----|----|----------------|----|---|---|---|---------------|
| 49 | 303 h | 89 | 7 ¹ | 41 ² | 31 | 10 | 56 | 9 ² | 32 | 4 | 7 | 5 | Overall Total |

¹Tornado warnings 1978 only

²Hail warnings 1978 only

reporting network, detailed site surveys by NSSL/NWS/JDOP personnel, extensive telephone surveys of local Civil Defense and law enforcement agencies, and State Agricultural Service reports. Participants believe that the 1977 and 1978 data make up probably the most complete verification list ever documented for severe storms. All tornadoes, but only a fraction (12%) of the severe reports (wind 50 kt, hail 3/4 in) are reproduced in Storm Data, partially because of \$50,000 minimum damage requirement.

The verified severe events were matched with WSFO warnings and Doppler advisories for all severe storms and tornadoes. All events were used for OKC WSFO warning verification and those events occurring during hours of operation (70% of OKC hits, misses and false alarms) were used to verify Doppler advisories. If any event fell into the warning or advisory area and time interval, it was considered a "hit". An event without a warning or advisory was a "miss", and a warning or advisory without events was a "false alarm". By definition, multiple events occurring simultaneously from the same storm were treated as one; if a severe weather event was judged in progress at advisory/ warning issuance time, a "hit" with negative lead time was recorded, but if the event had ceased, a "false alarm" ensued; no severe storm event "miss" was recorded during a tornado warning/advisory "false alarm". Multiple tornadoes occurring during one advisory or warning but distinctly separated in time and space were scored as multiple hits.

Doppler advisories issued during spring 1977 did not differentiate between severe storms (hail and wind) and tornadoes. The only advisory criteria were velocity observations (mesocyclones and strong low-level winds). Advisories for hailstorms were not issued until spring 1978. Data tabulations (Table 4) were used to derive parameters of "probability of detection", "false alarm rate" and "critical success index" displayed in Table 5.

The 1978 JDOP verification was judged representative for severe storms and OKC WSFO tornado warnings but perhaps unrepresentative for NRO DOP tornado advisories because of small sample size. Therefore, it was decided to add 1977 tornado results. In 1977 Doppler advisories were labeled solely as "mesocyclone" and not stratified "severe storm" and "tornado" as during 1978. Using the 1978 format, both data sets were tabulated alike, which led to a combination 1977-78 CSI analysis (Table 6).

The current NWS system has a relatively high POD for tornadoes but it is achieved with extreme FAR. The Doppler does miss some tornado events, apparently not severe tornadoes, but its POD is still good while having a significantly lower FAR. Doppler combined with spotters would probably provide the highest skill scores possible for severe weather warnings.

For events outside the OKC warning area, Storm Data was the verification source. Generally, only mesocyclone advisories were issued at long range. Results for both years (Table 7) are subdivided first using mesocyclones to determine severe or non-severe and, second, tornado or no tornado. Numbers are viewed as "lower limit" since JDOP experience has shown Storm Data fails to report a large percentage of severe events and unsurveyed tornadoes may simply be straight wind damage.

Table 4. JDOP 1977 and 1978 - Advisory/Warning Tabulation

| 1977 Severe Storms + Tornado | | | | | | | | |
|------------------------------|-----|------|-------------|------------------|--------------------------------|------|-------------|-------------------|
| OKC WSFO Warning | | | | | NSSL DOP Advisory ¹ | | | |
| Month | Hit | Miss | False Alarm | Lead Time | Hit | Miss | False Alarm | Lead Time |
| Apr | 3 | 2 | 2 | - | 2 | 1 | - | - |
| May | 45 | 29 | 54 | 0.5 | 15 | 4 | 5 | 23.0 |
| Jun | 5 | 8 | 6 | 1.0 | 1 | 1 | - | - |
| Total | 53 | 39 | 62 | 0.7 ² | 18 | 6 | 5 | 23.0 ² |
| 1978 Severe Storms | | | | | | | | |
| Apr | 25 | 18 | 14 | 11.1 | 29 | 8 | 2 | 14.1 |
| May | 12 | 17 | 13 | 18.7 | 13 | 12 | 7 | 19.7 |
| Jun | 5 | 13 | 1 | 13.8 | 4 | - | - | 8.0 |
| Total | 42 | 48 | 28 | 13.6 | 47 | 20 | 9 | 15.4 |
| 1978 Tornado | | | | | | | | |
| Apr | 8 | 1 | 17 | -1.4 | 5 | 3 | 2 | 19.8 |
| May | 1 | 1 | 9 | -10.0 | - | 1 | 1 | - |
| Jun | - | 1 | 7 | - | - | - | - | - |
| Total | 9 | 3 | 33 | -2.3 | 5 | 4 | 3 | 19.8 |

¹Only those advisories when radar not shared.

²Tornadoes only.

Table 5. JDOP Critical Success Index

X = Forecast severe event which occurs.
 Y = Forecast severe event which doesn't occur.
 Z = Forecast non-severe event which occurs severe.
 LT = Lead time between advisory/warning issuance and event occurrence (min).

$$\text{Probability of Detection (POD)} = \frac{X}{X+Z}$$

$$\text{False Alarm Ratio (FAR)} = \frac{Y}{X+Y}$$

$$\text{Critical Success Index (CSI)} = \frac{X}{X+Y+Z}$$

1977 Severe Storm + Tornado

| OKC WSFO | NSSL Doppler |
|---------------------------|----------------------------|
| POD = .58 | POD = .75 |
| FAR = .54 | FAR = .22 |
| CSI = .34 | CSI = .62 |
| LT = 0.7 ¹ min | LT = 23.0 ¹ min |

1978 Severe Storm

| OKC WSFO | NSSL Doppler |
|---------------|---------------|
| POD = .47 | POD = .70 |
| FAR = .40 | FAR = .16 |
| CSI = .36 | CSI = .62 |
| LT = 13.6 min | LT = 15.4 min |

1978 Tornado

| OKC WSFO | NSSL Doppler |
|---------------|---------------|
| POD = .75 | POD = .56 |
| FAR = .79 | FAR = .38 |
| CSI = .20 | CSI = .42 |
| LT = -2.3 min | LT = 19.8 min |

¹Tornado only

Table 6. 1977-78 Doppler CSI for Tornadoes

| Year | Hit | Miss | False Alarm | Time |
|---|-----|------|-------------|------|
| 1977 | 13 | 4 | 3 | 23.0 |
| 1978 | 5 | 4 | 3 | 19.8 |
| Total | 18 | 8 | 6 | 21.4 |
| POD = .692 FAR = .250 CSI = .563 Lead Time = 21.4 min. | | | | |

Table 7. JDOP Long Range Verification

| <u>All Severe</u> | | | |
|-------------------------------------|------|-------------|-----------|
| Hit | Miss | False Alarm | Lead Time |
| 30 | 35 | 22 | NA |
| POD = .46 FAR = .42 CSI = .35 | | | |
| <u>Tornado</u> | | | |
| Hit | Miss | False Alarm | Lead Time |
| 7 | 15 | 39 | 14.2 |
| POD = .32 FAR = .85 CSI = .12 | | | |

Table 8. OKC Warning Justification

| <u>Severe Storm Warnings</u> | | |
|------------------------------|--------|----------|
| Reason | Issued | Verified |
| 1. Radar Reflectivity | 43 | 20 |
| 2. Radar Tops | 24 | 14 |
| 3. Reflectivity + Tops | 38 | 19 |
| 4. Public Reports | 19 | 11 |
| 5. Doppler | 16 | 10 |

| <u>Tornado Warnings</u> | | |
|-------------------------|--------|----------|
| Reason | Issued | Verified |
| 1. Public Reports | 37 | 17 |
| 2. Radar (hook echo) | 27 | 5 |
| 3. Doppler | 23 | 10 |

To evaluate justifications behind current NWS system warnings, the OKC WSFO forecaster was asked to list reasons (radar, public report and Doppler) for issuing warnings. Many reasons were reported and listed in declining order of importance. However, subjective analysis of data showed that justifications were often listed in the same order as on the form provided. Therefore, results (Table 8) are derived by giving equal weight to all reasons for an individual warning. The verification data were used to determine warnings success. Because detection of reflectivity patterns signifying circulation (hook echoes) is subjective, few tornado warnings based on conventional radar verify. Often with tornado warnings, hook echoes are seen after public reports are received. Unfortunately, a majority of public tornado sightings and hook echoes cannot be verified after the fact with confirmed tornadoes. Particularly in metropolitan areas, a warning is followed with a deluge of false sightings. Initial reports of gust-front wind damage are frequently given as tornado-caused.

Table 9a. 1977 Thunderstorm Penetration Flight Summary

| A. Gust Front | | | |
|----------------|---------------|---------------------|----------------------|
| Altitude (AGL) | No. of Storms | No. of Runs | Total Length of Runs |
| ≤1500 ft | 5 | 13 | 488 km (263 nmi) |
| 2500 ft | 2 | 6 | 281 km (151 nmi) |
| 3000 ft | 1 | 4 | 77 km (42 nmi) |
| 3500 ft | 4 | 4 | 192 km (104 nmi) |
| 4500 ft | 1 | 1 | 31 km (17 nmi) |
| 5500 ft | 1 | 1 | 23 km (13 nmi) |
| 6500 ft | 1 | 1 | 13 km (7 nmi) |
| | 15 | 30 | 1105 km (597 nmi) |
| B. Penetration | | | |
| Altitude (AGL) | No. of Storms | No. of Penetrations | Total Length of Runs |
| 6000 ft | 1 | 1 | 54 km (29 nmi) |
| 7000 ft | 1 | 1 | 47 km (25 nmi) |
| 9000 ft | 1 | 3 | 73 km (39 nmi) |
| 10000 ft | 4 | 8 | 264 km (143 nmi) |
| 20000 ft | 1 | 1 | 38 km (21 nmi) |
| | 8 | 14 | 477 km (257 nmi) |

Besides the warning services provided by real time tests, the JDOP program conducted tests during 1977 and 1978 with the instrumented F-4-C aircraft described in Section 1.4. These were not real time tests of turbulence warning, but involved acquiring radar and aircraft data simultaneously for analysis. Penetrations were based on correlations between turbulence and radar echo intensity found from analysis of flights in 1975 and 1976. The aircraft was under the direct control of an FAA Air Traffic Controller assigned to the project. The flight data are summarized in Tables 9a and 9b. Detailed analysis is presented elsewhere in Lee, et al., (1978).

Table 9b. 1978 Thunderstorm Penetration Flight Summary

| Altitude (ft) | No. of Storms Penetrated | No. of Penetrations | Approximate total Distance Traversed "in cloud" during Penetrations |
|---------------|--------------------------|---------------------|---|
| 31,000 | 2 | 2 | 88 km (47 nmi) |
| 30,000 | 1 | 3 | 52 km (28 nmi) |
| 20,000 | 17 | 45 | 1373 km (740 nmi) |
| 16,000 | 1 | 1 | 27 km (15 nmi) |
| 15,000 | 3 | 10 | 344 km (185 nmi) |
| 12,000 | 1 | 1 | 34 km (18 nmi) |
| Total | 25 | 62 | 1916 km (1035 nmi) |

2.2 Air Weather Service Advisories

Through JDOP, AWS sought to determine the real-time capability of NSSL's Doppler radar for issuing point warnings to the seven military installations in Oklahoma (Tinker, Altus, Vance, Ft. Sill), southern Kansas (McConnell), and northern Texas (Sheppard, Carswell). Advisories were issued for winds greater than or equal to 50 kts, hail greater than or equal to 3/4 in, and tornado within 25 nmi. Several problems which surfaced during the 1977 experiment were corrected in 1978 by increasing operational control of the radar, improving communication procedures, and on-station training of AWS forecasters who might receive JDOP advisories.

During the spring 1977 experiment only five military advisories were issued and thus they could not be evaluated as a group because the sample was so small. Even with increased operational control and increased target points, the number of events and warnings did not increase to a statistically significant level during the 1978 experiment.

Table 10 shows the military point warnings issued and event occurrences during JDOP. Five additional events occurred at point warning locations when the Doppler radar was not operating. Table 11 shows the skill breakdown of the military point warnings. Some caution must be exercised in use of this data; the small data sample leads to statistically questionable results. A much more reliable measure of the system capabilities would be the skill statistics derived from the entire data base described earlier rather than these point warnings. This operation required the JDOP forecaster to issue

Table 10. JDOP Military Advisories

| Base | Date/Time (CST) | Advisory | Remarks |
|----------|-----------------|----------|--------------------------|
| Tinker | 3 May 77/2139 | W | Damage 5 mi west |
| Sheppard | 4 May 77/1544 | Meso(H) | Hail 2 mi west |
| Altus | 20 May 77/1406 | Meso(T) | Tornado at 1432 |
| Tinker | 20 May 77/1844 | TVS(T) | Tornado 2 mi west |
| Tinker | 28 Jun 77/1651 | W | Damage 7 mi northwest |
| Ft. Sill | 5 Apr 78/1905 | W | Hail 2 mi, Tornado 12 mi |
| Ft. Sill | 5 Apr 78/1943 | T+H | Hail 2 mi, Tornado 12 mi |
| Carswell | 22 Apr 78/1648 | H | 2 in hail at base |
| | /1656 | T | Tornado 12 mi southwest |
| | /1804 | H | Hail 14 mi southeast |
| Tinker | 30 Apr 78/1740 | T | Tornado 20 mi northwest |
| Carswell | 11 May 78/1555 | H | Hail 18 mi southeast |
| Tinker | 19 May 78/0025 | W | None reported |
| Ft. Sill | 27 May 78/1706 | W | 54 kt wind at base |
| | /1931 | H | Hail 11 mi northeast |

Table 11. JDOP Military Advisory Skill

| | Hit | Miss | FA | POD | FAR | CSI |
|---|-----|------|----|------|-----|------|
| Wind | 2 | 3 | 3 | .40 | .60 | .25 |
| Hail | 3 | 1 | 1 | .75 | .25 | .60 |
| Tornado | 5 | 0 | 0 | 1.00 | 0 | 1.00 |
| Composite | 10 | 4 | 4 | .71 | .29 | .56 |
| Composite w/o winds | 8 | 1 | 1 | .89 | .13 | .80 |
| Composite w/expanded verification circle | 13 | 4 | 1 | .76 | .07 | .72 |

point warnings for seven dispersed locations rather than simulating the actual weather warning responsibility of a base weather station. This could affect the number of Misses and False Alarms. Three of the four False Alarms occurred because the events were verified outside the allowed 5 nmi verification radius and not because they did not occur. The composite skill score (Table 11) shows a marked improvement when the radius of allowable verification is expanded to include these off-base events.

Wind advisories show the lowest skill of the three categories (Table 11). Wind advisories were based on the Doppler radial velocity component. Research into the development of Doppler radar techniques for severe thunderstorm wind advisories was begun by Bonewitz (1978) from JDOP 77 data. This study shows CSI = .80 for 1977 wind advisories (NWS plus military advisories) within 115 km. As seen in Table 11, when the wind data is dropped from the composite point warning skill score computation, the JDOP skill score improves appreciably. Follow-on research using JDOP data is planned on wind and hail advisories. Continued research should provide a significantly improved skill score.

An example of tornado advisory capability was provided when a tornado struck Altus AFB (LTS) on 20 May 1977. A list of events is as follows:

1. 1254 CST - LTS Weather Warning for hail and gusts to 45 kts.
2. 1350 CST - Marble-size hail reported at 240°/21 nmi from LTS.
3. 1356 CST - Doppler detected first shear.
4. 1400 CST - Marble-size hail reported at 200°/18 nmi from LTS.
5. 1406 CST - Doppler confirmed mesocyclone and called LTS
(information not understood and therefore not used).
6. 1410 CST - Pea-size hail reported at 240°/5 nmi from LTS.
7. 1420 CST - Tornado reported at 190°/9 nmi from LTS.
8. 1421 CST - LTS Weather Warning for a tornado in the vicinity.
9. 1423 CST - 3/8 in hail at LTS.
10. 1430 CST - Tornado 1/2 mile south of base moving NE, station evacuated.
11. 1432 CST - Tornado over runway.
12. 1445 CST - Tornado dissipated north of the base.

The Doppler 26-min lead time, as opposed to 9 min by the LTS forecaster, shows the increase in warning lead time and detection capability possible from Doppler. The LTS radar did not detect a hook echo and the AWS warning was based on Civil Defense reports. Damage to the base was extensive with losses in excess of one million dollars.

An example of wind advisory capability occurred with the storm that hit Ft. Sill on 27 May 78. As the storm moved toward the Norman Doppler radar site, high winds were observed in an advisory issued to Ft. Sill at 1706 CST.

The storm moved along the forecast track and beginning at 1749 CST, Ft. Sill recorded 16 min of winds greater than 50 kts. This successful forecast with a lead time of 43 min represents an important accomplishment.

In computing lead times, the small point warning sample is reduced by dropping the 22 April 78 advisories issued to Carswell AFB. The JDOP team watched the storm develop in the Carswell area, but were forced to switch the radar pulse repetition frequency to cover higher priority storms in Oklahoma. This resulted in a 30-min interruption in Carswell AFB coverage and resulting negative lead times. Dropping these advisories to Carswell leaves only 14 point warnings (5 Hail, 4 Tornado, 5 Wind) for lead time computation. The combined point warning average lead time is 30 min. A more realistic measure of the lead time capabilities would be the lead times computed from the entire data base rather than the more limited point warnings.

3. JDOP FACILITIES

3.1 NSSL Doppler Radar

The Doppler radar at Norman, Okla. (see frontispiece) is a custom built meteorological radar which operates at 10 cm wavelength. Radar characteristics (Table 12) include a narrow beamwidth, accurate reflectivity estimates and real time processing of mean velocity and spectral width information. The Norman Doppler includes a unique data processing system using two pulse repetition frequencies (PRF). We call the operation of this system "batch processing." Completed before the spring 1977 start of JDOP, the new equipment allows velocity data to be acquired during a short pulse repetition period (115 km range) and reflectivity data during an interspersed long period (1460 km unambiguous range).* The reflectivity and velocity samples are compared electronically so that each velocity estimate is positioned accurately on the display. In this way, unreliable data (e.g., multiple trip echoes) are filtered out and confidence is maintained in displayed velocity fields at any range. During spring 1978 the system also had a selectable PRF to allow weather targets to be separated from ground clutter annuli which repeat at multiples of the maximum unambiguous range.

Reflectivity estimates are made with an effective time average of eight intensity system periods (100 ms) and range integration over four pulse volumes, to give expected standard deviation of intensity about 1 dB. Velocity estimates consist of 56 samples processed in 8 blocks (batches) of 7 samples (batches are separated by the intensity samples). The standard deviation of the mean velocity estimate provided by the hardwired Pulse Pair Processor (operating at signal-to-noise ratios ≥ 10 dB) is between 0.5 and 1.0 m s⁻¹. Maximum unambiguous velocity of 34 m s⁻¹ (specified by 1300 Hz PRF for velocity estimation) is more than sufficient for severe storm observation.

* A rapid PRF is required to measure high winds, but a low PRF is required to "see" a great distance. These and other radar principles are discussed in Part II.

point warnings for seven dispersed locations rather than simulating the actual weather warning responsibility of a base weather station. This could affect the number of Misses and False Alarms. Three of the four False Alarms occurred because the events were verified outside the allowed 5 nmi verification radius and not because they did not occur. The composite skill score (Table 11) shows a marked improvement when the radius of allowable verification is expanded to include these off-base events.

Wind advisories show the lowest skill of the three categories (Table 11). Wind advisories were based on the Doppler radial velocity component. Research into the development of Doppler radar techniques for severe thunderstorm wind advisories was begun by Bonewitz (1978) from JDOP 77 data. This study shows CSI = .80 for 1977 wind advisories (NWS plus military advisories) within 115 km. As seen in Table 11, when the wind data is dropped from the composite point warning skill score computation, the JDOP skill score improves appreciably. Follow-on research using JDOP data is planned on wind and hail advisories. Continued research should provide a significantly improved skill score.

An example of tornado advisory capability was provided when a tornado struck Altus AFB (LTS) on 20 May 1977. A list of events is as follows:

1. 1254 CST - LTS Weather Warning for hail and gusts to 45 kts.
2. 1350 CST - Marble-size hail reported at 240°/21 nmi from LTS.
3. 1356 CST - Doppler detected first shear.
4. 1400 CST - Marble-size hail reported at 200°/18 nmi from LTS.
5. 1406 CST - Doppler confirmed mesocyclone and called LTS
(information not understood and therefore not used).
6. 1410 CST - Pea-size hail reported at 240°/5 nmi from LTS.
7. 1420 CST - Tornado reported at 190°/9 nmi from LTS.
8. 1421 CST - LTS Weather Warning for a tornado in the vicinity.
9. 1423 CST - 3/8 in hail at LTS.
10. 1430 CST - Tornado 1/2 mile south of base moving NE, station evacuated.
11. 1432 CST - Tornado over runway.
12. 1445 CST - Tornado dissipated north of the base.

The Doppler 26-min lead time, as opposed to 9 min by the LTS forecaster, shows the increase in warning lead time and detection capability possible from Doppler. The LTS radar did not detect a hook echo and the AWS warning was based on Civil Defense reports. Damage to the base was extensive with losses in excess of one million dollars.

An example of wind advisory capability occurred with the storm that hit Ft. Sill on 27 May 78. As the storm moved toward the Norman Doppler radar site, high winds were observed in an advisory issued to Ft. Sill at 1706 CST.

The storm moved along the forecast track and beginning at 1749 CST, Ft. Sill recorded 16 min of winds greater than 50 kts. This successful forecast with a lead time of 43 min represents an important accomplishment.

In computing lead times, the small point warning sample is reduced by dropping the 22 April 78 advisories issued to Carswell AFB. The JDOP team watched the storm develop in the Carswell area, but were forced to switch the radar pulse repetition frequency to cover higher priority storms in Oklahoma. This resulted in a 30-min interruption in Carswell AFB coverage and resulting negative lead times. Dropping these advisories to Carswell leaves only 14 point warnings (5 Hail, 4 Tornado, 5 Wind) for lead time computation. The combined point warning average lead time is 30 min. A more realistic measure of the lead time capabilities would be the lead times computed from the entire data base rather than the more limited point warnings.

3. JDOP FACILITIES

3.1 NSSL Doppler Radar

The Doppler radar at Norman, Okla. (see frontispiece) is a custom built meteorological radar which operates at 10 cm wavelength. Radar characteristics (Table 12) include a narrow beamwidth, accurate reflectivity estimates and real time processing of mean velocity and spectral width information. The Norman Doppler includes a unique data processing system using two pulse repetition frequencies (PRF). We call the operation of this system "batch processing." Completed before the spring 1977 start of JDOP, the new equipment allows velocity data to be acquired during a short pulse repetition period (115 km range) and reflectivity data during an interspersed long period (1460 km unambiguous range).* The reflectivity and velocity samples are compared electronically so that each velocity estimate is positioned accurately on the display. In this way, unreliable data (e.g., multiple trip echoes) are filtered out and confidence is maintained in displayed velocity fields at any range. During spring 1978 the system also had a selectable PRF to allow weather targets to be separated from ground clutter annuli which repeat at multiples of the maximum unambiguous range.

Reflectivity estimates are made with an effective time average of eight intensity system periods (100 ms) and range integration over four pulse volumes, to give expected standard deviation of intensity about 1 dB. Velocity estimates consist of 56 samples processed in 8 blocks (batches) of 7 samples (batches are separated by the intensity samples). The standard deviation of the mean velocity estimate provided by the hardwired Pulse Pair Processor (operating at signal-to-noise ratios ≥ 10 dB) is between 0.5 and 1.0 m s⁻¹. Maximum unambiguous velocity of 34 m s⁻¹ (specified by 1300 Hz PRF for velocity estimation) is more than sufficient for severe storm observation.

* A rapid PRF is required to measure high winds, but a low PRF is required to "see" a great distance. These and other radar principles are discussed in Part II.

Table 12. Norman Doppler Radar Characteristics

General

| | |
|---|-------|
| Wavelength (cm) | 10.52 |
| Peak power | 750 |
| Beamwidth (deg.) | 0.81 |
| Pulse length (m) | 150 |
| Antenna gain (dB) | 46.8 |
| Antenna rotation rate (deg. s ⁻¹) | 6.0 |

Reflectivity

| | |
|---------------------------------|-----|
| Pulse repetition frequency (Hz) | 325 |
| Maximum unambiguous range (km) | 460 |
| Range increment (m) | 600 |
| Number of data bins per radial | 762 |
| Intensity resolution (dB) | 1.3 |

Velocity

| | |
|---|------|
| Pulse repetition frequency (Hz) | 1300 |
| Maximum unambiguous velocity (m s ⁻¹) | ±34 |
| Maximum unambiguous range (km) | 115 |
| Range increment (m) | 150 |
| Number of data bins per radial | 762 |
| Velocity resolution (m s ⁻¹) | 1 |
| Spectral width resolution (m s ⁻¹) | 0.5 |

The Pulse Pair spectral width estimate is biased for weak signals and for extremely narrow or broad spectra. However, the worst bias reduces accuracy by only $2-3 \text{ m s}^{-1}$.

3.2 JDOP Control Room Configuration

The radar transmitter and receiver components are located directly below the 30 ft diameter antenna on the second floor of the hexagonal-shaped building (frontispiece). The downstairs area is subdivided into maintenance, radar control, computer support, and operations. Normal work areas of the staff of technicians (T), engineers (E), and meteorologists (M) (indicated by the circles) reflect the usual mode of operation for NSSL R & D programs, not necessarily the best configuration for an operational system.

Additional support staff within NSSL provide assistance in radar calibration and systems checks, scope photography, forecasting, and damage surveys.

Communications are mainly by telephone. NOAA Weather teletype and Service A circuits are available, and closed circuit TV from the Laboratory provides satellite and "nowcast" information at the discretion of the Laboratory forecaster who occasionally advises the JDOP team concerning severe storm watches, frontal positions, environmental winds, and damage reports. During 1978 equipment of the Air Force Geophysics Laboratory for receiving, data processing, recording, and display were operated from an instrumentation trailer located adjacent to the Doppler Building, and in parallel with the NSSL and NWS Systems. Information from these equipments is provided to JDOP meteorologists by color displays in the Doppler operations area.

3.3 NSSL Data Processing and Display

The Norman Doppler is interfaced to a Ling computer for data processing and display. The computer, for example, compares reflectivity estimates positioned with slow PRF to velocity estimates positioned with rapid PRF to remove range ambiguities as noted above. Operator input into the Ling is made by teletype.

Control functions consist of the software necessary to translate house-keeping information and operator commands into control variables used by all other programs. For example, if the PRT (Pulse-Repetition Time) is changed, various input constants change, and all appropriate adjustments are taken with no input from the operator. Operator control is required to change such things as the maximum range to be displayed, certain thresholds, or data resolution. Control functions are designed to make maximum use of pre-set thresholds and pre-programmed automatic decision making. Further development in these areas is necessary for routine operational uses.

The signal-to-noise ratio (SNR) for each reflectivity level is calculated from daily calibration. During real-time operation the SNR for each intensity estimate is generated and stored in a temporary buffer to be overwritten by

the next radial. If the SNR is below the threshold at which reliable velocity estimates can be used (default=10 dB, but operator adjustable), a no data code is stored.

The Ling controls a Vector General graphics display of Doppler spectral moments. The multimoment display (MMD) is a field of arrows (Fig. 15a) where arrow length is proportional to intensity, arrow deflection proportional to mean velocity and arrowhead size proportional to spectral width. Arrows pointing right indicate zero radial velocity, arrows toward display top and bottom are +17 and -17 m s⁻¹, respectively (positive velocity defined as away from radar) and arrows pointing left are at the unambiguous velocity interval of 34 m s⁻¹. (See Burgess et al., 1976, for further display explanation.) The display is unique in its provision of multiple data types simultaneously with a resolution comparable to radar output over a limited area. Single Doppler shears important to vortex recognition are emphasized by arrow orientations and arrowhead size (spectrum width is related to shear). It must be remembered that displayed velocities are radial component of motion and must not be taken as streamlines of horizontal air flow.

Arrow coordinates for the multimoment display are calculated from reflectivity, velocity, and width. The resulting coordinates are stored in the display area. The operator has a choice of eight different surveillance regions which he has previously defined by specifying the azimuth and range to locations of interest identified on the PPI display of reflectivity. Data resolution is determined automatically but may be overridden by the operator. Each region is updated as the antenna passes through it and is displayed either automatically or at the discretion of the operator.

The Ling computer also formats Doppler data for transfer to a Computer Automation (CA) computer which in turn presents the data on a color display (Fig. 15b). Operator control is maintained by color display keyboard and CA teletype.

The display format is an array of 256 x 256 elements with a variable grid mesh size, typically from 0.9 to 3.6 km. Radar data are considerably denser in range than the best possible resolution of the color display. Therefore, the data are reduced before time consuming computations in the "polar to rectangular" and "beamfill" routines.

All data values must be converted to a 4-bit code for the color display. Velocities and width codes change automatically with a change in PRT. Categorization is accomplished with a look-up table so that any desired code structure may be preprogrammed.

Twenty-four fields in color of each of velocity, reflectivity and spectral width are available for recall from a flow-through disk (the 25 fields in memory are automatically replaced by the newest data fields). A second disk storage area allows 24 total fields of any parameter to be saved indefinitely for later recall. Sixteen overlays and color mixes are also stored and available at operator discretion.

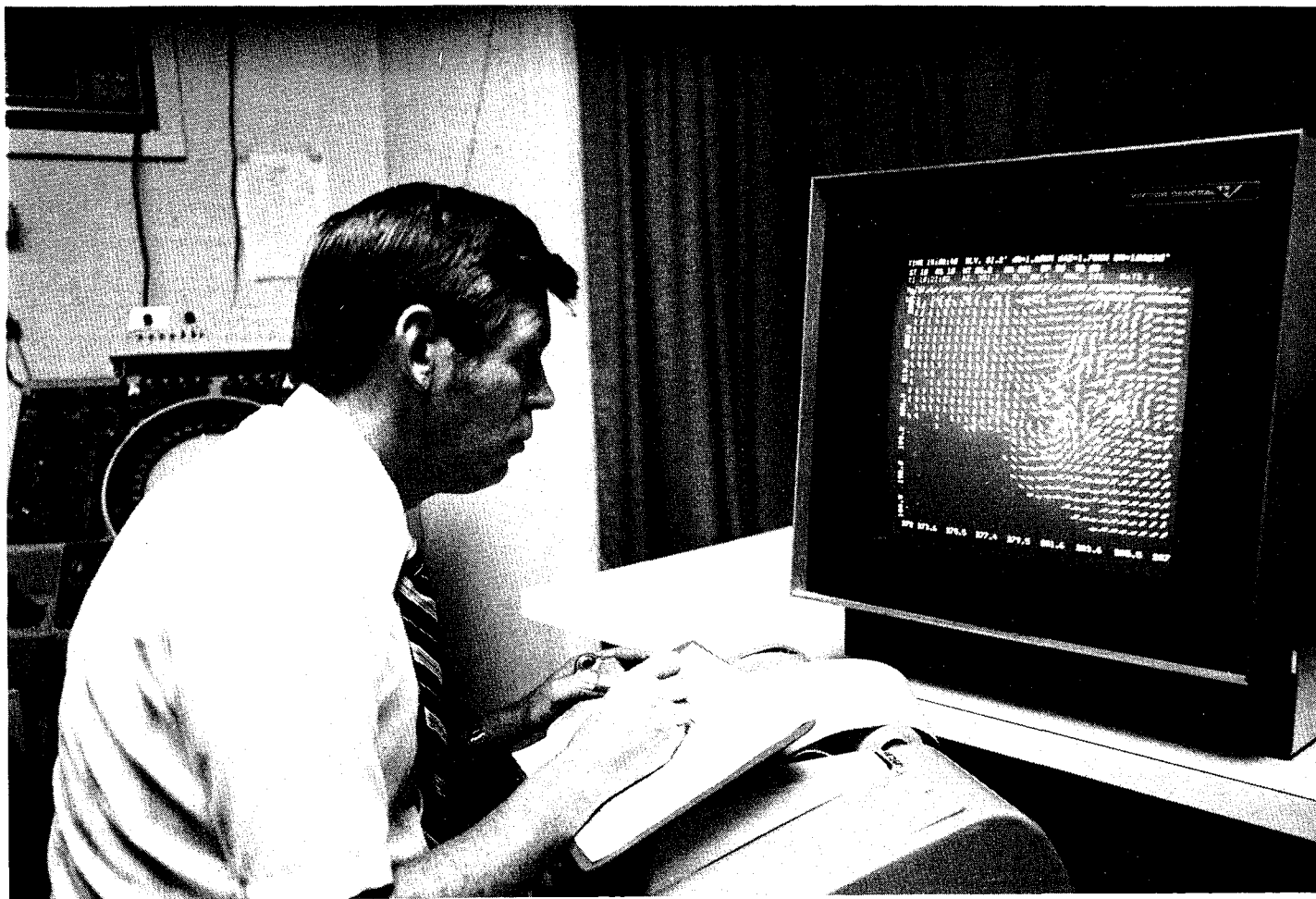


Figure 15a. Multimoment display. A field of arrows where each arrow length is proportional to reflectivity, arrow position proportional to single Doppler velocity, and arrowhead size proportional to velocity spectrum width.

of the trackball cursor to interrogate the SCRM and output the color pixel values to the operator. The magnetic disc unit has 10 megabytes of storage evenly divided between a fixed platter and a removable cartridge.

The Pulse Pair Processor (PPP) interface provides the major radar data input source. The data, either in real time or from the archived tapes, contain all the video data as well as the mean velocity and velocity variance data and ancillary data. The interface also does hardware bit reordering to provide the necessary format in the Interdata compatible 32 bit word. The data is transferred in blocks of 16 bytes of ancillary data followed by 1024 to 4096 bytes of radar data. Each azimuth's data is contained in such a data block.

The radar data is processed for output in six different stages. Because the software is still in the development stage, most of the processing is done in FORTRAN although drivers and input-output (I/O) operations are written in assembly language. Because of this, the total program is too long to be contained in memory at one time, so extensive use is made of overlays with the essential data stored in task commons for access by all subroutines.

The six stages of storm cell processing are data collection, range processing, azimuthal processing, area and weighted center processing, plotting and attribute listing.

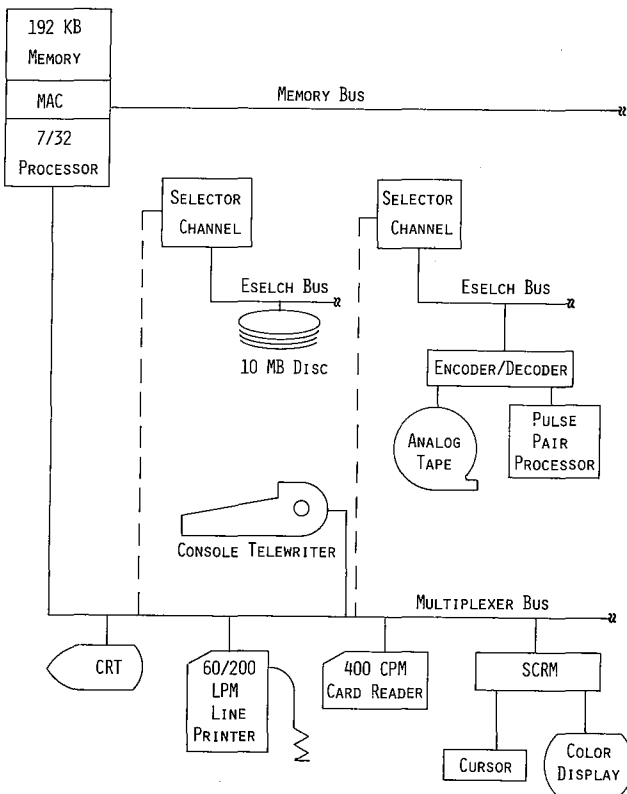


Figure 16. ETSE Block Diagram.

The data are collected by the PPP encoder and stored on discs. Data are collected based on selectable input parameters: beginning and ending azimuth for sector or PPI scans; lowest and highest allowable elevation angles; and continuous, on demand or time data collection options. During the spring of 1978, the system was operated to accept data every six minutes in a 360° PPI mode between elevation angles of 0.0° to 0.5°.

During the data collection, the beginning and end points of desired data segments are determined and stored in task common. The data segments are considered important only if their reflectivity exceeds a predetermined threshold, Z_{th} . Thirty dBZ was used during JDOP.

Various computer routines smooth and filter the data, and identify, locate, and characterize discrete areas from which echoes indicative of severe local storms are received. After the 12 largest areas are determined, the centers are correlated on past data using a nearest neighbor algorithm. A single attempt at correlation is made. If an area is not correlated, a new cell is assumed and a new track history begun. Once the areas are correlated, a least square fit extrapolation is made of the cell locations. During JDOP tests, 12- and 24-min forecasts were made, and the tracks plotted on the color display system with the same scale as the reflectivity data (Fig. 17). Each six minute cell location is plotted in one of twelve colors. Along with the cells' tracks, the forecast positions are plotted. The areas with reflectivities greater than Z_{th} are outlined and unique areas are labeled with the time associated with each past analysis annotated on the display.

After the cells' locations and forecasts are plotted, the program is returned to the data collection mode. At the same time, but in a different foreground task, an attribute listing is output to a CRT for use by the forecasters. In Oklahoma the same data were output to a printer for a hard copy.

Other programs can be run in parallel with the main program. For example, analysis parameters can be changed for comparisons without canceling the main program. Another program permits interrogation of the SCRM to determine color display pixel values. Along with the display number and pixel color, the azimuth, range and altitude of the pixel are output on the same display as the echo track display. The program runs concurrently with the main program.

During the entire spring 1978 JDOP program, the ETSE was operational, and no system failures occurred. The ETSE provided data to the forecasters in the same time frame as the data acquisition.

The analysis time is one or two minutes, and is dependent on the number of areas plotted on the color display and the listing of their corresponding attributes on the CRT and the printer. Since the processing is time bound by I/O operations and these drivers are written in assembly language, one way to decrease the processing time (by perhaps 20-30%) would be to do more processing during data collection stage via hard-wired devices or to convert the Fortran portions of the program to assembly language.

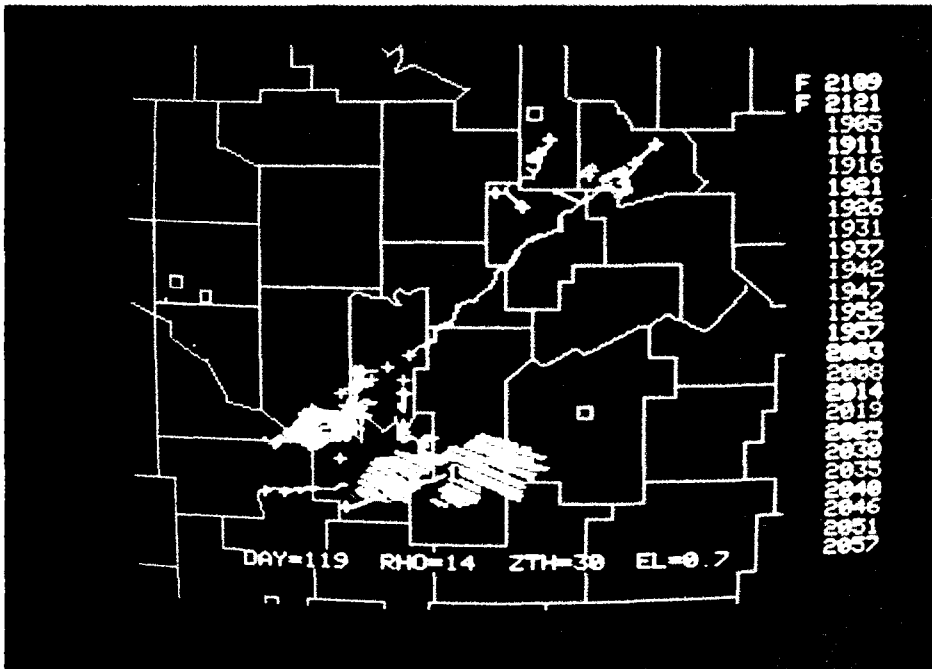
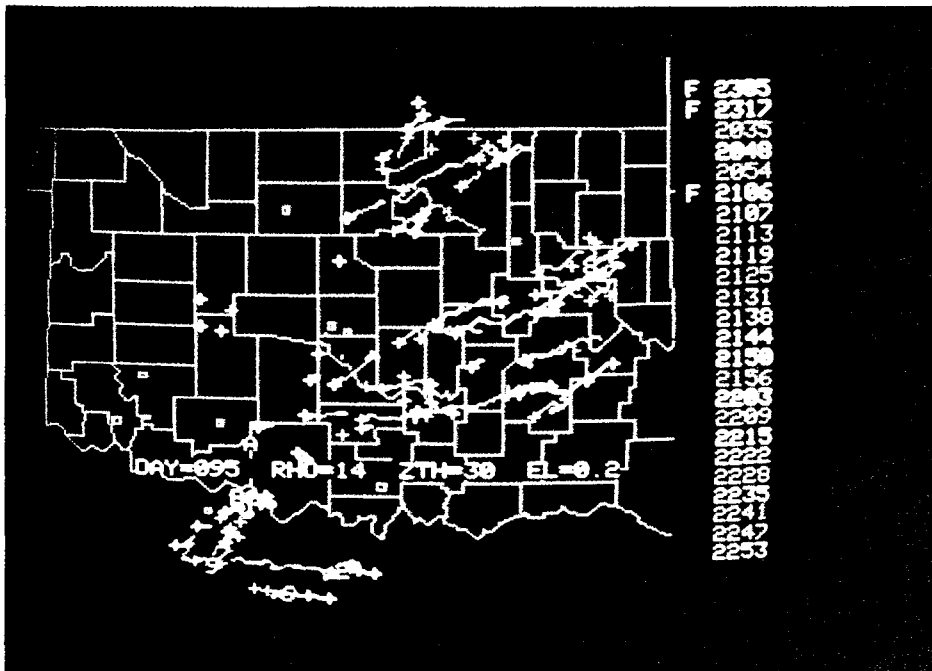


Figure 17. Echo track color display produced by echo track significance estimator (ETSE). Past, current, and forecast echo centroids are indicated by color code at right. (F) denotes forecast location color. Data are from 5 April 1978 (top) and 29 April 1978 (bottom) and show diversity of echo tracks across Oklahoma during two 3 h periods.

The Echo Track and Significance Estimator performed very well during the 1978 program. It provided the JDOP forecasters with valuable information on the past, current, and forecast positions of storm centroids. This information proved valuable not only in warning those areas that would be affected by the storm, but also in identifying the fact that a storm was deviating to the right of the mean flow and therefore was likely to be severe.

4. CONCLUDING REMARKS

The Joint Doppler Operational Project has concluded two seasons of weather observation and analysis in close collaboration with operating agencies, and in a real-time environment of severe storm forecasting and warning. The JDOP finds that:

1. Warning verification results indicate Doppler capability is superior to conventional radar and spotters. Its main advantages are increased lead time for tornadoes, reduced false alarm rates for tornado and severe thunderstorms, and improved probability of detection for severe thunderstorms.
2. Doppler radar with narrow beamwidth can distinguish between severe and nonsevere thunderstorms at long range (230-350 km) by observation of mesocyclones at storm mid-levels. Doppler capability for separating tornadic from non-tornadic storms is limited to close ranges (< 230 km).
3. Doppler radar can reduce dependence of the Weather Service on public reports of tornado occurrence and development. Interpretation of visual phenomena by laymen is often erroneous.
4. Doppler radar can provide precise location of signatures facilitating warnings more specifically directed to the rather small areas usually under threat. Thus, with Doppler radar, the size of warning areas can be markedly reduced and the phenomenon warned about can be more accurately identified.
5. Doppler radar can be of great value in improving the safety and economy of commercial flight in thunderstorm areas, through its identification of in-storm turbulence, wind shear, meso-scale vortices, and gust fronts.
6. The JDOP data are an essential part of the engineering analysis for specification of a Doppler radar system for operational use on a national basis.
7. JDOP participants agree that the next generation meteorological radar should have Doppler capability.

Radars built to a set of common specifications should provide data needed by all the federal agency users and private users who would draw on the advancing technology of data systems to provide processed materials at operating centers. Thus the diversity demanded by differing responsibilities would be provided by agency-specialized computer programs, communication modules, and display systems, and the Nation would benefit from the large capabilities and significant economies inherent in a single radar network.



PART II

DOPPLER RADAR ENGINEERING

Prepared by

Dale Sirmans, Kenneth Shreeve,
Kenneth Glover and Isadore Goldman

1. DOPPLER TECHNOLOGY

1.1 Historical Background

Unlike conventional radars, such as the WSR-57 and FPS-77, a Doppler radar is coherent, i.e., it can measure the phase difference between transmitted and received radar signals. The rate of change of the phase difference is directly proportional to the radial component of target motion relative to the radar (defined as the Doppler velocity). Thus, as a Doppler radar scans horizontally, it measures both the reflectivity and the component of target motion along the radar beam axis.

Doppler radars can be used to study clear air as well as precipitation. Thus Doviak and Jobson (1978) have used it to map the kinematic structure of the planetary boundary layer even when particulate matter does not offer significant reflectivity. Coherent processing of the echo data often improves the detectability of weather echoes by over an order of magnitude (Hennington, et al., 1976).

Reflectivity estimation requires only echo sample averaging to reduce statistical fluctuations. However, mean Doppler velocity estimation involves either the Fourier transform or covariance calculation and requires a large amount of data processing. Probably the long development and cost of Doppler processors (to estimate velocities simultaneously at all resolution volumes along the beam) was due to pursuit of measurement of the whole Doppler spectrum, from which the most interesting moments (mean Doppler velocity and spectrum width) must be extracted.

One of the first Doppler spectrum analyzers that could generate Doppler spectra for each continuous resolution volume in real time is described by Chimera (1960), and this machine, the Velocity Indicating Coherent Integrator, processed with a single electronic circuit, the echo signals to generate Doppler spectrum estimates simultaneously at all resolution volumes. Another machine, called the Coherent Memory Filter (CMF), employing the same principles, was developed for weather radar observations (Groginsky, 1965) and used by researchers at the Air Force Cambridge Research Laboratories (AFCRL)¹. This machine produced the first real-time maps of Doppler velocity shear fields on a plan-position indicator (PPI) (Armstrong and Donaldson, 1969).

¹Presently the Air Force Geophysics Laboratory.

In the early seventies, Sirmans and Doviak (1973) described a phase change estimator which circumvents spectral calculations and digitally processes echoes to estimate directly the Doppler velocity in contiguous resolution cells.

The need to obtain the principal Doppler moments economically and with minimum uncertainty, and have these in digital format (to facilitate processing and analysis with electronic computers) has prompted use of covariance estimate techniques. Hyde and Perry (1958) reported an early version of this method, but it was first used by ionosphere investigators at Jicamarca (Woodman and Hagfors, 1969). Independently, and at about the same time, Rummeler (1968a, b) introduced it to the engineering community. The advantages of covariance processing coupled with the new technology (medium scale integrated circuits, MSI) made possible the implementation of this signal processing technique on the pulse-Doppler radar (Lhermitte, 1972; Mueller and Silha, 1978; Novick and Glover, 1975; Sirmans and Bumgarner, 1975).

1.2 Inherent Characteristics

The nature of the weather echo imposes limitations and on the Doppler radar. Weather targets are distributed continuously over large regions (tens to hundreds of kilometers), the significant weather echoes easily span an 80 dB power range, and the signals themselves are semi-coherent (i.e., they are not a single pure sinusoid).

The unambiguous range, r_a , is the maximum distance a transmitted pulse can travel out and return echoes to the radar before the next pulse is transmitted. When a precipitation area is located beyond the unambiguous range, the echoes returning from that area arrive after the next pulse is transmitted. Uniform pulse repetition time (T_S) radars cannot discriminate between echoes coming from scatterers located in the different annuli (trips) of thickness $r_a = CT_S/2$ (where C is the velocity of light), so target range is ambiguous. Only by using a T_S long enough so that second trip (or higher) echoes are unlikely, can we be certain that range is measured unambiguously. Range ambiguities are detrimental only when echoes from different distances arrive at the same time causing interference with each other.

Target velocities are ambiguous because one cannot distinguish between real Doppler shifts and those spaced by pulse repetition frequency. All radial velocities must lie between $\pm v_a = \lambda/4T_S$ in order to be unambiguous; thus, the range velocity product (λ is the wavelength)

$$r_a v_a = C\lambda/8 \quad (1)$$

typifies the ambiguity resolution capabilities of conventional (i.e., uniform pulse spacing) Doppler radars. The equation shows the advantage of longer wavelengths, but other factors do influence the design.

Fully coherent pulse Doppler radars (i.e., coherency or phase sensitivity is maintained by the radar for more than one PRT) can measure precisely ranges and velocities of targets beyond the first range ambiguity. Similarly, good estimates of velocities past the ambiguous (Nyquist) velocity are possible. Some methods for achieving this and extending r_a and v_a well above the value given by (1) are discussed in Doviak, et al., 1978.

The most severe restriction imposed on the Doppler weather radar comes from the semi-coherency of the weather echo signal, i.e., the changing of resultant phase that arises from the motion of individual scattering elements (e.g., raindrops) relative to each other. Disregarding this property, one could in principle choose the pulse repetition time, T_s , large enough, as we do with incoherent radars, so that no second or higher order trip echoes would ever be received. But signal samples spaced T_s apart must be correlated for precise Doppler shift measurement. Correlation exists when

$$\frac{c\lambda}{4r_a} > 2\pi\sigma_v \quad (2)$$

where σ_v is the velocity spectrum width of echoes at range r (Atlas, 1964). Condition (2) merely states that Doppler width should be much smaller than the Nyquist interval $\lambda/2T_s$. When correlation decreases appreciably, the variance in mean-Doppler estimate increases exponentially, as does the variance of spectrum width estimate (Zrnic, 1977). Requirement (2) means that σ_v limits the largest unambiguous range for a given wavelength, whereas (1) restricts r_a only if ambiguities due to velocity aliases need to be resolved by choosing a large v_a .

When spectrum widths are greater than a few meters per second, it is unlikely that range ambiguities can be wholly eliminated with the PRT uniform and the wavelength 10 cm or shorter. The specification on r_a given σ_v established by (2) is more important than (1) because there is no limit in resolving velocity aliases if σ_v is sufficiently small; spectrum width limits the Doppler measurement and not ambiguities per se (Doviak, et al., 1978).

1.3 Spectral Moment Estimates

The pulse-Doppler radar should supply the three most important spectrum moment estimates: (1) the echo power or zero moment of the Doppler spectrum (this indicates liquid water content or precipitation rate in the resolution volume), (2) the mean Doppler velocity or the first moment of the spectrum normalized to the zeroth moment (this equals the mean motion of scatterers, which, for near-horizontal antenna orientations, is essentially the air motion towards or away from the radar), and (3) spectrum width σ_v , the square root of the second moment about the first of the normalized spectrum, a measure of velocity dispersion (i.e., shear or turbulence) within the resolution volume.

Moment estimates use samples of a randomly varying signal. In the case of weather echoes, single sample estimates have too large a statistical

uncertainty for meaningful data interpretation. Thus, a large number of echo samples (acquired during a few milliseconds) must be processed to provide the required accuracy. The accuracy of these estimates depends on radar system characteristics and meteorological conditions, such as the signal-to-noise ratio, the distribution of velocities within the resolution volume, the receiver transfer function, and the number of samples processed. Because samples are collected while the antenna is rotating, the desired precision that determines the collection time (dwell time) also restricts the rotation rate.

To obtain a quantitative estimate of echo power, samples must be averaged over a period long compared to the decorrelation time (reciprocal of Doppler spectrum width). A uniformly weighted average obtained from M complex video samples V_n 's is

$$\hat{P} = \frac{1}{M} \sum_{n=1}^M |V_n|^2 - N \quad (3)$$

where N is the radar white noise power. V_n 's are voltages with magnitude and phase corresponding to the electric field echoes from scatterers.

Although both coherent and incoherent radars can be used to estimate the zeroth and the second spectral moment,* only the Doppler radar provides the first spectral moment estimate. The autocovariance processor for mean velocity (popularly known as "pulse pair") is an excellent example of a blend between theoretical ingenuity (the algorithm) and technological advance (integrated digital circuits). Because the autocovariance $R(T_s)$ and the Doppler spectrum constitute a Fourier transform pair, the moments of the spectral density correspond to the derivatives of the complex autocovariance evaluated at zero lag. The pulse pair velocity estimate, v_{pp} , is defined as

$$\hat{v}_{pp} = \frac{v_a}{\pi} \arg [\hat{R}(T_s)] \quad (4)$$

where the autocovariance estimate $\hat{R}(T_s)$ is obtained from video samples V_n 's:

$$\hat{R}(T_s) = \frac{1}{M} \sum_{n=1}^M V_{n+1} V_n^* \quad (5)$$

and * denotes the complex conjugate.

Spectral analysis requires $\log_2 M$ times as many operations as the autocovariance method and M times more storage locations. However, new digital

* An incoherent radar senses the second moment by echo amplitude fluctuations, which reflect the relative velocities of particles (wind variations) within any sampled volume.

circuits made it possible to produce low cost and reliable processors with speed and accuracy to match the information inherent in the Doppler radar signals. The weather radar must make velocity estimates at a large number (several hundred) of contiguous range locations and at a rate compatible with radar PRF. Besides its efficiency and modest memory storage, the autocovariance algorithm is very close to a theoretical optimum, i.e., minimum variance estimator (Miller and Rochwarger, 1972).

Second moment estimators are necessarily more complex, and their optimum properties are more difficult to establish. Estimators based on Fourier methods and pulse pair processing have proved to be useful. The pulse pair algorithm for spectrum width σ_v reads:

$$\sigma_v = \frac{2v_a}{\pi} \ln[\hat{P}/|\hat{R}(T_s)|] \quad (6)$$

For (6) to be accurate, the spectrum shape must be nearly Gaussian (as it is for weather signals) and spurious signals must be kept at a minimum. Although spectrum width can indicate turbulence, shear, and vortices, it has not yet been as fully tested as the mean velocity.

2. RADAR SYSTEM CHARACTERISTICS

2.1 Design Criteria

Agencies such as NWS, AWS and FAA will formulate the engineering requirements of a Joint Use Radar, and the desired features will be subject to compromise.

Sample size, range spacing, and antenna rotation rate must be preselected for spectrum measurement calculations. Choice of these parameters can be automated so that the radar meteorologist has compatible signal processing characteristics for each mode of operation.

Coupling of $r_a v_a$ (Figure 1) is an inherent restrictive characteristic of Doppler radars giving rise to operational problems of velocity and range

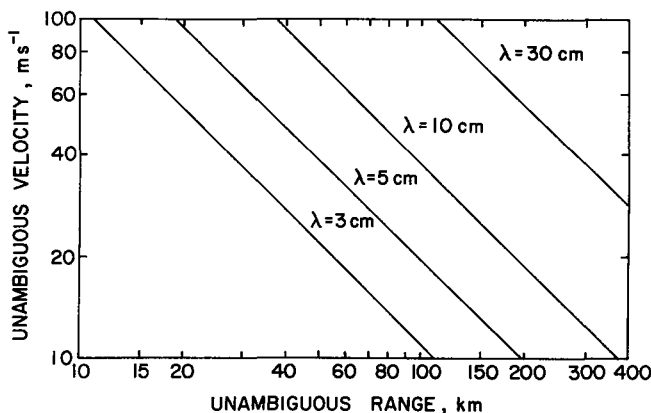


Figure 1. The unambiguous range--unambiguous velocity coupling for Doppler radar. International agreements with regard to frequency allocations have specified bands centered near 3, 5 and 10 cm for meteorological radars.

aliasing (Burgess et al., 1978; Doviak et al., 1978). Range aliasing results not only in range ambiguities but also in obscuration and velocity errors due to mixed multitrip signals. Velocity aliasing also results in ambiguities but is generally not as serious since true velocity can usually be retrieved via spatial continuity.

Choice of $r_a v_a$ must take into consideration aliasing and spectrum coherency as determined by anticipated spectrum width. For severe storms in the Midwest, velocity aliasing and coherency criteria are somewhat compatible (Doviak et al., 1978) and imply a minimum v_a of 20 to 25 m s^{-1} (Fig. 2). Although several techniques can alleviate the range and velocity ambiguities, the method used during JDOP operations was "batch" transmission and processing.

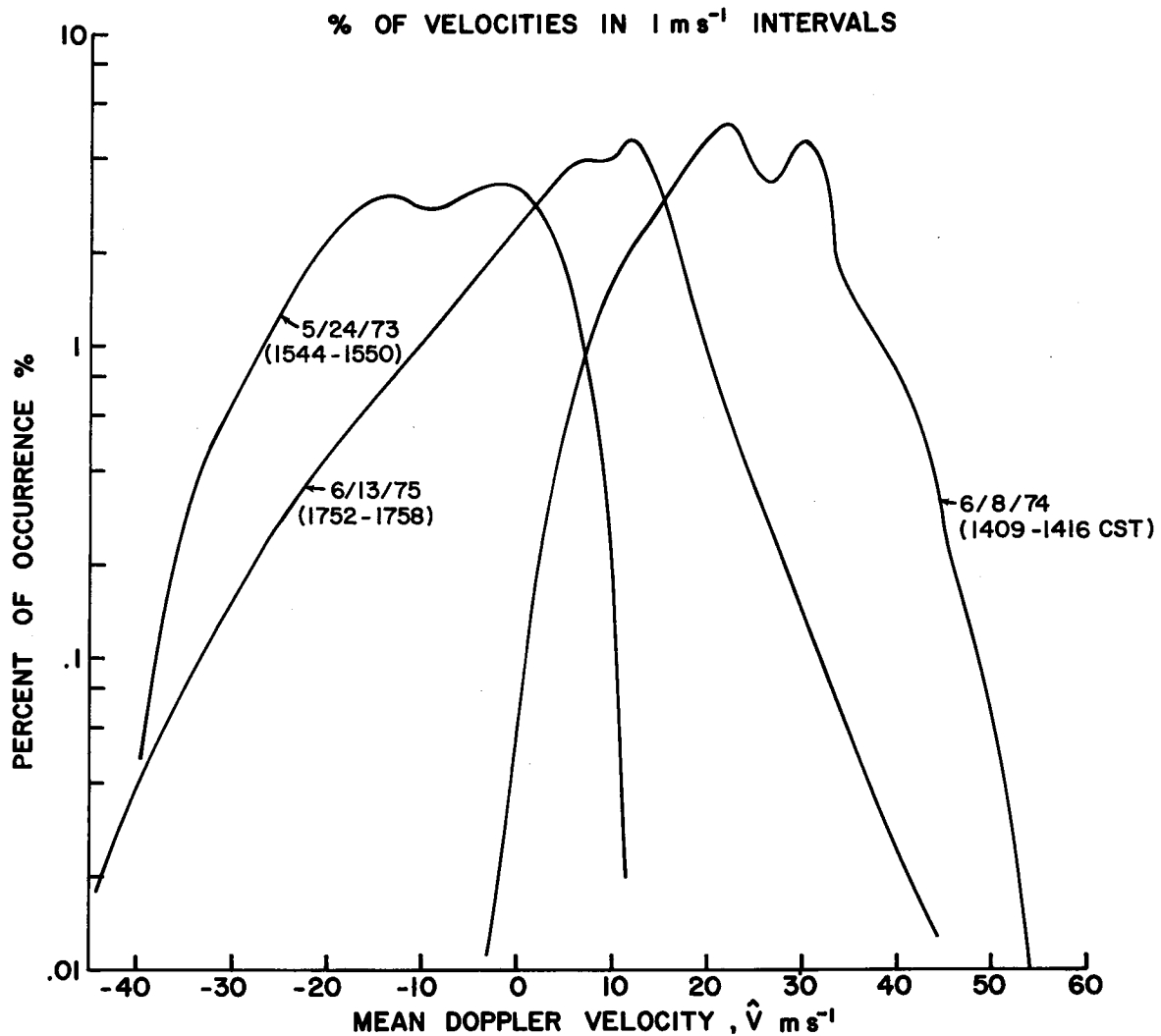


Figure 2. Percent occurrence of radial velocities for three tornadic storms. Note that the spread is typically less than 50 m s^{-1} .

Batch transmission consists of a series of equispaced transmitter pulses with internal separation dictated by the desired $r_a v_a$. These series are separated by an isolated transmitter pulse spaced at an interval sufficient to prevent significant range aliasing of the intensity data. Velocity estimation of first and multiple trip returns is made on the batches and usually limited to techniques capable of operating on signal pairs. Intensity estimation is made with the isolated pulse and the long range intensity field is used to detect regions where range aliasing has occurred during batch transmission.

As noted earlier, the unambiguous range r_a (for data processing on equispaced pulses) and unambiguous velocity, v_a , are coupled to wavelength through Eq. 1. A graph on Fig. 1, demonstrates that the choice of wavelength for this application ($r_a = 150$ km, $v_a = 25$ m s⁻¹) is limited to 10 cm or longer.

Shorter wavelength radars (3 cm) are usually less costly. Therefore there is interest in exploring means by which Doppler radars operating at wavelengths shorter than 10 cm can be made effective. For example, the range of effective velocity measurement might be extended, provided the Doppler spectrum is sufficiently narrow, through use of successive pairs of pulses at two different intervals. When the meteorological velocity exceeds v_a (the Nyquist velocity) for either or both pairs, the correct velocity would be deduced by analyzing the (unique) difference between the estimates provided by the two pairs. The smaller of the two v_a 's should not be less than twice the maximum spectrum width anticipated, about 20 m s⁻¹ for severe weather events. For example a 5 cm radar having the smaller v_a of 20 m s⁻¹ would have an r_a of about 100 km, however, the extended unambiguous velocity larger than 40 m s⁻¹ is at the expense of signal processing complexity and, more importantly, increased acquisition time (Sirmans et al., 1976).

Another argument against adoption of wavelength shorter than 10 cm, is the larger signal attenuation by rainfall at the shorter wavelength (Weible and Sirmans, 1976). Compensation via electronic means would be complex and most uncertain in the heavy rains of greatest interest (Joss et al., 1974; Hitschfeld and Bordan, 1954). Routine correction of rain attenuated signals has never been attempted in an operational environment. Because of the attenuation at shorter wavelengths, JDOP meteorology and engineering staffs alike believe that innovative engineering techniques to increase velocity measurement capability should be used to improve 10-cm equipment rather than to give shorter wavelengths a (marginal) Doppler velocity capability.

Longer wavelengths (> 10 cm) have an obvious advantage in minimizing the range velocity coupling. However, the required beamwidth would imply larger antenna apertures (e.g., 60-ft diameter for beamwidth of 1° at $\lambda = 25$ cm). A wavelength of 10 cm is recommended for the operational radars. This appears to be the best compromise between antenna size, range velocity coupling, and data acquisition time.

Because it determines spatial resolution, azimuthal and vertical beamwidth dictates the limiting range for detection of features in the velocity field (Burgess et al., 1978; Lemon et al., 1977; Burgess, 1976; Brown and

Lemon, 1976; Donaldson, 1970). Beamwidth is also reflected in range dependent velocity statistics by its influence on spectrum width and coherency (Doviak et al., 1978). Probably the velocity field feature of most concern is the mesocyclone signature associated with severe storms. Other significant features of even smaller scale are the tornado vortex signatures (Brown and Lemon, 1976; Donaldson, 1970). hail shafts, thermal plumes, and details of the radar "thin line", but the size of the mesocyclone and the required range of detection is the major consideration in specifying the beamwidth.

2.2 Detection of Mesocyclones

The mesocyclone can be modeled as a Rankine combined vortex, which consists of two regimes (Fig. 3a). The inner regime is in the vortex core ($R < R_m$) with R_m being the radius of maximum tangential velocity U_m . In this regime, the solid rotational core has the profile of tangential velocity given by $u = u_m R / R_m$. The outer regime is a potential vortex where $u = u_m R_m / R$. The model Doppler velocity azimuthal profile of a Rankine vortex measured with an antenna pattern of finite width is shown in Figure 3b (Brown and Lemon, 1976).

Resolution of the characteristic velocity signature pattern associated with the mesocyclone (after radar detection and signal handling) requires that the ratio of antenna beamwidth to core radius be small and the azimuthal sampling be dense to preserve the prominent features of the profile. To interpret measurement of cyclone signatures with rotating antennas, it is necessary to consider the effective beamwidth which depends on the product of rotation rate and dwell time. Effects of antenna beamwidth and sampling on mesocyclone features such as peak-to-peak velocity are presented in the JDOP report for 1978.

A histogram of mesocyclone diameters in Oklahoma thunderstorms, as measured by the NSSL Doppler radar at Norman, is presented as Fig. 4.* Data were taken to a slant range of 330 km. Azimuthal increments were generally 1° for ranges less than 230 km and 0.5° for greater ranges. Samples are taken during velocity estimation, and mean velocity estimates made from samples acquired over sectors of 0.6° or 0.3° are recorded at increments of 1° or 0.5° , respectively.

Equivalent beamwidth is

$$\begin{aligned} BW_e &\approx 1.38^\circ \text{ for } 1^\circ \text{ sampling} \\ BW_e &\approx 1^\circ \text{ for } 0.5^\circ \text{ sampling.} \end{aligned} \tag{1}$$

* This contains 35 entries representing mean diameter 5.7 km (uncorrected for beamwidth and sampling) and standard deviation 2.05 km from 1971-1975, and 40 entries with mean diameter 5.2 km and standard deviation 2.66 km from 1977. Systematic data acquisition on mesocyclones was begun in 1977 (Burgess et al.).

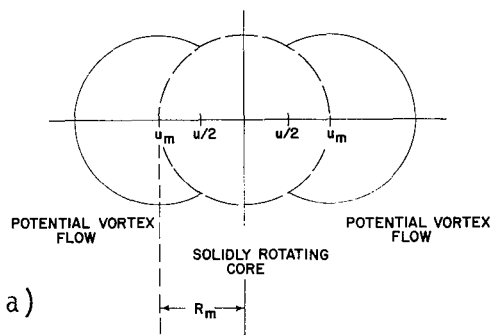


Figure 3. a) Single Doppler horizontal mesocyclone signature of a stationary Rankine combined radius. b) Theoretical mean Doppler velocity azimuthal profiles through a Rankine combined vortex (heavy line) for finite antenna beamwidth(s). Velocities are normalized by maximum tangential velocity. Azimuthal distance is normalized by vortex core radius. From Brown and Lemon, 1976.

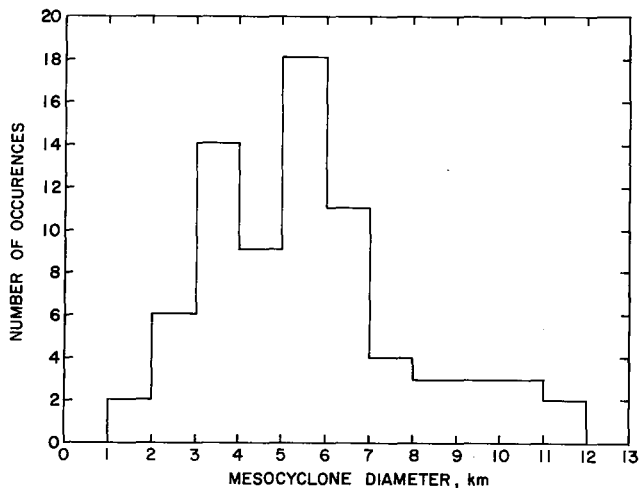
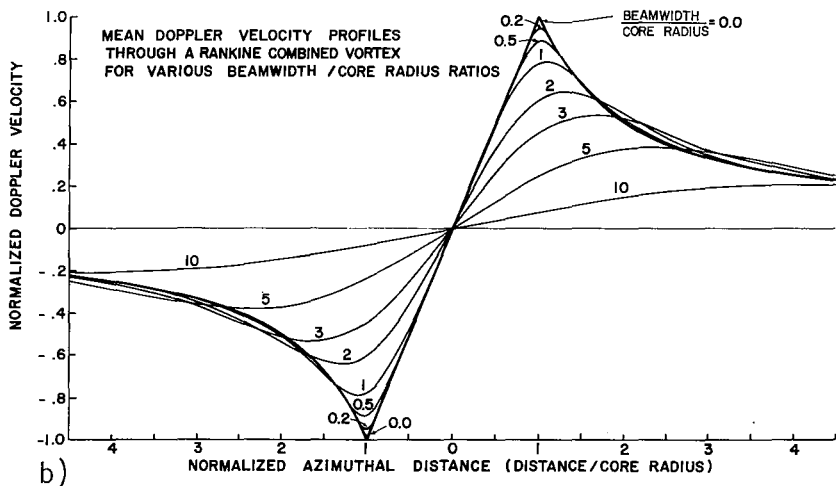


Figure 4. Frequency of occurrence of measured mesocyclone diameters. Data taken with NSSL Doppler radar, $\lambda = 10.7$ cm, $v_a = 34$ m s⁻¹, BW = 0.8°, sampling interval = 1° for range < 230 km, = 0.5° for range > 230 km. Data from Burgess (private communication).

Measured mesocyclone diameters and peak-to-peak velocities versus range are shown in Figs. 5a and 5b. Velocity measurements are based on the covariance technique. The range dependence of the measured parameters (diameter and peak to peak velocities) agrees well with the values (dashed line) obtained from the model using a mean diameter of 3.9 km and a mean peak to peak radial velocity of 54 m s^{-1} .

The implication of mesocyclone detection for the system beamwidth is seen to be stringent. Even if subjective detection of the signature could be accomplished with a beam broadening reduction of peak velocity to one-half of the true value (Burgess, et al., 1978; Sirmans, et al., 1976a), the effective beamwidth would have to be about 1.6° for a 4 km mesocyclone at 250 km and about 1.2° for detection of mesocyclones greater than the 90 percentile diameter of 3 km to a range of 250 km.

The recommended antenna beamwidth based on required detection of the mesocyclone is 1° (24 ft. reflector at $\lambda = 10 \text{ cm}$). In conjunction with azimuthal increments of 1° and 0.5° , this can provide effective beamwidths of 1.4° and 1.2° . It is not considered practical to resolve features significantly smaller than the mesocyclone beyond 200 km range or to control the apparent spectrum width profile across the mesocyclone by antenna beamwidth.

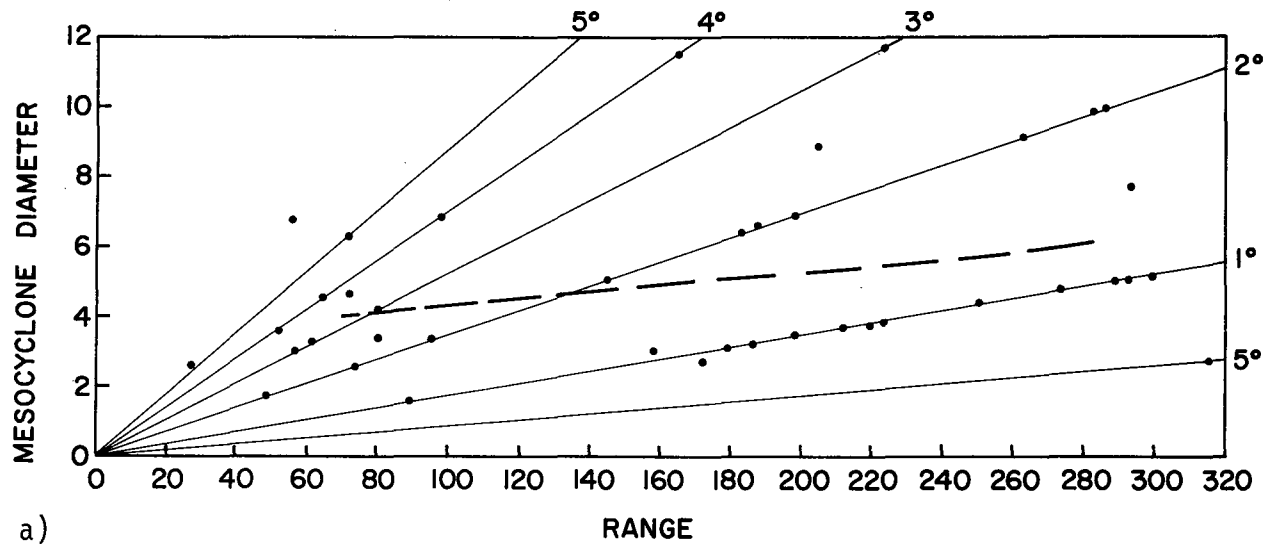
2.3 Spectrum Width Considerations

In most practical meteorological radar systems, the significant contributions to spectrum width, particularly in severe storms, are from shear and turbulence. Sustained shear over ranges necessary to produce large spectrum widths does not appear to exist routinely. In severe storms, the widths are principally due to eddies of scale size small compared to radar sample volumes 0.8° by 150 m (Doviak et al., 1978). Figure 6 shows a median width value of about 4 m s^{-1} due primarily to turbulence. Spectrum widths in the mesocyclone region of tornadic storms are shown in Fig. 7. Anticipated spectrum width (i.e., median about 4 m s^{-1} and extreme 8-12 m s^{-1}) is an important parameter in the design of meteorological radars since it determines Nyquist velocity (Eq. 1) for spectrum coherency. The operational system should be designed to provide quantitative measurements of populations having spectrum widths as large as 10 m s^{-1} .

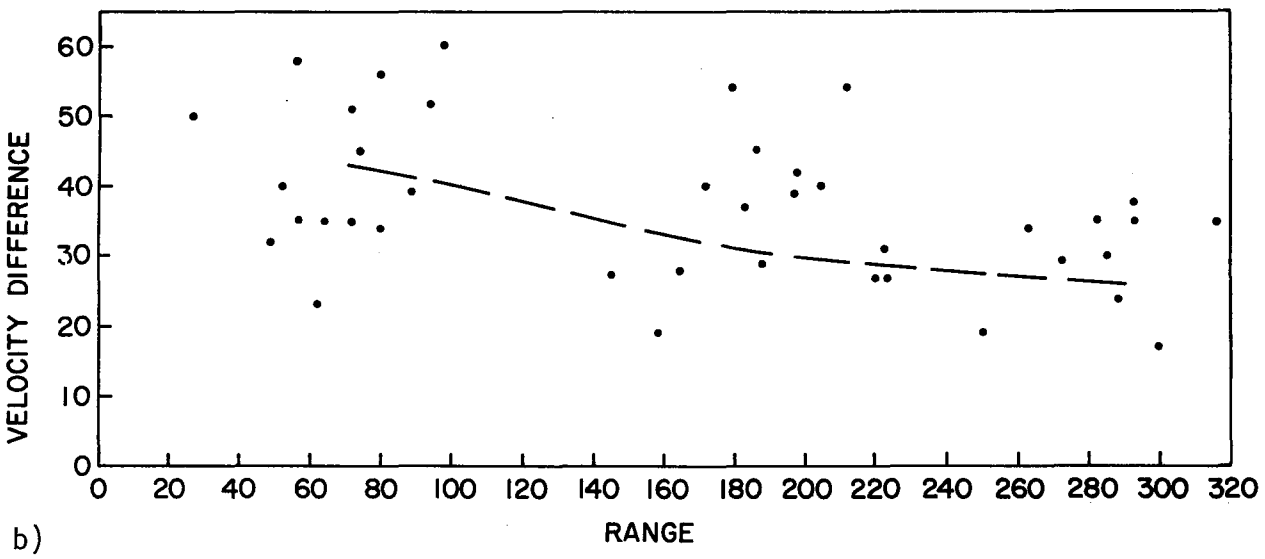
2.4 Engineering Possibilities

The new system can be developed with proven engineering and operational techniques. These techniques can be used innovatively, and little new engineering will be necessary. Since the beginning of JDOP the general philosophy has been that no "edge of the art" techniques or hardware requiring extensive engineering development would be considered.

Some signal sequencing schemes may prove attractive for the operational system. Those are depicted on Figure 8, and detailed descriptions are in Doviak et al. (1978) and Sirmans et al. (1976b). Here we present only the basic philosophy behind each including some potential advantages and drawbacks:



a)



b)

Figure 5. a) Measured mesocyclone diameters. Light lines are angular separations between velocity peaks. b) Measured peak-to-peak radial velocity. Dashed curves are theoretical for a mesocyclone of diameter 3.9 km and peak-to-peak radial velocity of 54 m s^{-1} , which are measured averages, corrected for beam-width and sampling effect. Data from Burgess (private communication).

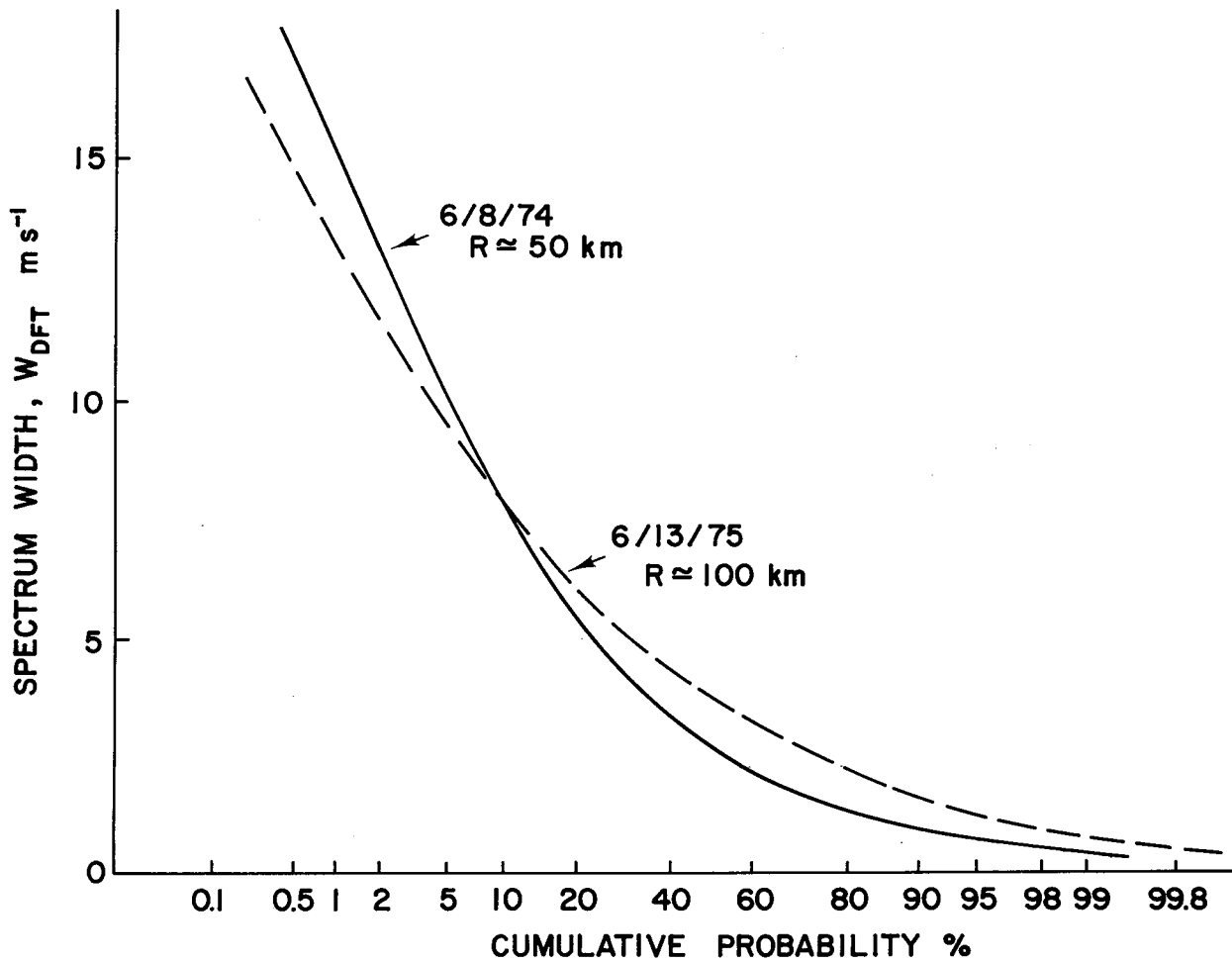


Figure 6. Cumulative probability (probability that width exceeds ordinate value) of spectrum width for two tornadic storms. Width calculated by DFT with threshold, bias removed by correction for Gaussian spectra. Note absence of strong range dependency in observed width. Radar resolution volume is $.8^\circ$ by 150 m.

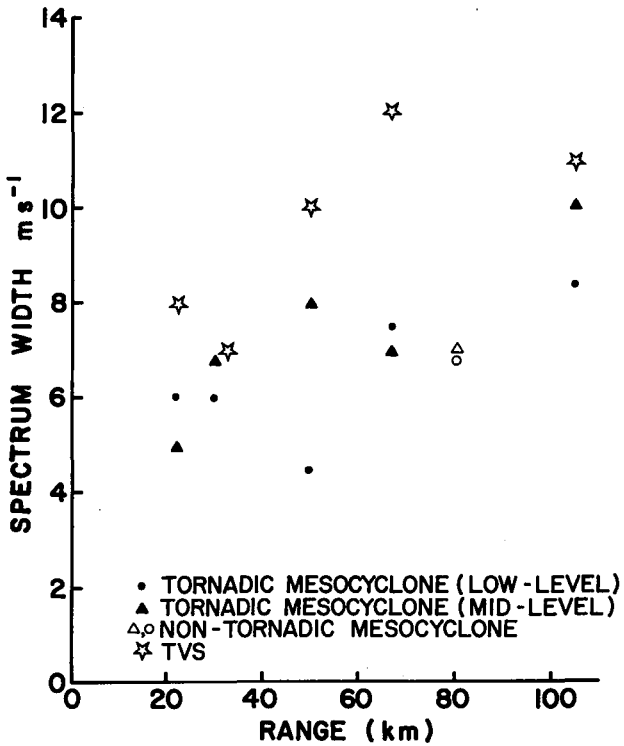


Figure 7. Velocity spectrum width versus range for the mesocyclone region. Each set of points (stratification by range) represents a different storm. Note extreme values in tornado vortex signature (TVS) and absence of strong range dependency.

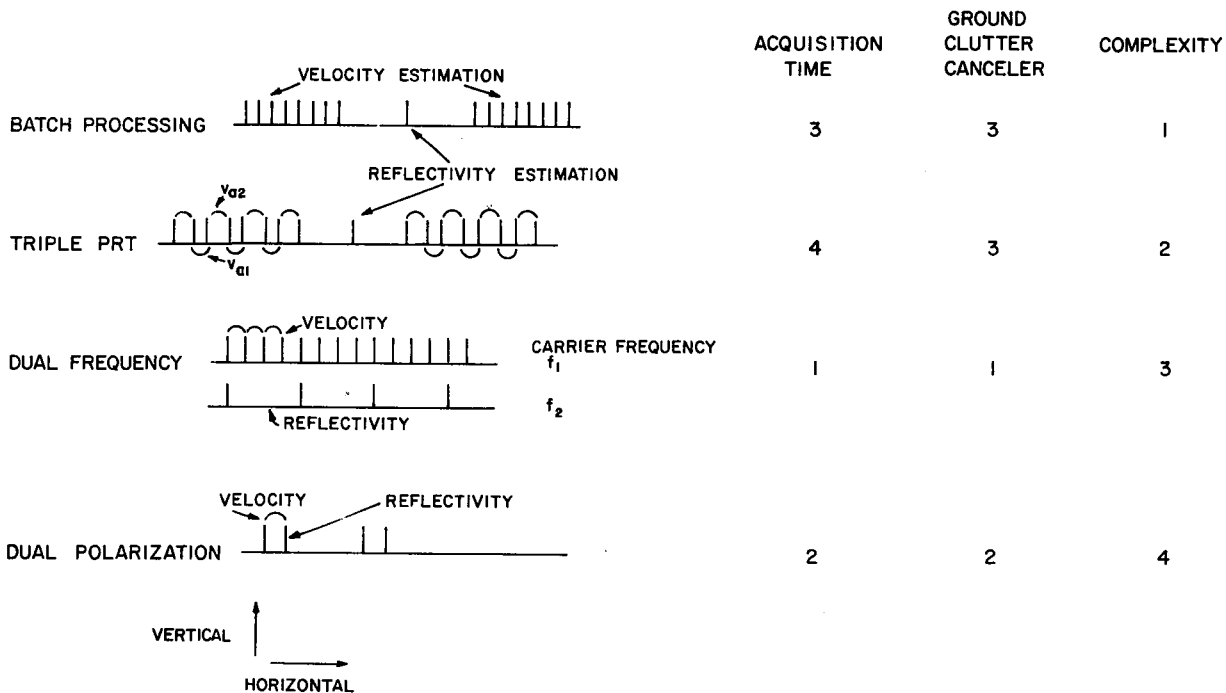


Figure 8. Signal schemes that can relax the range velocity ambiguity comparatively ranked. 1 means best; i.e., least acquisition time, most effective ground clutter canceler, or least complex system.

Batch processing is extensively discussed throughout this report and was successfully used during the experimental phase of JDOP. Batch processing is relatively simple to implement and gives accurate velocity estimates; reflectivity estimates are never contaminated with overlaid echoes. Although velocity estimates may become contaminated, this condition can be mitigated by change of PRF. Velocity aliasing can occur but is not detrimental. Spectral moments are determined by a technique that can operate on single pairs. Design of ground clutter cancelers is complicated except for removal of pure D.C. values.

The batch scheme with a single pair for velocity measurements is analogous to the double pulse technique described by Campbell and Strauch (1976). Those investigators did not use a separate pulse for reflectivity estimates, which is needed for unambiguous measurements of reflectivity to large distances (400-500 km) or the examination of erroneous velocities due to overlaid echoes.

Triple PRT uses two pulse separations for velocity measurements and a third for reflectivity measurement (Sirmans, et al., 1976b). The key to the technique is that velocity spectrum passes through two different Nyquist limits (v_{a1} and v_{a2}) when estimated with two different PRF's. Thus the two measurements differ by a known amount from which the true velocity can be determined. The two Nyquist limits can be made relatively small but not less than two to three times the spectrum width, or about 15 m s^{-1} , to preserve spectral shape. This increases the unambiguous range while the overall unambiguous velocity remains high. This requires twice as many calculations as does batch processing (Sirmans, et al., 1976a). The advantages are that velocity aliasing and contamination of velocity estimates with overlaid echoes are significantly reduced. As with the batch method, only the pure DC values produced by ground targets can be easily removed. The isolated transmitter pulse required for estimating intensity to large distances is also used to identify velocity estimates contaminated by multitrip echoes.

Dual Frequency: The use of two transmitted frequencies allows simultaneous but decoupled estimation of reflectivity and velocity (Fig. 8) in two separate channels at the receiver. This is equivalent to batch processing except that the velocity estimates are made on truly contiguous and uniformly spaced pulse returns that lend themselves to more effective ground clutter cancelation. Also, the scan time required to achieve the same standard error in estimates is somewhat reduced. Those improvements are at the expense of a more complicated (i.e., dual frequency) radar. Although two receiver chains are needed (as in batch), one broadband transmitter would probably suffice. Similarly, both signals would be transmitted through the same antenna and waveguide assembly.

Polarization Diversity: If the receiver could distinguish which of previous transmitted pulses correspond to a given return signal, range and velocity (r_a , v_a) would become decoupled. This idea has motivated researchers (Doviak and Sirmans, 1973) to suggest use of two orthogonally polarized pulses in a pair for velocity estimation. The scheme need not use a separate pulse for reflectivity measurements because ideally the two echoes would be separated in the receiver. However, meteorological targets are not perfect

spheres and each echo contains portions of both orthogonal polarizations; this limits separation. The added complexity is in the microwave section of the transmitter-receiver combination.

All the discussed schemes adapt readily to a selectable interpulse spacing for automatic or operator positioning of multiple trip signals into regions of minimal interference. As engineering technology advances, these types of systems will probably be more widely used in research programs for tornado detection, rainfall estimation, vertical air motion (when the antenna is oriented to the vertical), and the nature of scattering. More complex radars may also be developed such as the multibeam electronically steerable radar. The acquisition time with such a radar is vastly reduced because echoes from several elevation angles are received and processed simultaneously.

Although the techniques above are worth investigating, the 10 cm Doppler radar does not need refinements beyond those used during the JDOP experiment (batch processing) before operational implementation.

3. RADAR DESIGN CONSIDERATIONS

General performance guidelines for the operational Joint Use Doppler radars established by NWS, AWS, and FAA are the following:

- (1) detection and quantitative measurement of severe storm events to a range of at least 250 km;
- (2) quantitative measurement of intensity to a range of 250 km, surveillance to a range of 450 km;
- (3) detection of rainfall rates greater than 0.65 mm h^{-1} ($\log Z = 2$) to a range of 250 km (detection implies $\text{SNR} \geq 3\text{db}$);
- (4) antenna scan rate not less than 1 rpm for velocity data acquisition;
- (5) unambiguous velocity (v_a) not less than 25 m s^{-1} and range r_a (for velocity measurements) not less than 125 km, with quantitative velocity and spectrum width measurements over at least two times the unambiguous range interval (to 250 km);
- (6) standard deviation of intensity estimate should be about 1 dB and the standard deviation of mean velocity and spectrum width should be about 1 m s^{-1} .

Radar design parameters compatible with the characteristics listed above are given in Tables 1 and 2.

Table 1. Illustrative Doppler Radar Characteristics

Antenna

| | |
|-----------------------|-------------------------------|
| Shape | Parabolic |
| Diameter | 7.32 m (24 ft) |
| Half Power Beamwidth | 1° |
| Gain | 45 dB |
| First Side Lobe Level | -25 dB max (with radome) |
| Polarization | Linear-horizontal |
| Antenna Scan Rate | 0.5 to 3 rpm (both planes) |
| RHI | Yes |
| PPI | Yes |
| Manual Scan Control | Yes (both planes) |

Transmitter

| | |
|------------------------|---|
| Wavelength | 11.1 cm to 10.3 cm |
| Frequency | 2.7 GHz to 2.9 GHz |
| Peak Power | 500 kW min |
| Pulse Width | 1 μ s |
| Pulse Repetition Time* | Selectable equally spaced or batch discrete values of 835 μ s, 1024 μ s, 1167 μ s* |
| Duty Cycle | 1.2×10^{-3} max |

Receiver

| | |
|---|---------------|
| System Noise Figure (including radome and waveguide losses) | 4 dB |
| Transfer Function-Doppler | Linear |
| Transfer Function-Intensity | Logarithmic |
| Dynamic Range | 80 dB min |
| Doppler AGC | By range gate |

*See Table 2

Table 2. Illustrative System and Signal Processing Characteristics
(Batch Processing)

| | | | |
|------------------------------------|-----------------------|--|-----------------------|
| Pulse Repetition Time for velocity | 835 μs | 1024 μs | 1167 μs |
| Unambiguous Velocity | 31.5 ms^{-1} | 25.6 ms^{-1} | 22.5 ms^{-1} |
| Unambiguous Range | 125 km | 154 km | 175 km |
| Intensity Surveillance Range | 500 km | 460 km | 525 km |
| Velocity Range Cell Spacing | 122 m | 150 m | 170 m |
| *Intensity Range Cell Spacing | 488 m | 450 m | 510 m |
| No. of Intensity Range Cells | 1024 | 1024 | 1024 |
| No. of Velocity Range Cells | 1024 | 1024 | 1024 |
| Range Sampling | 122 m | 112.5 m | 127.5 m |
| <u>Reflectivity</u> | | | |
| No. of Range Samples Averaged | | 4 | |
| Output Resolution (8 bits) | | <.4 dB | |
| No. of Time Samples | | Selectable 4 to 32 | |
| <u>Velocity</u> | | | |
| No. of Samples Averaged | | Selectable 16 to 256 | |
| Output Resolution (8 bits) | | <.25 ms^{-1} | |
| Estimated Standard Deviation | | | |
| Intensity | | 1 dB to 1.7 dB | |
| Velocity | | 0.5 ms^{-1} to 0.9 ms^{-1} | |
| Width | | 0.6 ms^{-1} to 1 ms^{-1} | |

* In equally-spaced pulse mode, the intensity and velocity range resolution is the same.

4. NEXRAD

The advisory and warning programs of NWS and AWS are in jeopardy because the weather radars, some of the most important observation tools, are approaching the end of their useful lives. In response to this need, the NEXRAD Program has been established.

The NEXRAD system, by using Doppler radar, will improve the accuracy and timeliness of warnings. Modern data processing techniques will improve the accuracy and speed of precipitation rate analyses and area motions, and the data will be made available more quickly to the users.

The term NEXRAD encompasses all the next generation radar data system including radars, data processors, facilities for communication and display of processed data, staff and its training, administration, and supporting funds.

The JDOP has clearly shown that training will be an important problem in NEXRAD. Handling Doppler velocity data is different from handling reflectivity data. Therefore, operators will have to be retrained beginning with an introduction to basic Doppler radar principles. Although computerized echo tracking routines are already well established and identification of storm signatures by computer is a promising early capability, meteorologists who understand the computer programs and who can interpret the velocity data for themselves are needed when the programs fail. They also must understand mesocyclone and tornado vortex signatures and the limitations of Doppler radar, such as range and velocity ambiguities in relation to pulse repetition frequency. Training can be facilitated by playback of recorded data from special events and by audio-visual training methods. During JDOP, an intensive 5-day training course was followed by several weeks of on the job training with experienced operators. The training needs of the various agencies will be similar, and important economies would be realized by a common training program.

A discussion of Doppler data display systems is contained in Appendix A.

* A course outline is given in the JDOP report for 1977.

APPENDIX A
RADAR DATA DISPLAYS

Kenneth Shreeve

Equipment Development Laboratory
National Weather Service
Silver Spring, Md.

1. INTRODUCTION

A major system design problem with radar displays is transformation of radar information into an easily understandable form. Large quantities of reflectivity and velocity data have little value unprocessed and communication to users is difficult and costly. The data must be processed, either by machine or by well-trained operational staff, to extract information needed for warning and forecast programs. The JDOP experiments show that automated data reduction is needed to assure accurate evaluation and timely recognition of all significant weather events within the radar coverage area. The 1979 tests explored techniques for automated processing and remote display.

Graphic displays that combine more than one parameter to depict events are needed to use the radar data effectively. The radar operator must extract from these displays all important events and a situation summary, without spending many minutes in visual analysis. Without some automatic data processing to help the radar operator's interpretation some storm events may go undetected.

Several kinds of radar data displays are needed. The recognition of patterns requires graphic displays, especially where three dimensions are involved. Alpha-numeric displays are needed for point-type data, system dialogue, and messages. Graphic displays, including vector and symbolic annotations, seem to be the most effective way to display radar data for operations. Radar system control, including remote communications, data review, and scheduling, is best handled by an alpha-numeric display and associated keyboard.

2. DISPLAYS RECOMMENDED FOR NEXT GENERATION WEATHER RADAR

Two general radar site configurations are possible: those with the transmitter-receiver and antenna assembly located with the operator work station (within 200-300 cable ft) and those sites where they are not collocated (up to 25 mi away). In both cases the equipment and location are the same

except that an additional PPI display at remote transmitter-receiver sites is recommended to facilitate maintenance.

The general recommended equipment grouping can be broken down into three sections listed below:

(1) Transmitter - receiver - antenna site:

At this site only equipment calibration and maintenance equipment is located. The A/R-scope display is the only one recommended, except for remote sites where a small PPI display is also needed.

The A/R-scope display should be designed to monitor all real time video streams at different points throughout the system and be able to display up to four in combination, for quality control and manual calibration checks. In older radar systems this display was used by radar operators to help distinguish weather from non-weather targets and determine point reflectivity values. In a new radar system these functions will be available on the color graphic display by using a keyboard and cursor to identify points of interest.

(2) Maintenance - control console:

This equipment is located with the operator's work station. Besides being used for maintenance and control, it serves as fall-back equipment for the operator if the primary data processing equipment fails. At this location an A/R-scope and PPI displays are available.

(3) Operator's work station:

At this location alpha-numeric and color graphic displays are recommended for any next-generation radar system. With these the operator has access to the memory and can control the system and regulate the dissemination of external communications. The operator should be able to monitor all major scheduled tasks including active communications. All system alarms, including general systems operations and meteorologically significant messages, should be displayed on this unit.

The primary weather monitor is the color graphic display. All meteorological and hydrological situation depictions can be displayed in area contoured color with alpha-numeric annotations and graphic overlays. Echo reflectivity can indicate general storm motion and severity. Storm severity can be diagnosed from Doppler information with display of mean radial velocity or horizontal shear. These provide information on surface and upper level winds and identify gust fronts and severe circulations associated with mesocyclones and tornadoes. A display of hydrologic data such as accumulations or accumulation rates are valuable for flash flood warnings and as an input to river stage forecasting. Three dimensional hydrologic summaries such as the vertical integrated liquid water content (VIL) also are important for severe weather and flash flood alarms.

The computer-driven color graphic display seems to be the best currently available to depict summaries of general meteorologic and hydrologic situations. The graphic display equipment should be located so that forecasters and other operational personnel can share information if they are both located within the radar facility.

3. RECOMMENDED DISPLAY SPECIFICATIONS

3.1 A/R-Scope Display

The A/R-Scope Display is normally a plot of range vs. signal amplitude. The R-Scope provides an expanded section of the A-Scope presentation. With the advent of more advanced frontend signal processing, the conventional A/R-Scope Display has been modified to include unprocessed output of the logarithmic receiver, I and Q components of the linear receiver and processed video streams including mean velocity and velocity spectral-width data. It allows real time monitoring of signal characteristics, which is an invaluable tool for technical personnel for maintenance and quality control.

The following performance specifications are recommended:

Size: 8 vertical x 10 horizontal cm minimum.
Bandwidth: 15 mHz minimum.
Sweep Range: A-Scope, 0-50 to 0-1000 km; R-Scope, 0-10 to 1-100 km.
Sweep Delay, R-Scope: 0 to 450 km.
Range Strobe (marker): operator adjustable with 1 km resolution out to 450 km.
Range Markers: available at several operator selected intervals.
Number of traces (channels): 4 minimum.

3.2 Plan Position Indicator (PPI) Display

The common PPI display presents reflectivity, velocity, and other processed videos as Z-axis modulation on a polar plot with the radar usually located at the center of the display. The PPI is still probably best to show echo locations where computer driven displays are not available, and it is the optimum fallback display when onsite computer systems have temporarily failed. During maintenance of equipment, it is also helpful for distinguishing radar problems from data processing problems.

Recommended performance specifications for a PPI Display include the following:

Size: 9 in diameter minimum.
Bandwidth: 10 mHz minimum.
Sweep ranges: 0-125 km, 0-450 km.
Range marks: several operator selectable.
Gray scale: 6 minimum.

Geographic linearity: 2% or better.
Range Strobe: provided, same as for A/R scope.
Phosphor: P7.

3.3 Alpha-Numeric Display

Speed, flexible symbology, and economy make the alpha-numeric display superior to the rigid formats of hard copy printers. This display is needed for system dialogue, operator generated messages, system alarm messages, and control and monitoring of communications.

Recommended performance for an alpha-numeric display is as follows:

Display size: 12 in diagonal minimum with a display area of 50 square in minimum.

Number of displayed characters: 1,920 minimum.

Number of characters per line: 80 minimum.

Number of lines: 24 minimum.

Displayable characters: full ASCII set.

Minimum character size: 0.12 in high x 0.075 in wide.

Resolution: 800 TV lines at 50-ft-lumens minimum.

Phosphor: P31 or P39.

Geometric linearity: 2% of picture height.

Contrast ratio: 10:1 at 50-ft-lumens minimum.

3.4 Color Graphic Display

Another consideration in designing a weather radar display is visual dynamic range. Both black and white and color displays are available with more than adequate equivalent gray shades, but the visual dynamic range is considerably different. The color display has better feature separation (high-lighting), facilitates subjective interpretation of data categories, and helps emphasize important features.

Three kinds of color displays are available: Raster-Scan, Penetron, and stroke-generator types. The Penetron is good for displaying areal data but has only three to six distinct colors and is very expensive. Stroke-generator displays are very efficient for alpha-numeric and vector-graphic presentations but produce area contours only in a cross-hatching mode. The Raster-Scan display appears to be the most practical for daily use. Further research on specialized displays is required.

Generally, area contouring is superior to isoline contouring, since the latter produces rather crude outlines. Unless smoothed artificially, the fine structure associated with contouring three or more categories using thin lines makes the display unreadable.

One drawback of any color display is the difficulty that an operator with abnormal color vision has in color interpretation. Selectable color mixing capability allows the operator to color-encode as suits his visual

perception. Since this prevents having standard color category representations for a given data display, a standardized color table is encouraged except for those operators with abnormal color vision.

General recommended performance specifications are the following:

- CRT size: 19 in diagonal minimum.
- CRT type: color, negative black matrix, high resolution shadow mask
- Type display: red-green-blue (RGB) color
- Geometric linearity: 2% of picture height
- Color convergence, in terms of color separation (misconvergence):
 - less than 0.5 mm within a central area bounded by a circle equal to the picture height and 1.0 mm outside that area
- Color triad spacing: 0.31 mm or smaller
- Display pixel resolution: 320 H x 256 V x 16 categories (bits) per pixel for radar data and 640 H x 512 V for each of 2 overlays
- Vertical frame rate: nominal 60 Hz synchronized to the input power line
- Contrast ratio: 10:1 at 50 ft lamberts minimum
- Color mix table size: 16 shades for each of the red, green, and blue for each of 64 pixel categories.
- Vector and conic section generation: provided for overlay use.
- Character generation: full ASCII set in two font sizes, one for data areas and a smaller set for overlays.

3.5 Stroke-generator Displays

A stroke-generator display is one designed to draw short and long thin lines in any place and in any direction on the display. This type display is optimized for thin line drawing of all kinds. The NSSL multi-moment display consisting of a matrix of arrows is an excellent example. To date, little work has been done with this type display in the weather radar field. It provides the ability for excellent fine line detail but has little effective gray scale range. Further study and development of this type display may make it attractive and desired in NEXRAD.

Recommended performance specifications include:

- CRT size: 21-in diagonal minimum.
- Addressable and viewable display locations: 2,048 x 2,048 minimum.
- Spot size: 0.020-in maximum.
- Minimum drawing speed: 2000 inch long vectors, at 30 frames per second.
- Frame rate: Sufficient to provide flicker-free display.

4. REMOTE DISPLAYS

Little experience has been gained in remoting displays from the radar site in the JDOP program. Remoting requires a long time to communicate a

high resolution display over conventional phone lines. For example, transmitting a 256 x 256 rasterscan display takes approximately 2 min at 2400 baud. Transmitting a more desirable display with 320 x 256 x 6-bit resolution (similar to that used in the JDOP experiment) requires approximately 3.75 min. These times can be reduced by more expensive and faster equipment, e.g., 4800 or 9600 baud equipment. The cost of communications equipment approximately doubles as the speed doubles.

At the radar site the operator has the data display storage at hand and can quickly review a variety of them. At a remote site, equipment must be provided to store several displays for call-up by the remote user, or the user must be satisfied with a single or alternating display in a serial format.

APPENDIX B
PLANS FOR 1979

Kenneth Glover

Weather Radar Branch
Air Force Geophysics Laboratory
Sudbury, Massachusetts

1. GENERAL CONSIDERATIONS

During these investigations, the subject of common requirements for a new generation weather radar system among NOAA, USAF and FAA has received considerable attention. Initially, discussions centered around integrated specifications for the basic radar and manual techniques for its use; however, as each of the JDOP participants became more familiar with the requirements of the other agencies, it became apparent that the original concept might be expanded to take advantage of economies afforded by the coordinated location, use, and operation of the proposed radar system.

The rationale behind this expanded concept of operations is based in large measure on success by the JDOP in defining specifications of a system which meets the needs of each of the three agencies. Although the agencies' uses of Doppler information will differ, one data source should suffice. With judicious placement of radars and full coverage data remoted to the various users in a cost effective manner, national Doppler coverage can be provided with considerable savings in both initial and ongoing costs.

An important technical problem is the transmission of data to the users. All data may be transmitted by microwave in real time, or a smaller amount of processed data may be transmitted less expensively by telephone lines. FAA and USAF require more computer-automated products, whereas NOAA's National Weather Service places more emphasis on man and machine in an interactive role.

2. THE 1979 EXPERIMENT

The need for a test to compare "automated analysis" information with man-machine interactive capability at sites remote from the radar was discussed at several meetings of the JDOP participants. During the August 1978 meeting of the Working Group on Next Generation Weather Radar (WG/NGWR), AFGL offered use of equipment for automated Doppler analysis and combination with manual analysis techniques that would provide a summary of Doppler information at one and possibly two remote locations. A joint agency meeting was held on 18-19 September 1978 at the AFGL Weather Radar Facility, Sudbury, MA, to plan the test given the limitations of manpower, funding and equipment.

The NSSL radars are assigned to the Severe Environmental Storms and Mesoscale Experiment (SESAME) through the spring of 1979. During this time, AFGL's 5.5 cm Doppler radar will be deployed at NSSL to acquire data for an independent hail research program. This program requires a continuous volumetric scanning sequence for the radar antenna as in earlier JDOP tests. The AFGL remote color display and the on-line computer facility are not required for the real time portion of their hail research program. Thus these facilities and the Doppler information they provide can be available for JDOP '79 tests. Participants agreed that most problems arising from using the 5.5 cm wavelength (rather than the 10 cm as in previous years) should be resolved by locating AFGL computer and display equipments with those of NSSL.

The members decided on the following objectives for the spring 1979 JDOP:

- a. Evaluate one or more methods for transmitting data to a remote site;
- b. Evaluate one or more types of systems for data display;
- c. Provide input to warning agencies from the remote site.

To accomplish these objectives, the experimental configuration shown in Fig. 1 is proposed. The plan calls for remoting the computer/ manual processed data every five minutes or less* to the Oklahoma City Weather Service Forecast Office (OKC WSFO) and the FAA Traffic Control Center (TRACON) at Tinker AFB. The same data will be transmitted to both locations.

Most storms in western and central Okla. will be scanned by the NSSL 10 cm Doppler radar and signature information will be given to JDOP personnel. Therefore, JDOP annotated displays may contain a mix of 5 cm and 10 cm information.

The man/computer generated color display planned for JDOP 79 (built by AFGL and NWS) is a modified version of the AFGL computer display described earlier in this report. The reflectivity data will consist of two different colored areas for each identified cell. One area will represent the low-level, weak reflectivity (e.g., greater than 15 dBZ) pattern. The second area will represent higher reflectivity (e.g., 30 dBZ) cores of the cells. Super-imposed on this pattern will be the cells' past tracks and future extrapolated positions in unique color coded segments associated with a particular analysis time period, indicated on the right side of the display. Ten past positions and two forecast positions (prefaced by the letter F) and their associated times will be displayed. A unique hexadecimal number will be plotted next to the beginning of each cell track. This location will prevent blocking out of the high reflectivity core area under most circumstances. Beneath the analysis times on the right side of the display will be a numerical listing of the detected cells and their associated severe weather events determined by the AFGL radar meteorologist. Overlaid on the radar data will be an Oklahoma county map for reference purposes.

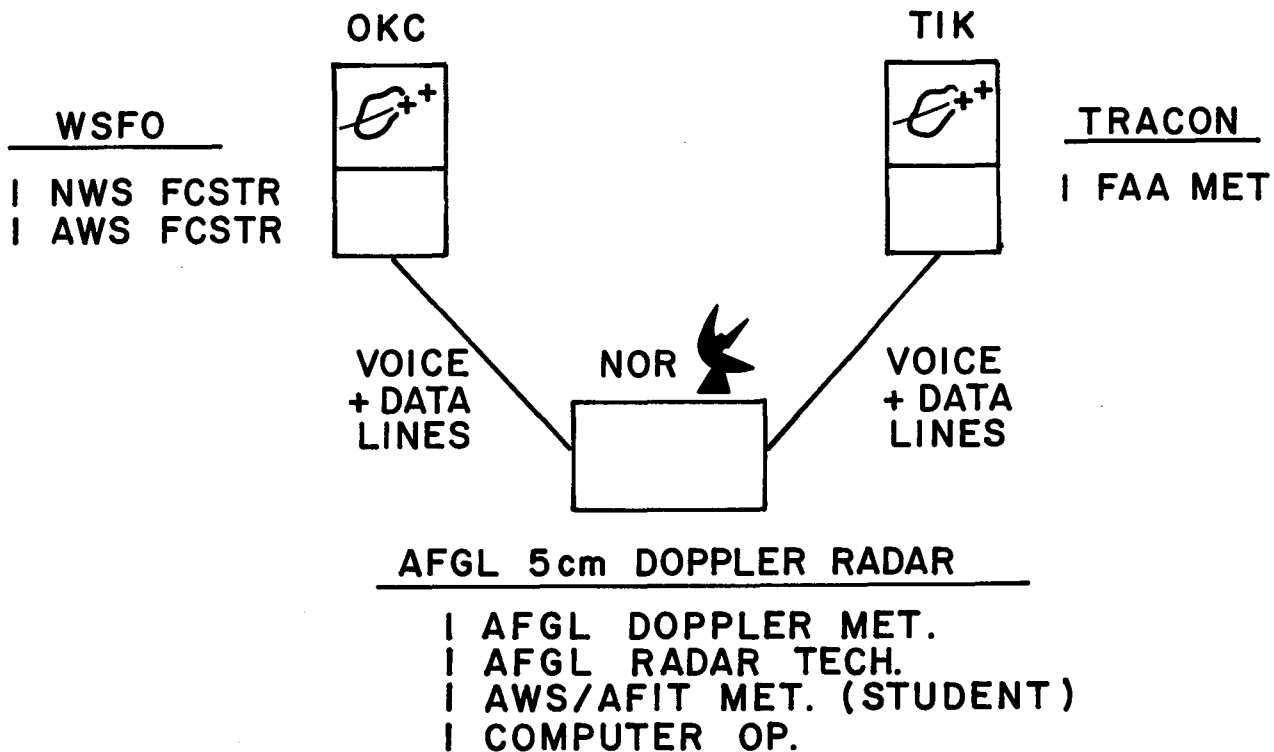
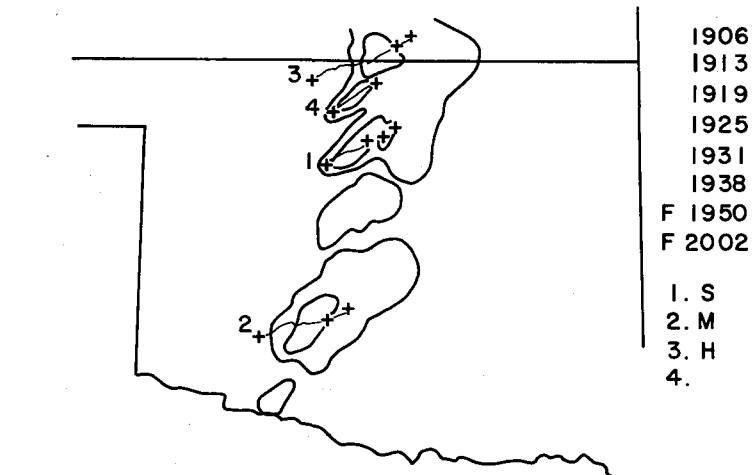


Figure 1. Experimental Configuration for JDOP '79.

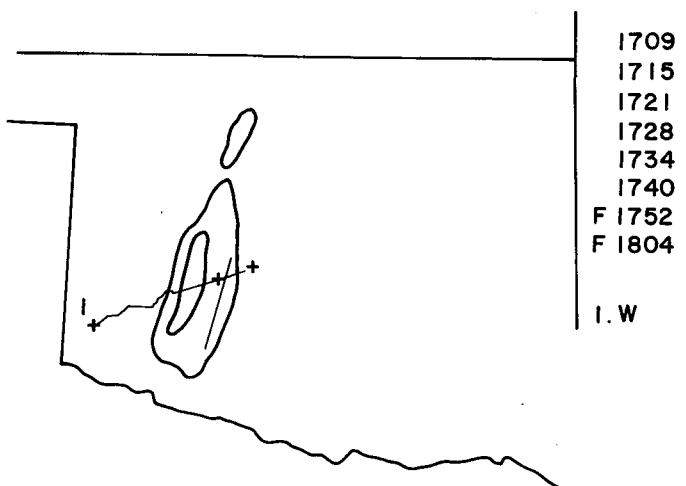
An artist's conception of the display for April 5, 1978 is shown in Fig. 2a. The two reflectivity contours are the 15- and 30-dBZ levels. The associated severe weather events, as determined by the radar meteorologist,

are strong shear with echo one, a mesocyclone with echo two, hail with echo three and none with echo four. These are signified by 1.S, 2.M, 3.H, and 4., respectively.

Figure 2b shows a gust front core similar to the one on May 2, 1978. The line drawn ahead of the echo area is the gust front location and strong surface winds are indicated by the 1.W on the right side.



a)



b)

Figure 2a & b. Schematic drawings of display data to be remoted to NWS and FAA operations.

The severe weather indicators are as follows: H, large hail, S; strong shear; M, mesocyclone; T, tornado vortex signature; W, damaging surface winds; and B, bad data. Up to three letters can be used with any one echo. Shears, mesocyclones and TVS's are assumed to be the same phenomena in different stages of development; thus only one would be used at a given time for a given echo. Although hail and damaging surface winds are often associated with a mesocyclone or TVS but not necessarily with strong shear, these three (H, W and S) could be used concurrently. The bad data indicator, B, could be used to show echoes where the nature of the flow field cannot be determined because of velocity folding or range folding.

Attempts have been made to provide the type of information in the display format that one would expect to be generated automatically, by a computer, in the foreseeable future. The data presented will not be a final product for a new generation system, but rather an example of a computer-generated display synthesized from the reflectivity, Doppler velocity, and shear displays.

ACKNOWLEDGMENTS

The authors gratefully acknowledge efforts of Edwin Kessler, Kenneth Wilk, and Dusan Zrnic in organizing and editing this report. The figures were prepared by Charles Clark and Jennifer Moore, and the manuscript typed by Connie Hall.

REFERENCES

- Armstrong, G. M. and R. J. Donaldson, Jr., 1969: Plan shear indicator for real time Doppler radar identification of hazardous storm winds. J. Appl. Meteor., 8(3), 376-383.
- Atlas, D., 1976: Overview: The prediction, detection, and warning of severe storms. Bull. Amer. Meteor. Soc., 57(4), 398-401.
- _____, 1964: Advances in radar meteorology. Chapter in Advances in Geophysics, Landsberg and Mieghem, Editors. New York: Academic Press, 317-478.
- Bjerkaas, C. L., and R. J. Donaldson, 1978: Real time tornado warning utilizing Doppler velocities from a color display. Preprints, 18th Radar Meteorology Conf., AMS, Boston, Mass., 449-452.
- Boak, T. I. S., A. J. Jagodnik, R. B. Marshall, D. Rice and M. J. Young, 1977: R & D Equipment Information Report, Tracking and Significance Estimator. AFGL-TR-77-0259, 118.
- Bonewitz, J. D., 1978: Development of Doppler radar techniques for severe thunderstorm wind advisories. Master's Thesis, University of Oklahoma, Norman, Oklahoma, 67 pp.
- Brown, R. A., and L. R. Lemon, 1976: Single Doppler radar vortex recognition Part 2 - Tornadic vortex signature. Preprints, 17th Radar Meteorology Conf., AMS, Boston, Mass., 104-109.
- _____, D. W. Burgess, and Kenneth C. Crawford, 1973: Twin tornado cyclones within a severe thunderstorm: Single Doppler radar observations. Weatherwise, 26(2), 63-71.
- Burgess, D. W., 1976: Single Doppler radar vortex recognition: Part I - Mesocyclone signatures. Preprints, 17th Radar Meteorology Conf., AMS, Boston, Mass., 97-103.
- _____, J. D. Bonewitz, and D. R. Devore, 1978: Joint Doppler operational project: Results year 1. Preprints, 18th Severe Local Storms Conf., AMS, Boston, Mass., 442-448.
- _____, L. D. Hennington, R. J. Doviak, and P. S. Ray, 1976: Multi-moment Doppler display for severe storm identification. J. Appl. Meteor., 15(12), 1302-1306.
- _____, L. R. Lemon and R. A. Brown, 1975: Tornado Characteristics revealed by Doppler radar. Geo. Res. Lett., 2(5), 183-184.
- Campbell, W. C., and R. G. Strauch, 1976: Meteorological Doppler radar with double pulse transmission. Preprints, 17th Radar Meteorology Conf., AMS, Boston, Mass., 42-44.

- Chimera, A. M., 1960: Meteorological radar echo study. Final Rept. Contract AF33(616)-6352, Cornell Aero. Labs., Buffalo, New York.
- Cooley, J. R., 1978: Cold air funnel clouds. Mon. Wea. Rev., 106(9), 1368-1372.
- Donaldson, R. J., Jr., 1970: Vortex signature recognition by a Doppler radar. J. Appl. Meteor., 9(4), 661-670.
- Doviak, R. J., D. Sirmans, D. Zrnica and G. B. Walker, 1978: Considerations for pulse-Doppler radar observations of severe thunderstorms. J. Appl. Meteor., 17(2), 189-205.
- _____, and C. T. Jobson, 1978: Dual Doppler-radar observations of clear air wind perturbations in the planetary boundary layer. J. Geophys. Res., 84(C2), 697-702.
- _____, and D. Sirmans, 1973: Doppler radar with polarization diversity. J. Atmos. Sciences, 30(4), 737-738.
- Fujita, T. T., 1973: Tornadoes around the world. Weatherwise, 26(2), 56-62.
- Groginsky, H. L., 1965: The coherent memory filter. Electron Prog., (Raytheon Co.), 9(3), 7-13.
- Hennington, L., R. J. Doviak, D. Sirmans, D. Zrnica, and R. G. Strauch, 1976: Measurements of winds in the optically clear air with microwave pulse-Doppler radar. Preprints, 17th Conf. on Radar Meteor., Am. Meteor. Soc., Boston, Mass., 342-348.
- Hitschfield, W., and J. Bordan, 1954: Errors inherent in the radar measurement of rainfall at attenuating wavelength. J. Meteor., 11(1), 58-67.
- Houbolt, J. C., R. Steiner and K. Pratt, 1964: Dynamic response of airplanes to atmospheric turbulence including flight data or input and response. NASA Technical Report TR R-199 NASA Washington, D.C., 7-18.
- Hyde, G. H. and K. E. Perry, 1958: Doppler phase difference integrator. M.I.T. Tech. Rep. 189.
- Joss, J., Cowalli and R. K. Crane, 1974: Good agreement between theory and experiment for attenuation data. J. de Recherches Atmospheriques, VII, 299-318.
- Kraus, M. J., R. J. Donaldson, Jr., and C. L. Bjerkass, 1977: Severe thunderstorm and tornado warning in real time by color display of Doppler velocities. Preprints, 10th Severe Local Storms Conf., AMS, Boston, Mass., 81-83.
- Lee, J. T., J. Stokes, Y. Sasaki, and T. Baxter, 1978: Thunderstorm Gust Fronts--Observations and Modeling. Final Rpt. #FAA-RD-78-145 to Systems Research and Development Serv., FAA, Wash. D.C. 20590.

- Lee, J. T., 1977: Application of Doppler weather radar to turbulence measurements which affect aircraft. Final Rpt. #FAA-RD-77-145 to Systems Research and Development Serv., FAA, Wash. D.C. 20590.
- Lemon, L. R., 1977: New severe thunderstorms radar identification techniques and warning criteria: A preliminary report. NOAA Technical Memo NWS NSSFC-1.
- _____, R. J. Donaldson, Jr., D. W. Burgess and R. A. Brown, 1977: Doppler radar application to severe thunderstorm study and potential real-time warning. Bull. Amer. Meteor. Soc., 58(11), 1187-1193.
- Lhermitte, R. M., 1972: Real time processing of meteorological Doppler radar signals. Preprints, 15th Conf. on Radar Meteor., Am. Meteor. Soc., Boston, Mass., 364-367.
- Miller, K. S. and M. M. Rochwarger, 1972: A covariance approach to spectral moment and estimation. IEEE Trans. Inf. Theory, IT-18, 588-596.
- Mueller, E. A. and E. J. Silha, 1978: Unique features of the CHILL radar system. Preprints, 18th Conf. on Radar Meteor., Am. Meteor. Soc., Boston, Mass., 381-382.
- Novick, L. R. and K. M. Glover, 1975: Spectral mean and variance estimation via pulse pair processing. Preprints, 16th Conf. on Radar Meteor., Am. Meteor. Soc., Boston, Mass., 1-5.
- Rummler, W. D., 1968: Introduction of a new estimator for velocity spectral parameters. Tech. Memo MM-68-4121-5, Bell Telephone Labs., Whippany, N.J.
- _____, 1968: Accuracy of spectral width estimators using pulse pair waveforms. Bell Telephone Labs., Whippany, N.J., Tech. Memo.
- Sirmans, D., D. W. Burgess and D. S. Zrnic, 1976a: Consideration for the Doppler conversion of NWS radars. (NWS report)
- _____, D. S. Zrnic and W. C. Bumgarner, 1976b: Extension of maximum unambiguous Doppler velocity by use of two sampling rates. Preprints, 17th Radar Meteorology Conf., AMS, Boston, Mass, 23-28.
- _____, and W. C. Bumgarner, 1975: Estimation of spectral density mean and variance by covariance argument techniques. Preprints, 16th Radar Meteorology Conf., AMS, Boston, Mass., 6-13.
- _____, and R. J. Doviak, 1973: Pulsed-Doppler velocity isotach displays of storm winds in real time. J. Appl. Meteor., 12(4), 694-697.
- Weible, M., and D. Sirmans, 1976: Simulations of attenuation by rainfall at a wavelength of 5 cm. Preprints, 17th Radar Meteorology Conf., AMS, Boston, Mass., 75-78.

Wilk, K., K. Gray, C. Clark, D. Sirmans, J. Dooley, J. Carter, and W. Bumgarner, 1976: Objectives and accomplishments of the NSSL 1975 Spring Program. NOAA Tech. Memo ERL NSSL-78.

Woodman, R. F. and T. Hagfors, 1969: Methods for the measurement of vertical ionospheric motions near the magnetic equator by incoherent scattering. J. Geophys. Res., 75(5), 1205-1212.

Zrnic, D. S., 1977: Spectral moment estimates from correlated pulse pairs. IEEE Trans. on Aero. and Elec. Systems., AES-13(4), 344-354.

_____, and W. C. Bumgarner, 1975: Receiver chain and signal processing effects on the Doppler spectrum. Preprints. 16th Radar Meteorology Conf., AMS, Boston, Mass., 163-168.

NATIONAL SEVERE STORMS LABORATORY

The NSSL Technical Memorandum, beginning with No. 28, continue the sequence established by the U. S. Weather Bureau National Severe Storms Project, Kansas City, Missouri. Numbers 1-22 were designated NSSL Reports. Numbers 23-27 were NSSL Reports, and 24-27 appeared as subseries of Weather Bureau Technical Notes. These reports are available from the National Technical Information Service, Operations Division, Springfield, Virginia 22151, for \$3.00 and a microfiche version for \$0.95. NTIS numbers are given below in parentheses.

- No. 1 National Severe Storms Project Objectives and Basic Design. Staff, NSSP. March 1961, 16 p. (PB-168207)
- No. 2 The Development of Aircraft Investigations of Squall Lines from 1956-1960. B. B. Goddard. 34 p. (PB-168208)
- No. 3 Instability Lines and Their Environments as Shown by Aircraft Soundings and Quasi-Horizontal Traverses. D. T. Williams. February 1962. 15 p. (PB-168209)
- No. 4 On the Mechanics of the Tornado. J. R. Fulks. February 1962. 33 p. (PB-168210)
- No. 5 A Summary of Field Operations and Data Collection by the National Severe Storms Project in Spring 1961. J. T. Lee. March 1962. 47 p. (PB-165095)
- No. 6 Index to the NSSL Surface Network. T. Fujita. April 1962. 32 p. (PB-168212)
- No. 7 The vertical structure of Three Dry Lines as Revealed by Aircraft Traverses. E. L. McGuire. April 1962. 10 p. (PB-168213)
- No. 8 Radar Observations of a Tornado Thunderstorm in Vertical Section. Ralph J. Donaldson, Jr. April 1962. 21 p. (PB-174859)
- No. 9 Dynamics of Severe Convective Storms. Chester W. Newton. July 1962. 44 p. (PB-163319)
- No. 10 Some Measured Characteristics of Severe Storms Turbulence. Roy Steiner and Richard H. Rhyne. July 1962. 17 p. (N62-16401)
- No. 11 A Study of the Kinematic Properties of Certain Small-Scale Systems. D. T. Williams. October 1962. 22 p. (PB-168216)
- No. 12 Analysis of the Severe Weather Factor in Automatic Control of Air Route Traffic. W. Boynton Beckwith. December 1962. 67 p. (PB-168217)
- No. 13 500-Kc./Sec. Sferics Studies in Severe Storms. Douglas A. Kohl and John E. Miller. April 1963. 36 p. (PB-168218)
- No. 14 Field Operations of the National Severe Storms Project in Spring 1962. L. D. Sanders. May 1963. 71 p. (PB-168219)
- No. 15 Penetrations of Thunderstorms by an Aircraft Flying at Supersonic Speeds. G. P. Roys. Radar Photographs and Gust Loads in Three Storms of 1961 Rough Rider. Paul W. J. Schumacher. May 1963. 19 p. (PB-168220)
- No. 16 Analysis of Selected Aircraft Data from NSSL Operations, 1962. T. Fujita. May 1963. 29 p. (PB-168221)
- No. 17 Analysis of Methods for Small-Scale Surface Network Data. D. T. Williams. August 1963. 20 p. (PB-168222)
- No. 18 The Thunderstorm Wake of May 4, 1961. D. T. Williams. August 1963. 23 p. (PB-168223)
- No. 19 Measurements by Aircraft of Condensed Water in Great Plains Thunderstorms. George P. Roys and Edwin Kessler. July 1966. 17 p. (PB-173048)
- No. 20 Field Operations of the National Severe Storms Project in Spring 1963. J. T. Lee, L. D. Sanders, and D. T. Williams. January 1964. 68 p. (PB-168224)
- No. 21 On the Motion and Predictability of Convective Systems as Related to the Upper Winds in a Case of Small Turning of Wind with Height. James C. Fankhauser. January 1964. 36 p. (PB-168225)
- No. 22 Movement and Development Patterns of Convective Storms and Forecasting the Probability of Storm Passage at a Given Location. Chester W. Newton and James C. Fankhauser. January 1964. 53 p. (PB-168226)

- No. 23 Purposes and Programs of the National Severe Storms Laboratory, Norman, Oklahoma. Edwin Kessler. December 1964. 17 p. (PB-166675)
- No. 24 Papers on Weather Radar, Atmospheric Turbulence, Sferics and Data Processing. August 1965. 139 p. (AD-621586)
- No. 25 A Comparison of Kinematically Computed Precipitation with Observed Convective Rainfall. James C. Fankhauser. September 1965. 28 p. (PB-168445)
- No. 26 Probing Air Motion by Doppler Analysis of Radar Clear Air Returns. Roger M. Lhermitte. May 1966. 37 p. (PB-170636)
- No. 27 Statistical Properties of Radar Echo Patterns and the Radar Echo Process. Larry Armijo. May 1966. The Role of the Kutta-Joukowski Force in Cloud Systems with Circulation. J. L. Goldman. May 1966. 34 p. (PB-170756)
- No. 28 Movement and Predictability of Radar Echoes. James Warren Wilson. November 1966. 30 p. (PB-173972)
- No. 29 Notes on Thunderstorm Motions, Heights, and Circulations. T. W. Harrold, W. T. Roach, and Kenneth E. Wilk. November 1966. 51 p. (AD-644899)
- No. 30 Turbulence in Clear Air Near Thunderstorms. Anne Burns, Terence W. Harrold, Jack Burnham, and Clifford S. Spavins. December 1966. 20 p. (PB-173992)
- No. 31 Study of a Left-Moving Thunderstorm of 23 April 1964. George R. Hammond. April 1967. 75 p. (PB-174681)
- No. 32 Thunderstorm Circulations and Turbulence from Aircraft and Radar Data. James C. Fankhauser and J. T. Lee. April 1967. 32 p. (PB-174860)
- No. 33 On the Continuity of Water Substance. Edwin Kessler. April 1967. 125 p. (PB-175840)
- No. 34 Note on the Probing Balloon Motion by Doppler Radar. Roger M. Lhermitte. July 1967. 14 p. (PB-175930)
- No. 35 A Theory for the Determination of Wind and Precipitation Velocities with Doppler Radars. Larry Armijo. August 1967. 20 p. (PB-176376)
- No. 36 A Preliminary Evaluation of the F-100 Rough Rider Turbulence Measurement System. U. O. Lappe. October 1967. 25 p. (PB-177037)
- No. 37 Preliminary Quantitative Analysis of Airborne Weather Radar. Lester P. Merritt. December 1967. 32 p. (PB-177188)
- No. 38 On the Source of Thunderstorm Rotation. Stanley L. Barnes. March 1968. 28 p. (PB-178990)
- No. 39 Thunderstorm - Environment Interactions Revealed by Chaff Trajectories in the Mid-Troposphere. James C. Fankhauser. June 1968. 14 p. (PB-179659)
- No. 40 Objective Detection and Correction of Errors in Radiosonde Data. Rex L. Inman. June 1968. 50 p. (PB-180284)
- No. 41 Structure and Movement of the Severe Thunderstorms of 3 April 1964 as Revealed from Radar and Surface Mesonet Data Analysis. Jess Charba and Yoshikazu Sasaki. October 1968. 47 p. (PB-183310)
- No. 42 A Rainfall Rate Sensor. Brian E. Morgan. November 1968. 10 p. (PB-183979)
- No. 43 Detection and Presentation of Severe Thunderstorms by Airborne and Ground-based Radars: A Comprehensive Study. Kenneth E. Wilk, John K. Carter, and J. T. Doolley. February 1969. 56 p. (PB-183572)
- No. 44 A Study of a Severe Local Storm of 16 April 1967. George Thomas Haglund. May 1969. 54 p. (PB-184970)
- No. 45 On the Relationship Between Horizontal Moisture Convergence and Convective Cloud Formation. Horace R. Hudson. March 1970. 29 p. (PB-191720)
- No. 46 Severe Thunderstorm Radar Echo Motion and Related Weather Events Hazardous to Aviation Operations. Peter A. Barclay and Kenneth E. Wilk. June 1970. 63 p. (PB-192498)
- No. 47 Evaluation of Roughness Lengths at the NSSL-WKY Meteorological Tower. Leslie D. Sanders and Allen H. Weber. August 1970. 24 p. (PB-194587)

- No. 48 Behavior of Winds in the Lowest 1500 ft in Central Oklahoma: June 1966-May 1967. Kenneth C. Crawford and Horace R. Hudson. August 1970. 57 p. (N71-10615)
- No. 49 Tornado Incidence Maps. Arnold Court. August 1970. 76 p. (COM-71-00019)
- No. 50 The Meteorologically Instrumented WKY-TV Tower Facility. John K. Carter. September 1970. 18 p. (COM-71-00108)
- No. 51 Papers on Operational Objective Analysis Schemes at the National Severe Storms Forecast Center. Rex L. Inman. November 1970. 91 p. (COM-71-00136)
- No. 52 The Exploration of Certain Features of Tornado Dynamics Using a Laboratory Model. Neil B. Ward. November 1970. 22 p. (COM-71-00139)
- No. 53 Rawinsonde Observation and Processing Techniques at the National Severe Storms Laboratory. Stanley L. Barnes, James H. Henderson and Robert J. Ketchum. April 1971. 245 p. (COM-71-00707)
- No. 54 Model of Precipitation and Vertical Air Currents. Edwin Kessler and William C. Bumgarner. June 1971. 93 p. (COM-71-00911)
- No. 55 The NSSL Surface Network and Observations of Hazardous Wind Gusts. Operations Staff. June 1971. 20 p. (COM-71-00910)
- No. 56 Pilot Chaff Project at the National Severe Storms Laboratory. Edward A. Jessup. November 1971. 36 p. (COM-72-10106)
- No. 57 Numerical Simulation of Convective Vortices. Robert P. Davies-Jones and Glenn T. Vickers. November 1971. 27 p. (COM-72-10269).
- No. 58 The Thermal Structure of the Lowest Half Kilometer in Central Oklahoma: December 9, 1966-May 31, 1967. R. Craig Goff and Horace R. Hudson. July 1972. 53 p. (COM-72-11281)
- No. 59 Cloud-to-Ground Lightning Versus Radar Reflectivity in Oklahoma Thunderstorms. Gilbert D. Kinzer. September 1972. 24 p. (COM-73-10050)
- No. 60 Simulated Real Time Displays of Velocity Fields by Doppler Radar. L. D. Hennington and G. B. Walker. November 1972. 10 p. (COM-73-10515)
- No. 61 Gravity Current Model Applied to Analysis of Squall-Line Gust Front. Jess Charba. November 1972. 58 p. (COM-73-10410)
- No. 62 Mesoscale Objective Map Analysis Using Weighted Time-Series Observations. Stanley L. Barnes. March 1973. 60 p. (COM-73-10781)
- No. 63 Observations of Severe Storms on 26 and 28 April 1971. Charles L. Vlack. April 1973. 19 p. (COM-73-11200)
- No. 64 Meteorological Radar Signal Intensity Estimation. Dale Sirmans and R. J. Doviak. September 1973. 80 p. (COM-73-11923/2AS)
- No. 65 Radisonde Altitude Measurement Using Double Radiotheodolite Techniques. Stephan P. Nelson. September 1973. 20 p. (COM-73-11932/9AS)
- No. 66 The Motion and Morphology of the Dryline. Joseph T. Schaefer. September 1973. 81 p. (COM-74-10043)
- No. 67 Radar Rainfall Pattern Optimizing Technique. Edward A. Brandes. March 1974. 16 p. (COM-74-10906/AS)
- No. 68 The NSSL/WKY-TV Tower Data Collection Program: April-July 1972. R. Craig Goff and W. David Zittel. May 1974. 45 p. (COM-74-11334/AS)
- No. 69 Papers on Oklahoma Thunderstorms, April 29-30, 1970. Stanley L. Barnes, Editor. May 1974. 147 p. (COM-74-11474/AS)
- No. 70 Life Cycle of Florida Key's Waterspouts. Joseph H. Golden. June 1974. 147 p. (COM-74-11477/AS)
- No. 71 Interaction of Two Convective Scales Within a Severe Thunderstorm: A Case Study and Thunderstorm Wake Vortex Structure and Aerodynamic Origin. Leslie R. Lemon. June 1974. 43 p. (COM-74-11642/AS)
- No. 72 Updraft Properties Deduced from Rawinsoundings. Robert P. Davies-Jones and James H. Henderson. October 1974. 117 p. (COM-75-10583/AS)

- No. 73 Severe Rainstorm at Enid, Oklahoma - October 10, 1973. L. P. Merritt, K. E. Wilk, and M. L. Weible. November 1974. 50 p. (COM-75-10583/AS)
- No. 74 Mesonet Array: Its Effect on Thunderstorm Flow Resolution. Stanley L. Barnes. October 1974. 16 p. (COM-75-10248/AS)
- No. 75 Thunderstorm-Outflow Kinematics and Dynamics. R. Craig Goff. December 1975. 63 p. (PB-250808/AS)
- No. 76 An Analysis of Weather Spectra Variance in a Tornadic Storm. Philippe Waldteufel. May 1976. 80 p. (PB-258456/AS)
- No. 77 Normalized Indices of Destruction and Deaths by Tornadoes. Edwin Kessler and J. T. Lee. June 1976. 47 p. (PB-260923/AS)
- No. 78 Objectives and Accomplishments of the NSSL 1975 Spring Program. K. Wilk, K. Gray, C. Clark, D. Sirmans, J. Dooley, J. Carter, and W. Bumgarner. July 1976. 47 p. (PB-263813/AS)
- No. 79 Subsynoptic Scale Dynamics As Revealed By The Use Of Filtered Surface Data. Charles A. Doswell III. December 1976. 40 p. (PB-265433/AS)
- No. 80 The Union City, Oklahoma Tornado of 24 May 1973. Rodger A. Brown, Editor. December 1976. 235 p. (PB-269443/AS)
- No. 81 Mesocyclone Evolution and Tornado Generation Within the Harrah, Oklahoma Storm. Edward A. Brandes. May 1977 28 p. (PB-271675/AS)
- No. 82 The Tornado: An Engineering-Oriented Perspective. Joseph E. Minor, James R. McDonald, and Kishor C. Mehta. December 1977. 196 p. (PB-281860/AS)
- No. 83 Spring Program '76. R. L. Alberty, J. F. Weaver, D. Sirmans, J. T. Dooley, and B. Bumgarner. December 1977. 130 p. (PB280745/AS)
- No. 84 Spring Program '77. P. S. Ray, J. Weaver, and NSSL Staff. December 1977. 173 p. (PB-284953/AS)
- No. 85 A Dual-Doppler Variational Objective Analysis as Applied to Studies of Convective Storms. Conrad L. Ziegler. November 1978. 116 p. (PB-293581/AS)